An Experimental Investigation of Glacial Till Erodibility and the Impacts of Slaking

by

Brodie Lane Blight

A thesis submitted to the Faculty of Graduate Studies of
the University of Manitoba
in partial fulfilment of the requirements for the degree of

Master of Science

Department of Civil Engineering
University of Manitoba
Winnipeg, Manitoba, Canada

Abstract

A better understanding of the glacial till erosion process and specifically the impacts of slaking (the disintegration/fragmentation of unsaturated soil after immersion in water) could be used to improve the design and operation of the proposed Lake St. Martin Outlet Channel, as well as other infrastructure affected by glacial till erosion. To study this, a total of 48 erosion tests were conducted on intact glacial till samples in a hydraulic flume located at the University of Manitoba. The critical shear stress of till which had not been subjected to slaking was found to be greater than 13 Pa for all sample locations and was typically in excess of 17 Pa (the maximum shear stress that could be applied by the apparatus). Conversely, the critical shear stress of slaked till was found to be less than 2 Pa. Due to this significant difference in critical shear stress, it is suggested that slaking may in some ways govern the rate of erosion. To better understand slaking, the slaking threshold (the minimum matric suction that will result in slaking) was estimated for material from the various sample locations by iteratively drying till samples to increasing matric suction prior to immersion in water. This threshold ranged from approximately 4 Pa to 400 Pa and was found to increase with increasing density and decrease with increasing clay content. Furthermore, slaking was found to be dependent on the rate of wetting, as samples saturated through capillary rise prior to immersion did not slake. Finally, recompacting till material with hydrated lime was found to effectively prevent slaking and it is suggested that lime stabilization could be considered as an alternative to conventional erosion protection depending on the project scale, location, and the local material present.

Acknowledgements

First and foremost, I would like to thank my advisor Dr. Shawn Clark. I have greatly benefited from your guidance and expertise not just during this project, but throughout most of my academic and young professional career. I thoroughly enjoyed working with you these past few years and I hope to continue to collaborate in the future, at very least on a softball diamond.

I would like to acknowledge the generous funding contributions from Manitoba Transportation and Infrastructure, the Natural Sciences and Engineering Council of Canada, and the University of Manitoba, without which this project would not have been possible.

A huge thank you to KGS Group for initiating and supporting this research. Special thanks to Dr. Lucas Wazney who served on the examining committee as well as to Mr. Patrice Leclercq and Mr. Shawn Beaudry for their insights from the engineering design perspective.

Thanks to Dr. Marolo Alfaro and Dr. Hartmut Hollaender who also served on the examining committee and offered technical guidance from their respective disciplines.

Thank you to research technicians Mr. Kerry Lynch and Mr. Alex Wall for your sampling/testing assistance, technical support, and ideas, but also for the fishing and meat smoking tips and discussions.

Lastly, I would like to thank my family and friends. In particular, my parents Pat and Tracy for their hard-working example and unconditional support. Finally, I would like to thank my fiancé, Kristina. I could not have done this without your endless patience, support, and encouragement.

Table of Contents

Abstract ..... **ii**

Acknowledgements ..... **iii**

Table of Contents ..... **iv**

List of Figures ..... **vii**

List of Tables ..... **x**

Chapter 1: Introduction **1**

1.1 Background 1

1.2 Motivation 2

1.3 Objectives 3

Chapter 2: Literature Review **4**

2.1 Introduction 4

2.2 Flow Characteristics of Open Channels 4

2.2.1 Discharge, Velocity, and Flow Depth 4

2.2.2 Shear Stress 6

2.3 Glacial Till Properties 8

2.4 Erosion Mechanisms 9

2.5 Characteristics of Cohesive Sediments and Their Effect on Erodibility 11

2.6 Erodibility of Glacial Till – Testing Methods and Results 16

2.6.1 In-situ Jet-Tests 19

2.6.2 Hydraulic Flume Tests 21

2.7 Softening / Weathering of Glacial Till and other Cohesive Sediments 23

2.7.1 Slaking 23

2.7.2 Freeze/Thaw Process 26

2.8 Lime Stabilization of Soils 27

2.8.1 Stabilization Process and Construction Procedures 27

2.8.2 Safety Considerations 28

2.8.3 Environmental Considerations 28

2.8.4 Economic Considerations 29

2.8.5 Testimonials 29

Chapter 3: Methodology 31

3.1 Introduction 31

3.2 Field Reconnaissance 31

3.2.1 St. Laurent Quarry Site 31

3.2.2 Lake St. Martin Emergency Outlet Channel – Reach 1 36

3.3 Preparation of Intact Shelby Tube "Puck" Samples 40

3.4 Slaking Observation Procedure 41

3.5 Increasing and Decreasing Initial Moisture Content of Puck Samples 42

3.6 Reconstituting Puck Samples 43

3.7 Reconstituting Puck Samples with Hydrated Lime 43

3.8 Hydraulic Flume Testing 44

3.8.1 Variable Slope Flume Overview 44

3.8.2 Design and Construction of Modifications to Variable Slope Flume 46

3.8.3 Varying the Applied Shear Stress 48

3.8.4 Validation of Applied Shear Stress Using ADV 50

3.8.5 Quantifying Erosion 51

3.8.6 Comparison to Previous Experiments Using Buffstone Clay 53

Chapter 4: Results and Analysis 55

4.1 Material Properties 55

4.2 Slaking Experiments 60

4.2.1 St. Laurent Quarry Till (Phase 1) 61

4.2.2 LSMEOC Till (Phase 2) 65
4.3 Cohesive Strength Meter (CSM) Testing 70
4.4 Hydraulic Flume Tests 70
4.4.1 St. Laurent Quarry Till 70
4.4.2 Lake St. Martin Emergency Outlet Channel Till 71
4.4.3 Hydraulic Flume Test Results Summary 72
4.4.4 General Observations 76
4.4.5 Defining the Critical Shear Stress 77
4.5 Effects of Slaking on Erosion 79
4.6 Effect of Material Properties on Erosion and the Slaking Threshold 79
4.6.1 Effect of Dry Density 80
4.6.2 Effect of Grain Size Distribution 81
4.6.3 Effect of Atterberg Limits 83
4.6.4 Effect of Cation Exchange Capacity (CEC) 83
4.6.5 Stepwise Multiple Linear Regression 84
4.7 Effects of Lime Stabilization 84
4.7.1 Effects of Lime Stabilization on Slaking 84
4.7.2 Effects of Lime Stabilization on Freeze/Thaw Deterioration 85
4.7.3 Effects of Lime Stabilization on Erosion (Post Freeze/Thaw and Wetting/Drying Cycle) 86
Chapter 5: Discussion 88
Chapter 6: Conclusion 96
6.1 Conclusions 96
6.2 Recommendations for Future Work 97
Chapter 7: References 99

List of Figures

Figure 1: Velocity distribution in trapazoidal channel section (adapted from Chow, 1959) 5
Figure 2: Shear stress distribution in a trapeziodal channel section (adapted from Chow, 1959) 7
Figure 3: Shear stress distribution on the bed of a rectangular channel with aspect ratio (base width over flow depth) of 8 (Adapted from Mirauda & Russo, 2020) 7
Figure 4: Shear strength at various normal stresses for a non-cohesive coarse-grained soil and a cohesive fine-grained soil 13
Figure 5: Stress-strain relationship under direct shear for cemented and uncemented soils 14
Figure 6: Channel Armouring (Adapted from Lagasse et al. 2012) 18
Figure 7: Shelby tube with guide attached (left) and Shelby tube with guide attached and hammer (right), showing yielded steel at holes 33
Figure 8: Deformed bevelled (bottom) edge of Shelby tube after sample extraction 34
Figure 9: CSM used in dewatered area (left) and dry area (right) at St. Laurent quarry site 35
Figure 10: Phase 2 sample locations relative to existing and proposed channels 37
Figure 11: Shelby tube sample extraction near inlet of LSMEOC 39
Figure 12: Rill erosion along banks of LSMEOC (person is 1.94 m tall) 40
Figure 13: Shelby tube being cut by chop saw with masonry blade and jig for cutting 50 mm lengths 41
Figure 14: Tray with constant water level for saturating samples via capillary rise 42
Figure 15: Shelby tube puck sample weight over time (one side sealed) 43
Figure 16: Variable slope flume located in the University of Manitoba Hydraulic Research and Testing Facility 45
Figure 17: Variable slope flume headwater box (left) and tailwater gate (right) 46
Figure 18: Subfloor HDO panels and C-channel girders (attached for weight) pictured during construction 47
Figure 19: Reconstituted block sample panel (left) and Shelby tube “puck” sample panel (right) 47

Figure 20: ADV transducer (left) and transducer mounted to point gauge and movable frame with laptop for recording data (right) 50
Figure 21: Measured and theoretical relationship between dimensionless velocity (u^+) and dimensionless distance from bed (y^+) under 9.3 Pa applied shear stress condition 51
Figure 22: Example of erosion progression and calculated pitted areas (shown with and without paint to highlight depressions) – Sample R1-L6-D1 53
Figure 23: Erosion of Buffstone clay observed using modified variable slope flume and EMD (unpublished data from Jianfar, 2014) 54
Figure 24: Plasticity chart for till samples used in this study 56
Figure 25: Grain size distribution of till samples used in this study 57
Figure 26: In-situ degree of saturation variation of Reach 1 samples with overburden material depth and height above channel water level. 58
Figure 27: In-situ matric suction variation of Reach 1 samples with overburden material depth 58
Figure 28: In-situ matric suction variation of Reach 1 samples with height above water level 59
Figure 29: Conceptual representation of matric suction relative to different boundary conditions (adapted from Fredlund et al., 2012) 60
Figure 30: Submerged Shelby tube puck sample with LVDT to measure vertical displacement 62
Figure 31: Swelling of reconstituted St. Laurent till sample submerged at in-situ moisture content 62
Figure 32: Point gauge used to measure vertical displacement (swelling) of air-dried reconstituted (left) and intact (right) St. Laurent till samples. 63
Figure 33: Swelling of Air-dried Intact and Reconstituted St. Laurent Till Samples 63
Figure 34: Effect of groundwater boundary condition on swelling/slaking 65
Figure 35: Minor (top) and major (bottom) slaking – Sample Location R1-L1 67
Figure 36: Example soil-water characteristic curve (adapted from Fredlund et al., 2012) 69
Figure 37: Portion of sample area pitted at increasing increments of applied shear stress 75

Figure 38: Intact till sample with centre pit drilled prior to testing 77
Figure 39: Effect of dry density on slaking threshold 81
Figure 40: Effect of median particle diameter on slaking threshold 82
Figure 41: Effect of clay fraction on slaking threshold.....82
Figure 42: Effect of plasticity index on slaking threshold 83
Figure 43: Effect of cation exchange capacity on slaking threshold.....83
Figure 44: Observed and predicted slaking threshold based on two variable (clay content and density) linear regression model shown with 1:1 line 84
Figure 45: Swelling of LSMOC till reconstituted with 4% (left), 2% (centre), and 0% (right) hydrated lime content - subjected to air-drying prior to submergence.....85
Figure 46: Portion of sample area pitted at increasing increments of applied shear stress – lime stabilized 86
Figure 47: Double-layer repulsive and interparticle attraction (van der Waals) forces as a function of interparticle distance (adapted from Principles of Soil Chemistry) 90
Figure 48: Matric suction at a point along a channel bank relative to channel and groundwater levels at an initial condition (light blue) and during immersion (dark blue) 93

List of Tables

Table 1: Critical shear stress estimates for glacial till 19
Table 2: Phase 2 sample summary 38
Table 3: Applied shear stress conditions 49
Table 4: Soil Sample Properties 56
Table 5: Suction and slaking determined for various initial moisture conditions 68
Table 6: Ranges Determined for Slaking Thresholds – Initial Suction and Moisture Content 70
Table 7: Hydraulic Flume Testing Summary 73
Table 8: Critical Shear Stresses for Glacial Till Material 79

Chapter 1: Introduction

1.1 Background

A system of artificial channels and control structures mitigates Assiniboine River flooding downstream of Portage la Prairie and through Winnipeg by diverting a portion of the natural river flow to Lake Manitoba and eventually the North Basin of Lake Winnipeg. In its current configuration, the system includes the Portage Diversion which connects the Assiniboine River to Lake Manitoba, the Fairford River Water Control Structure (FRWCS) which regulates Lake Manitoba outflows to Lake St. Martin, and the Lake St. Martin Emergency Outlet Channel which was constructed in 2011 to increase the outlet capacity of Lake St. Martin to Lake Winnipeg and is intended to only be used again for a similar emergency scenario.

In 2011 and 2014, Manitoba experienced record or near-record flooding throughout the Assiniboine River Basin (Manitoba, 2013; Manitoba, 2022). During the 2011 flood event, the total volume of flood waters entering the Portage Reservoir was unprecedented - twice as large as the previous record amount recorded in 1976 and for comparison; approximately equivalent to the flow volume recorded at Ste. Agathe on the Red River in 1997 during the "Flood of the Century". To prevent the Assiniboine River flows from exceeding the capacity of the river's banks and/or dyke system downstream of Portage la Prairie and through Winnipeg, flows were diverted through the Portage Diversion and into Lake Manitoba. This unprecedented flow volume entering Lake Manitoba, along with several compounding factors (high lake levels in 2010, above average precipitation, record inflows from Lake Winnipegosis, high winds), resulted in thousands of acres of agricultural land being flooded and the damage or destruction to hundreds of homes and other buildings adjacent to Lake Manitoba and the downstream Lake St. Martin (KGS Group, 2016).

First Nations communities were among those most severely impacted by the flooding in 2011 and accounted for 62% of total evacuees in 2014. Members of Lake St. Martin, Dauphin River, Little Saskatchewan, and Pinaymootang First Nations alleged their residents were forced to leave their homes in 2011 as a result of the Manitoba government's decision to divert water from the Assiniboine River to reduce the risk of flooding in Winnipeg in a lawsuit that was eventually settled for $90 million (Lambert,

2018)In 2017, 1,953 evacuees remained, mostly from the Lake St. Martin First Nation, and the evacuation was eventually declared over in 2020 when the entire community was rebuilt in a new location at a higher elevation (Government of Canada, 2022).

In the summer and fall following the peak of the 2011 flood event, the Lake St. Martin Emergency Outlet Channel (LSMEOC) was designed and constructed to help reduce Lake Manitoba and Lake St. Martin Water Levels on an emergency basis. Although this channel effectively provided a flood protection benefit during the emergency periods when it was operated, permanent flood control infrastructure is required to provide additional outlet capacity from both Lake Manitoba and Lake St. Martin to better regulate the water levels in these lakes during non-emergencies. In 2018, the Province of Manitoba awarded the design and construction oversight of the Lake St. Martin and Lake Manitoba Outlet Channels to Hatch Ltd. and KGS Group, respectively (Manitoba, 2022).

1.2 Motivation

The design of any permanent artificial channel excavated through native material requires an understanding of how the hydraulic conditions within the channel will impact erosion of the channel bed and bank material. Bed or bank substrate which is highly resistant to erosion allows for faster channel velocities, increasing the allowable channel slope which reduces the number of control structures required to “step down” the hydraulic grade line from the channel inlet to its outlet. If left unchecked, over time channel bed and bank erosion could result in undesirable changes to the channel alignment and geometry, slope failure of the channel banks, and a significant increase to the sediment load which could have detrimental impacts on fish and other aquatic life within or downstream of the channel.

The way in which hydraulic conditions impact erosion is unique to the material which lines a given channel. The majority of the Lake St. Martin and Lake Manitoba Outlet channels are to be constructed through various subclassifications of glacial till (silt till, clay till, and silty clay). For typical applications, a sufficient understanding of the relationship between the hydraulic conditions within the channel and the resulting erosion can be gained from the literature. However, just as its composition can vary, the reported erosion parameters of glacial till vary widely and the overall mechanisms

which cause erosion are not well understood (Pike, 2014). Furthermore, the large scale of these outlet channel projects increases the cost and environmental implications of the channel design, thus simply selecting conservative erosion parameters could result in significant unnecessary expenditure. As such, gaining a better understanding of glacial till erosion and its mechanisms would help improve the design of artificial channels such as these, as well as be useful in the design and analysis associated with the erosion of natural watercourses through glacial till or other cohesive sediments.

1.3 Objectives

The overall objective of this research is to better understand the erosion process of glacial till and specifically the impacts of slaking (i.e. the disintegration/fragmentation of unsaturated soil after immersion in water). The specific technical objectives are as follows:

- Develop a method for extracting intact cohesive sediment samples and determining their critical shear stress for erosion using a hydraulic flume.
- Determine the critical shear stress for erosion of several different intact glacial till sediments collected along Reach 1 of the Lake St. Martin Emergency Channel and at the St. Laurent quarry site, both before and after being subjected to slaking.
- Estimate the slaking threshold (i.e. the minimum matric suction that will result in slaking) for several intact glacial till sediments collected along Reach 1 of the Lake St. Martin Emergency Outlet Channel.
- Evaluate the effects of various material properties on till slaking and erosion.
- Evaluate the effects of lime stabilization on till slaking and erosion.

Chapter 2: Literature Review

2.1 Introduction

This chapter will first provide an introduction to basic hydraulic concepts of flow, velocity, and how a fluid imparts a shear stress on a flow boundary. The properties of glacial till are then discussed, followed by an introduction to the mechanisms that cause erosion. Since it is typically intended for artificial channels such as the Lake St. Martin and Lake Manitoba outlet channels to be non-eroding, this review focusses on the shear stress threshold for erosion or the "critical shear stress". Since glacial till is a cohesive sediment, cohesive sediment properties and how they influence erosion are discussed. A review of existing studies on the erodibility of glacial till is then provided, and lastly, the impact of weathering and soil stabilization on the erodibility of cohesive sediments is discussed.

2.2 Flow Characteristics of Open Channels

2.2.1 Discharge, Velocity, and Flow Depth

Three of the simplest and most commonly referenced flow characteristics in open channels are velocity, depth, and discharge. In one-dimensional space, an average flow depth, average velocity, and discharge can be attributed to a given cross-section of flow oriented perpendicular to the flow direction. Average velocity is simply the total discharge through the cross-section divided by the cross-sectional area of flow. The relationship between discharge/velocity and depth can most simply be examined under the uniform flow condition using the empirically-based Manning equation:

$$Q = A \times V_{avg} = \frac{k_n}{n} A R^{2/3} \sqrt{S} \tag{2-1}$$

Where Q is the channel discharge, A is the cross-sectional area of flow, V_{avg} is the average flow velocity, k_n is a unit conversion factor, n is the empirical Manning's roughness coefficient, R is the hydraulic radius (flow area divided by wetted perimeter), and S is the slope of the energy grade line, which is equivalent to the slope of the channel bed under uniform flow conditions.

The Manning's roughness coefficient is intended to account for the effect of frictional resistance of the wetted channel boundary (known as the wetted perimeter) on flow

characteristics such as depth and velocity. In addition, Manning's n also accounts for any other features that cause flow resistance, such as channel sinuosity, expansion and contraction, vegetation, etc. Coefficients for various channel boundary surfaces have been determined experimentally and can be obtained from the literature. For a given channel boundary material, the Manning's roughness coefficient can vary slightly depending on the flow depth and velocity, however in practice this variation is often neglected.

In reality, water velocity varies both vertically and laterally (perpendicular to flow) across a given cross section, as shown in Figure 1. This velocity distribution is influenced by shear forces along the boundaries, and inertia in cases where the channel bends.

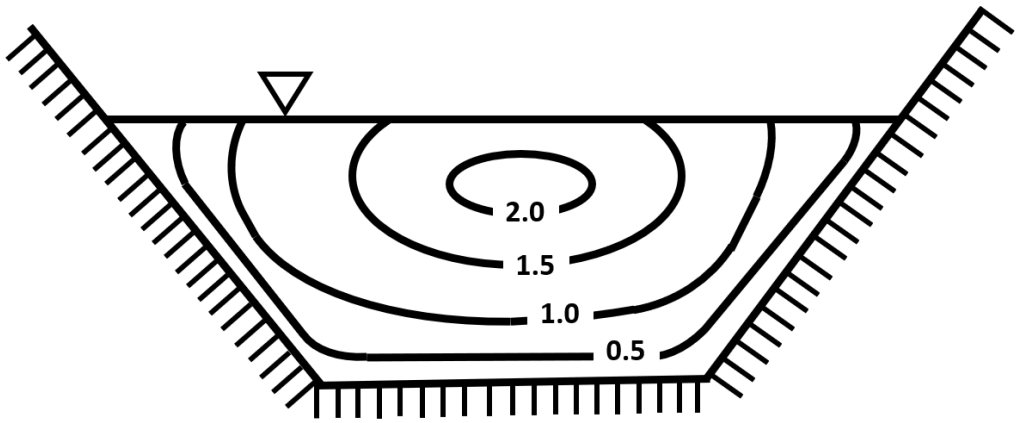

Figure 1: Velocity distribution in trapazoidal channel section (adapted from Chow, 1959)

For a given column of flow, the vertical distribution of streamwise velocity is often described by either a logarithmic or power relationship such as the log-law, velocity defect law, or Cole's law of the Wake (Peters, 2015). Each law is theoretically applicable for only a specific depth region. Due to the no-slip boundary condition, fluid in contact with a stationary boundary (e.g. a channel bed) will also be stationary and flow velocities within the region immediately adjacent to this boundary (known as the viscous sublayer) will be very low (Munson et al., 2002). As a result, viscous effects dominate very close to the channel boundary. Conversely, in the turbulent region a sufficient distance from the stationary boundary (known as the outer region), there is considerable mixing and randomness to the flow and Reynolds stresses dominate. Through dimensional analysis, the log-law was developed to represent the velocity

profile between the viscous sublayer and the outer layer (known as the overlap region):

$$\bar{u}/u_* = \frac{1}{\kappa}\ln\left(\frac{u_* z}{v}\right) + 5 - \Delta B \quad (2\text{-}2)$$

Where $\bar{u}$ is the average streamwise velocity, u_* is the shear velocity, v is the kinematic viscosity, κ is the von Karman constant (0.41), z is the distance from bed, and ΔB is the roughness shift.

2.2.2 Shear Stress

Due to the no-slip boundary condition, the velocity of a fluid immediately adjacent to a boundary will have the same velocity as the boundary. Under steady uniform flow conditions, momentum effects acting on a control volume of fluid cancel out, and a simple force balance can be used to calculate the shear force which counter-acts the down-slope component of the fluid weight (Munson et al., 2002). When simplified, the force balance equation becomes:

$$\tau_{mean} = \gamma RS \quad (2\text{-}3)$$

Where τ_{mean} is the average shear stress along the entire wetted perimeter and γ is the specific weight of the fluid.

It is this shear stress (also known as tractive force) acting on the channel boundary that may cause erosion, depending on the erodibility of the channel boundary material. As shown in equation (*2-3*), the average shear stress applied to the channel boundary is directly proportional to the hydraulic radius and channel slope (under uniform flow conditions).

However, shear stress distribution along the wetted perimeter is not uniform, and areas will experience higher or lower shear stresses than the average. An example of a shear stress distribution in a trapezoidal channel section is provided in (note the specific weight of the fluid is denoted as w instead of γ). As shown, the maximum shear stress applied to the channel banks is less than the maximum shear stress applied to the channel bottom.

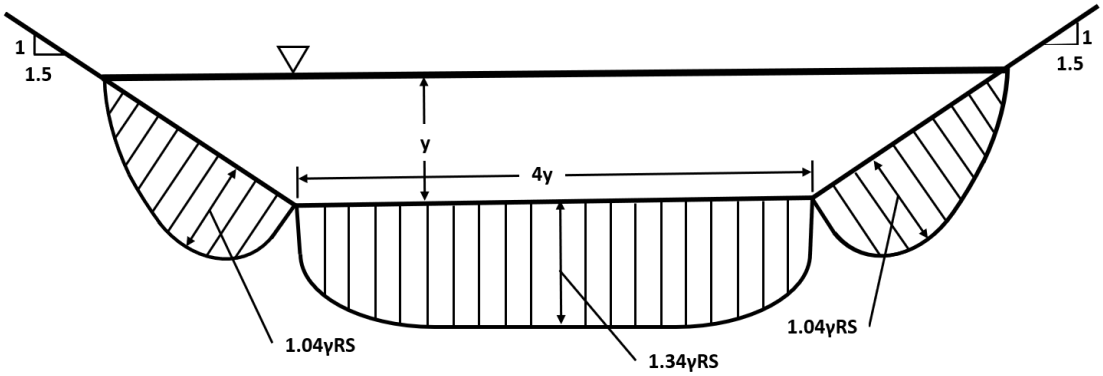

Figure 2: Shear stress distribution in a trapeziodal channel section (adapted from Chow, 1959)

Similarly, Mirauda & Russo (2020) reviewed experimental data and developed a model of the shear stress distribution in open rectangular channels. Figure 3 shows the shear stress distribution applied to the channel bed relative to the average shear stress for flow conditions with an aspect ratio (base width divided by flow depth) of eight. As shown, the applied shear stress is relatively constant when farther than 15% of the base width from the channel sidewall, where it is approximately 1.12 times the average shear stress based on the experimental data.

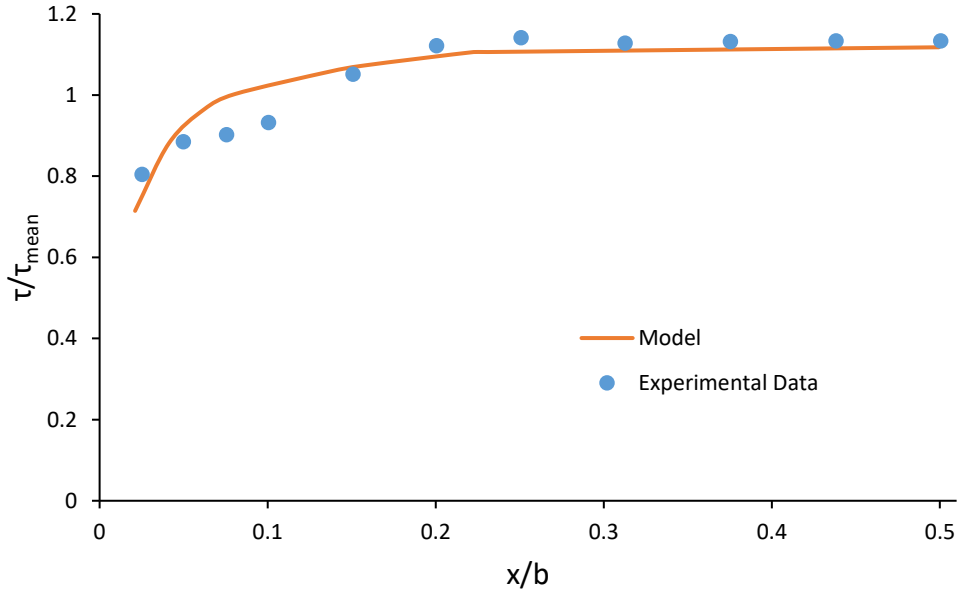

Figure 3: Shear stress distribution on the bed of a rectangular channel with aspect ratio (base width over flow depth) of 8 (Adapted from Mirauda & Russo, 2020)

While experimentally derived models of the shear stress distribution, such as those shown in Figure 2 and Figure 3, are useful in estimating the applied shear stress at a particular location along a channel cross section, the actual applied shear can be more accurately determined by fitting the vertical velocity profile measured at a location to the log-law. For this method, the shear velocity (u_*) and roughness shift (ΔB) are used as fitting parameters to make the measured and theoretical velocity profiles align within the overlap region. Once u_* is determined, it can be used to obtain the shear stress applied to the channel boundary at a particular location using the following equation:

$$\tau_b = \rho {u_*}^2 \tag{2-4}$$

Where τ_b is the boundary shear stress at a specific location along the wetted perimeter and ρ is the density of the fluid.

2.3 Glacial Till Properties

Glacial till (or just "till") is a heterogeneous sediment formed through the glacial processes of erosion, transportation, and deposition (Clarke, 2018). Glaciers erode a particular substrate through either abrasion or quarrying (also known as plucking). Abrasion breaks down larger particles into smaller particles at the interface between glacial ice and the substrate, while quarrying "plucks" particles of various sizes from the substrate without completely breaking them down. The eroded material can be transported a large distance before being deposited through subglacial traction (lodgement till) or melt-out (ablation till), depending on whether the glacial ice is advancing or retreating. Due to the varied modes of glacial erosion, glacial till contains a distinctly broad array of particle sizes, ranging from large boulders to microscopic clay particles. Conversely, alluvial deposition tends to sort particles by size since larger particles settle out at locations or during time periods where the water velocity is higher and the size of particles deposited decreases as the water velocity decreases.

As noted, lodgement till is deposited by subglacial traction or the "lodgement" of glacial debris beneath a glacier by pressure melting or when the frictional resistance between a clast and the underlying substrate exceeds the frictional drag forces of the glacier on the clast (Dreismanis, 1986 as cited in Clarke, 2018). Lodgement tills are typically very dense (often considered over-consolidated) due to the pressure and

shear forces that were present during their deposition. The immense shear forces can also result in slip planes or planes of weakness within the soil structure.

Ablation till is formed when a glacier carrying material either entrapped within (englacial) or carried on top the ice (supraglacial) melts in place without further deformation or transport (Benn and Evans, 2010 as cited in Clarke, 2018). Particles deposited through ablation are typically more angular since abrasion did not occur during their deposition. Furthermore, ablation tills have not been subject to the same high pressure and shear during deposition as lodgement tills and are typically less dense and without slip planes.

In addition to the variability of till resulting from the different modes of deposition, further variability can be introduced into previously deposited till via "ploughing". Ploughing occurs when a new glacier passes over previously deposited till and a clast that protrudes across the ice-till interface is dragged through the upper layer of the till, which can lead to a local reduction in strength.

Glacial till is predominantly considered a cohesive material (IOWADOT, 2015). Despite its composition often including a significant percentage of sand, gravel, cobbles and boulders, the portion of finer material typically results in relatively high undrained shear strength.

2.4 Erosion Mechanisms

In general, channel erosion is a function of the hydraulic conditions within the channel, mainly the applied shear stress, and the composition of the channel bed and bank material. This material can be classified as either cohesive or non-cohesive. Erosion of non-cohesive material is more easily understood since there are no inter-particle attractive forces and erosion can be quantified based on the lift, drag, gravitational, and friction forces acting on an individual particle. Larger particles are acted on by larger gravitational forces and are therefore more resistant to erosion. Erosion characteristics can be determined using the well-known Shields diagram and related equations. In contrast, cohesive soil particles are attracted to one another due to electrochemical forces acting on the surface of the particles (Garcia, 2008). Since cohesion acts on the surface of particles, the degree of cohesion depends on the ratio of the particle's mass to the particle's weight (known as its specific surface area). Clay

particles, defined as particles with a diameter of less than 2 µm, are plate-like and therefore have a high specific surface area resulting in stronger electrochemical forces between particles (cohesion). Studies have shown that as little as 10% clay can affect soil behaviour (Debnath & Chaudhuri, 2010). Non-cohesive sediments typically erode on only a "particle by particle" basis (Mier and Garcia, 2011), whereas cohesive sediments may also erode in larger clasts or chunks of smaller particles bonded together, separating from the bed along planes of weakness (typical of glacial till).

Two of the most fundamental concepts of sediment transport are *critical shear stress* and *erosion rate*. Put most simply (but somewhat inaccurately), the critical shear stress is the shear stress applied by a moving fluid which is the threshold of sediment movement (Sturm, 2010). However, according to Mantz (1977, as cited in Mier & Garcia), "there is no single value of bed shear stress below which not a single particle will move". Similarly, Paintal (1971, as cited in Mier & Garcia, 2011) points out that "there does not seem to be any limit below which there is no movement. At very low shear stress values, one has to wait a longer time to see movement, as the probability of movement becomes very small, but this probability is never zero except in still water". Therefore, determining the erosion threshold (critical shear stress) of a particular sediment is more of a stochastic problem than a deterministic problem and thus the concept of a "critical shear stress" requires a more practical definition. Paintal (1971) defines it as the shear stress "below which the bed load transport is of no practical importance", while others tend to define it as the lowest shear stress which results in erosion that is "visible to the eye" (Mier and Garcia, 2011). These definitions are somewhat subjective, however Mier and Garcia noted that for glacial till collected along the St. Clair River the threshold for erosion was very sharp and the initiation of erosion was easily observed with the naked eye.

Once the applied shear stress exceeds the critical shear stress of the bed material, particles either begin to slide, roll, and/or saltate downstream (non-cohesive sediment) or dislodge from the bed as flocs or chunks of particles (cohesive sediment). This type of sediment transport is referred to as the bed load. If the magnitude of the vertical velocity fluctuations exceed the fall velocity of the bed load particles, they will become suspended in the flow, which is referred to as the suspended load. The

combined bed and suspended loads can be expressed in terms of volume or mass over time, referred to as the *erosion rate*. The erosion rate is often a function of the applied shear stress relative to the critical shear stress (McAnally, 1968).

Since it is typically intended for artificial channels such as the Lake St. Martin and Lake Manitoba outlet channels to be non-eroding, this review focusses on critical shear stress rather than erosion rate.

2.5 Characteristics of Cohesive Sediments and Their Effect on Erodibility

Unlike non-cohesive sediments which resist erosion primarily through gravitational forces acting on individual particles, the critical shear stress of cohesive sediments may be dependent on several different soil properties, in addition to the water chemistry, abrasion, and weathering. Due to the large number of variables, there are currently no standardized methods for estimating critical shear stress of cohesive soils based on specific soil parameters, and experience with laboratory testing of the local material is therefore recommended for design (USDA, 2007). Nonetheless, attempts have been made to correlate cohesive soil parameters to erodibility for various sample sets with some success. Kimiaghalam (2016) categorized the main characteristics of cohesive soils (in the context of erodibility) as follows:

Physical properties:

a) Grain size distribution: This is the measure of relative composition of particle sizes of a given soil. It is often expressed in terms of the percentages of clay, silt, sand, gravel, cobbles, and boulders (all of which can be present in glacial till). Studies have shown that a larger fraction of fine grained particles (silt and clay) can increase the erosive resistance of a material; however this can also increase the materials susceptibility to weathering (Couper, 2003).
b) Plasticity Index (PI): This is a measure of the plasticity of a soil and is taken as the difference between the liquid limit (water content at which soil behaviour changes from plastic to liquid) and plastic limit (water content at which soil behaviour changes from semisolid to plastic). These water contents are referred to as the Atterberg limits. Several relationships between the critical shear stress of cohesive soils and their plasticity index have been found which

show that the critical shear stress typically increases as the plasticity index increases (Dunn, 1959; Smerdon and Beasley, 1961; Carlson and Enger, 1962 as cited in Kimiaghalam, 2016).

Mechanical properties:

c) Cohesion (C) and Friction angle (ϕ): Both cohesion and friction angle are measures of a soil's shear strength and can be determined with a Direct Shear Test. A Direct Shear Test subjects a cylindrical sample of undisturbed soil to an increasing shear stress under various normal stresses and determines the shear stress required to shear the sample. The normal stresses and corresponding shear strengths are then plotted (see example on Figure 4). In soil mechanics, the portion of the shear strength that is proportional to the normal stress (the slope of the line) is referred to as the friction angle and is caused by the friction between soil particles sliding past one another (Mitchell & Soga, 2005). The portion of the shear strength present without any normal stress (the Y-intercept) is referred to as cohesion and is most often attributed to the electrochemical forces between particles. Erosion of cohesive soils is by definition governed by cohesion and cohesion measured using a Direct Shear Test has successfully been used to estimate the critical shear stress of cohesive soils (Kimiaghalam, 2016). Friction angle increases with increasing particle size (Roy & Dass, 2019), and is generally not a good indicator of the critical shear stress of cohesive soils.

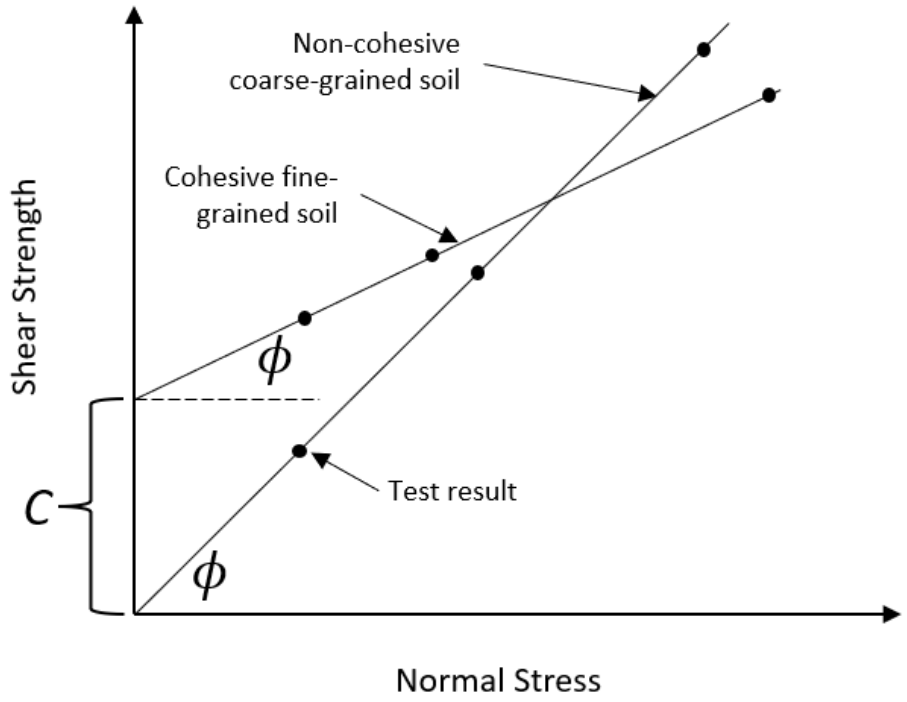

Figure 4: Shear strength at various normal stresses for a non-cohesive coarse-grained soil and a cohesive fine-grained soil

While cohesion in soil mechanics is most often attributed to electrochemical forces, there are a few different sources of cohesion (Mitchell & Soga, 2005):

- True Cohesion: True cohesion is the "shear strength in excess of that generated by frictional resistance to sliding between particles, the rearrangement of particles, and particle crushing" (Mitchell & Soga, 2005). Even with a Direct Shear Test conducted under no applied normal stress, some of the shear strength may still be attributed to frictional resistance due to the particulate nature of the soil and the fact that particle contacts are not oriented in the plane of the applied shear stress. As a result, true cohesion is difficult to quantify, especially in soils with a higher friction angle. Mitchell & Soga (2005) proposed three sources of true cohesion:
    - <u>Cementation:</u> Cementation is the chemical bonding between soil particles, typically by carbonates, silica, alumina, iron oxide, and organic compounds, and can account for a large portion of true

cohesion. Figure 5 shows how a small amount of cementation can significantly increase the shear strength, and that this strength is diminished at large strains, when the cementitious bonds become broken.

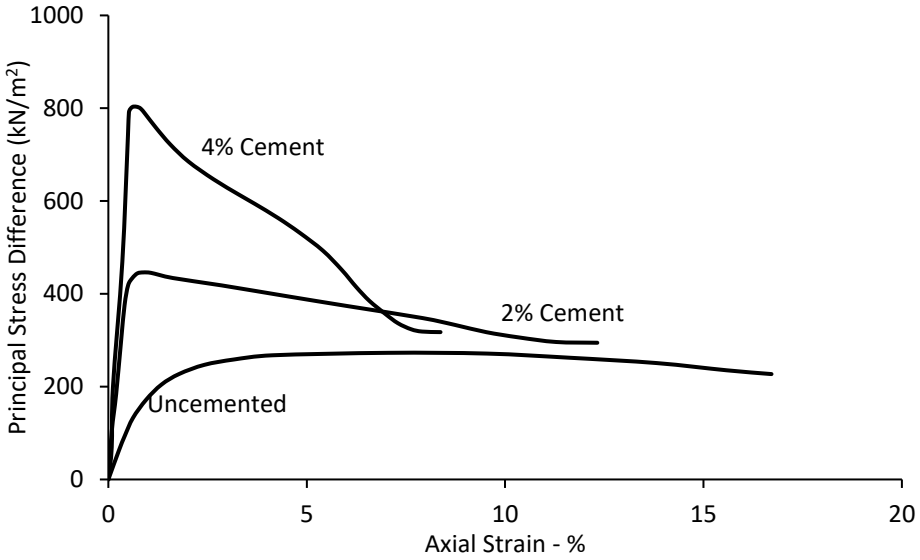

Figure 5: Stress-strain relationship under direct shear for cemented and uncemented soils

Cementation can develop naturally through the precipitation of minerals over time, or artificially through the addition of stabilizers such as cement or lime. The tensile strength of cemented bonds depends on the amount of particle contact in addition to the amount of precipitates, therefore tensile strength increases with decreased void ratio and increased density. However, when a natural cemented soil under high overburden stress is unloaded, elastic rebound can result in tensile stress between particles, and possibly break cemented bonds.

- Electrostatic Attractions: If the edges and surfaces of particles are oppositely charged, electrostatic attraction adds to the tensile strength between particles. Electrostatic attraction becomes significant for separation distances less than 2.5 nm.

Electrostatic forces can also be repulsive, resulting in dispersion, as described in Chapter 2.7.1.

- Electromagnetic Attraction: Electromagnetic attraction is caused by van der Waals forces, which are attractive forces always acting on all matter, but are very weak and usually only influence small particles at close distances (less than 1000 nm). Casimir-Polder theory suggests that these forces are related to the distance between particles as follows:

$$F \propto \frac{Ak}{d^3} \quad (2\text{-}5)$$

Where A, and k are constants, and d is the distance between particles.

- Preliminary Valence Bonding: Preliminary valence bonding is a chemical interaction similar to cementation and occurs at very short particle distances (less than 0.3 nm). This type of bonding is not well understood, but it is speculated that it may occur without any cementing agents.

- Apparent Cohesion: In unsaturated soils, surface tension causes attraction between soil particles, which is referred to as apparent cohesion. Apparent cohesion is eliminated when the soil becomes saturated.

d) Dry or Bulk Density: This is simply the dry mass of an undisturbed soil sample divided by its volume. Alshameri et al. (2017) found that cohesion increases with increasing density. This could be explained by the reduced fraction of water/voids interrupting the electro-chemical bonds between soil particles. This relationship consistent with findings from Owen (1975, as cited in Kimiaghalam, 2016) and Thorn & Parsons (1980 as cited in Kimiaghalam, 2016) who developed similar equations for estimating critical shear stress based on dry density (Kimiaghalam, 2016).

Electro-chemical properties:

e) Cation Exchange Capacity (CEC): Cation exchange capacity is a measure clay mineral cohesion (McAnally, 1968) and is calculated as follows (expressed as milliequivalents per 100g of soil):

$$CEC = \frac{\frac{[k]}{39.0983} + \frac{[Ca]}{20.039} + \frac{[Mg]}{12.1525} + \frac{[Na]}{22.9897}}{10} \quad (2\text{-}6)$$

Kaolinite has a low CEC and exhibits a lower degree of cohesion, while smectite has the highest CEC and is the most cohesive (illite and chlorite fall in between).

f) Sodium Adsorption Ratio (SAR): This is the ratio of sodium ions (Na^{+}) to the sum of calcium Ca^{++} and magnesium Mg^{++}ions within the pore fluid (McAnally, 1968) and is defined as:

$$SAR = \frac{Na^{+}}{[0.5(Ca^{++} + Mg^{++})]^{1/2}} \quad (2\text{-}7)$$

Since SAR is a measure of the relative salinity of the pore fluid, it can be altered by the salinity and pH of the eroding fluid which saturates the sediment. Studies attempting to relate SAR with erodibility have found both positive and negative correlations between SAR and critical shear stress (Medina-Cetina, 2019).

g) Exchangeable Sodium Percentage (ESP): This is the ratio of sodium ions (Na^{+}) to the CEC for a particular soil. ESP is considered the most important factor affecting dispersion in soils (Laker & Nortjé, 2019) which can greatly impact their critical shear stress.

2.6 Erodibility of Glacial Till – Testing Methods and Results

Glacial till erosion could be conservatively estimated by assuming the till would not exhibit any cohesive behaviour. Since glacial till contains a very wide range of particle sizes, shear stress imparted by water under a given hydraulic condition would be sufficient to move smaller particles but insufficient to move larger particles. As the smaller particles are transported downstream, the remaining bed material becomes

increasingly coarse and eventually thick enough to prevent the underlying material from being eroded (Lagasse et al., 2012). This process is referred to as "armouring" and the depth of scour required to form the armour layer can be predicted using the following equation:

$$Y_s = y_a\left(\frac{1}{P_c} - 1\right) \tag{2-8}$$

Where Y_s is the depth of scour required to form the armour layer, y_a is the thickness of the armour layer, and P_c is the percent of material coarser than the critical particle size, as shown in Figure 6. The critical particle size is the smallest particle which is large enough to resist the applied shear stress and can be determined using the Shields diagram or using the following equation:

$$D_c = \frac{\tau_0}{K_s(\gamma_s - \gamma)} \tag{2-9}$$

Where D_c is the critical particle size, τ_0 is the applied shear stress, γ is the specific weight of water, γ_s is the specific weight of the sediment, and K_s is a dimensionless coefficient often referred to as the Shields parameter (often taken as 0.047 for sand and 0.03 for gravel). The thickness of the armour layer is taken as one to three times the critical particle size.

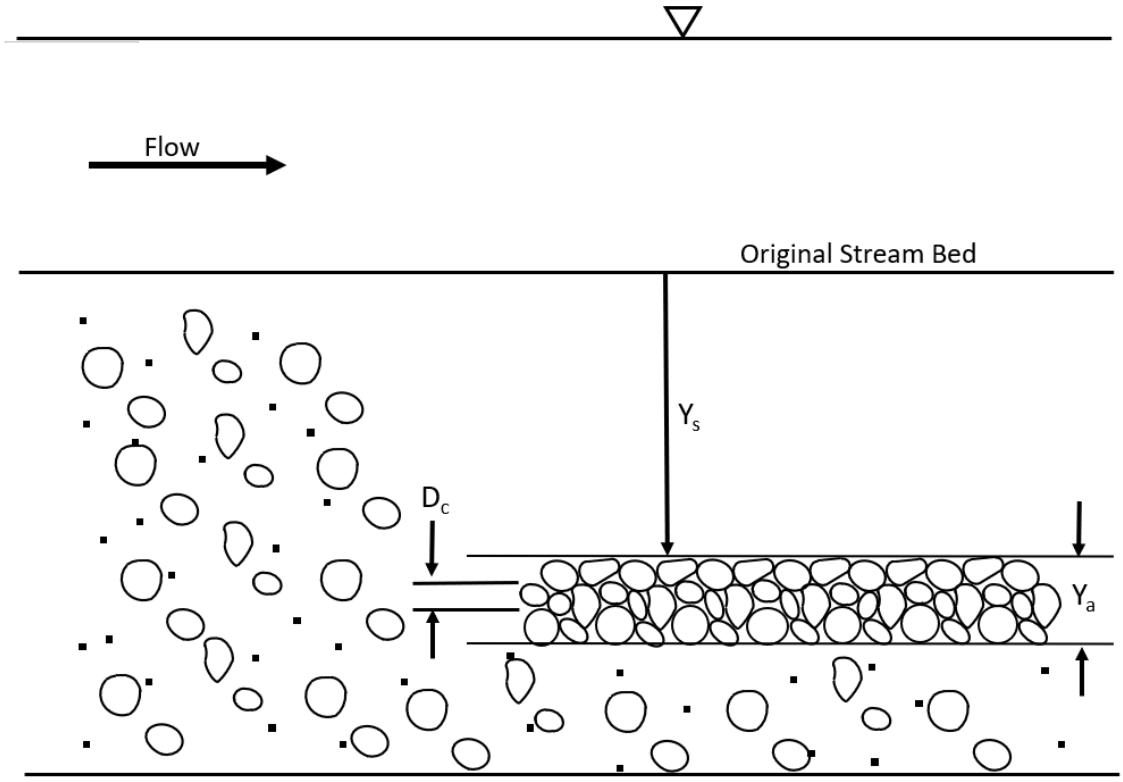

Figure 6: Channel Armouring (Adapted from Lagasse et al. 2012)

While the concept of armouring is useful to define the upper limit of the expected scour, the till material through which the Lake St. Martin and Lake Manitoba Outlet Channels will be constructed contains a large fraction of sediment particles smaller than the critical particle size for a practical applied shear stress. As a result, a very large volume of sediment would need to be transported downstream and into natural water bodies before the armour layer develops - which may have a significant ecological impacts. To minimize the ecological impact, the proposed channels are to be designed such that they are non-eroding. This requires an estimation of the critical shear stress of the native glacial till which considers the cohesive bonds that would be present within the soil matrix.

As discussed, to date there are no standardized methods for estimating the critical shear stress of cohesive sediments based on soil characteristics. Therefore, laboratory and in-situ field tests are considered the most dependable way to determine this parameter (Mier & Garcia, 2011). These tests can generally be grouped into either in-situ jet tests or hydraulic flume tests. A summary of some experimentally determined critical shear stresses for glacial till sediments is provided in the Table 1 below. As

shown, there is considerable variability in the critical shear stresses estimated, making it difficult to a select a value for design purposes.

Table 1: Critical shear stress estimates for glacial till

Study	Material Description	Critical Shear Stress (Pa)	
		Range	Average
In-situ Jet Tests			
Shugar et al. (2007)	Fletcher's Creek Till	0-20	2.24
Khan & Kostaschuk (2011)	Submerged Highland Creek Till	17.5-63.3	38.7
	Exposed Highland Creek Till	0.0-0.2	0.1
	Submerged Fletcher's Creek Till	0-9.6	3.7
	Unexposed Fletcher's Creek Till	0-17.3	8.5
Hydraulic Flume Tests			
Kamphuis et al. (1990)	Dingman Creek Till	0-2	1.1
(Mier & Garcia, 2011)	Clair River Till	-	4.2*
Pike (2014)	Medway Creek Till – In-situ Moisture Content	7.9-8.3	8.1
	Medway Creek Till – In-situ Moisture Content with Abrasion	-	6.8*
	Medway Creek Till – Air Dried	0.9-1.2	1.1

*Only one test result reported

2.6.1 In-situ Jet-Tests

In-situ jet-testers are portable devices which submerge a small area of in-situ material (usually the bed or banks of a river) and subject it to a jet of water. These devices may quantify the erodibility of the material by either gradually increasing the jet velocity and recording the velocity at which the water becomes turbid (Tolhurst et al., 1999), or by applying a constant jet velocity and recording the scour depth once equilibrium is reached (Mazurek, 2010). The critical shear stress can then be calculated using either empirical or theoretical equations specific to the device being used. In-situ jet tests are typically easier to conduct than hydraulic flume tests because test set-up and duration is relatively short, and in-situ jet tests negate the difficulties of trying to collect and transport "intact" samples which maintain their in-situ properties (especially in the case of glacial till) to a lab. However, with in-situ jet testers the shear stress is applied to only a very small area which may not be representative depending on the homogeneity of the material and whether the material erodes through mass erosion (separation of larger chunks along planes of weakness, typical of glacial till) which is a process larger than the scale of the testing device. ASTM D5852-00 (2007) suggests

that this test should not be used for materials which erode through mass erosion. Furthermore, the applied shear stress at the threshold or equilibrium condition is measured indirectly, and some variability has been documented between methods used to determine the applied shear stress based on the jet and scour conditions (Mazurek, 2010).

In situ jet-testers have been used by Shugar et al. (2007) and Khan and Kostaschuk (2011) to measure the critical shear stress of glacial tills in southern Ontario. Shugar et al. performed 10 in-situ jet-tests at various locations along Fletcher's Creek and obtained values for critical shear stress which ranged from approximately 0.001 Pa to 20 Pa, with an average of 2.24 Pa. The author attributes this significant variability to variable erosion and weathering history amongst the tested locations. Khan and Kostaschuk conducted over 50 in situ jet tests on two distinct glacial tills located along Highland Creek and Fletcher's Creek (same reach as tested by Shugar et al.) at submerged and exposed locations. For the submerged Highland Creek till, Khan and Kostaschuk found that critical shear stresses varied from 17.5 Pa to 63.3 Pa, with an average of 38.7 Pa. The critical shear stress determined for the exposed till along the same reach ranged from 0.8 Pa to 1.6 Pa, with an average of 1.1 Pa. This suggests that weathering of exposed till can greatly reduce its critical shear stress. This distinction was less pronounced for the Fletcher's Creek till as the critical shear stress for the submerged till exhibited a wide range of critical shear stress values (0.01 Pa to 9.61 Pa). However, as Shugar et al. notes, this could be due to some history of subaerial exposure (caused by fluctuating water levels) at some of the test locations resulting in a significant reduction to critical shear stress values. Several unexposed areas along Fletcher's Creek were tested by removing some easily eroded overburden material. Of the six areas tested, most exhibited a relatively high critical shear stress greater than 10 Pa, while two values less than 1 Pa were also determined (possible that not all the weathered overburden material was removed). This again supports the idea that weathering can significantly reduce the critical shear stress of till material. In addition, Khan and Kostaschuk found that critical shear stress generally increases with increased fines (silt and clay) content, increased density, increased shear strength (used E-285 Pocket Vane Shear Tester), increased compressional strength, and increased depth from surface.

2.6.2 Hydraulic Flume Tests

Hydraulic flume tests can be used to determine erodibility parameters such as critical shear stress of a particular soil sample by subjecting it to a unidirectional current and resulting shear stress, similar to how one would be applied to the channel bed or banks of a river or channel. Chapter 2.2.2 describes how a current imparts a shear stress on a flow boundary. Most often the sample is placed in the bed of a flume such that the top of the sample is flush with the channel bed. The applied shear stress is gradually increased by increasing the channel slope or discharge until the initiation of erosion is identified. Most often flume tests are performed in a laboratory since hydraulic flumes are difficult to transport and set up. However, as noted, it can be challenging to obtain and transport intact cohesive sediment samples. As such, hydraulic flumes are sometimes installed in the field with an open bottom (Herrier et al., 2018; Debnath, 2007 as cited in Pike, 2014). To circumvent having to obtain and transport an intact sample, some researchers have attempted erosion experiments in hydraulic flumes using reconstituted or remoulded cohesive sediment samples. However, Lefebvre et al. (1985) notes that remoulded cohesive sediments are homogenized, eliminated structural effects present in intact sample such as planes of weakness (known to be present in glacial till) and that the necessity to obtain undisturbed samples should be emphasized.

Hydraulic flume tests have been used to estimate the erodibility of glacial tills by Kamphuis et al. (1990), Mier & Garcia (2011), and Pike (2014). In each study, mass erosion was observed with clasts or chunks of sediment breaking off once the critical shear stress is reached along discontinuities or planes of weakness. Although difficult to confirm, it is anticipated that additional planes of weakness could develop during the extraction and transportation process of a sample which could influence where and under what conditions a sample erodes (Pike, 2014). Kamphuis et al. collected four samples of undisturbed sediment (three clays and one clayey silty till) approximately one meter below the ground surface by forcing a rectangular cutting frame into the ground. The material was trimmed flush with each side of the frame such that a test could be performed on each exposed side (some difficulties were noted with the sampling and trimming of the till sample) and the samples were subjected to a unidirectional current (maintained in extraction frame). Critical shear stresses for the

till sample ranged from 0 Pa to 2 Pa. The author suggests the suspension of and abrasion by sand particles was a controlling factor for the initiation or erosion of the sediment samples, however the presence of sand was not shown to decrease the critical shear stress of the till sample.

Mier & Garcia (2011) obtained a block sample of glacial till from the St. Clair River bed in southern Ontario which was divided into smaller samples and subjected to various shear stresses in a unidirectional flume. Vertical velocity profiles were measured using a Laser Doppler Velocimiter (LDV) and the applied shear stresses at incipient erosion (critical shear stress) of 4.2 Pa was determined using the Log Law (equations (2-2) and (2-4)). Although there was considerable scatter, the authors found a linear relationship between the Particle Reynolds Number and the Shields Parameter at incipient erosion on the classic Shields diagram with their data and data from similar experiments conducted on cohesive sediments. This suggests that mean particle diameter and density can be important predictors of the critical shear stress for cohesive sediments, in addition to non-cohesive sediments. With more experiemental data, it is suggested that much of the scatter could be collapsed with a bulk density correction factor since critical shear stress tends to increase with increased bulk density.

Pike (2014) obtained four block samples of glacial till material along the bed of Medway Creek in southern Ontario. The samples were situated flush with the flume bed on an adjustable platform (sample could be raised to remain flush with the bed as it eroded) and subjected to various shear stresses in a unidirectional flume by changing the flow rate and slope. The shear stresses applied to the sample were determined using equation (*2-3*), assuming uniform flow and a uniform shear stress distribution. Based on the model proposed by Mirauda & Russo (2020), it is anticipated that the shear stress applied to the samples would have been slightly larger than the mean shear stress determined using equation (*2-3*). The samples were cut to fit the flume platform using a concrete masonry saw and were fully saturated through submergence prior to testing. It was noted that some submerged samples split when submerged, which was thought to be due to the samples drying. Shear stresses were increased every 15 minutes if no erosion was observed, as Pike notes that previous experiments have suggested that if erosion were to occur at a given shear stress, it would occur

early in the given time period. Four samples were tested at their in-situ moisture content (prior to submergence). Two of these samples were tested without abrasion and critical shear stresses of 7.9 Pa and 8.3 Pa were obtained; while the two samples tested with gravel abrasion (gravel continuously placed upstream of the sample and allowed to roll over the sample) exhibited critical shear stresses of 6.8 Pa and 4.3-6.1 Pa. The two remaining samples were allowed to air dry prior to submergence, which drastically reduced their critical shear compared to the other samples to 1.2 Pa and 0.9 Pa. The critical shear stress reduction due to weathering, or specifically drying prior to submergence, is consistent with other research and suggests that material subject to frequent wetting and drying cycles (e.g. the lower bank material) is more susceptible to erosion.

2.7 Softening / Weathering of Glacial Till and other Cohesive Sediments

Unlike non-cohesive sediments which depend only on the particle mass to resist erosion, cohesive sediments depend on the electrochemical bonds between particles. It is widely reported that environmental processes such as wetting and drying or freezing and thawing can greatly reduce the strength of these bonds, which can reduce the critical shear stress of a cohesive soil by several orders of magnitude (Pike, 2011; Khan and Kostaschuk, 2011). Sediments adjacent to a watercourse can be subjected to cyclic wetting and drying by rising and falling water levels, in addition to rainfall and local runoff. These processes affect only the portion of a channel that is not permanently saturated which typically includes a portion of the channel banks where local shear stresses are relatively low.

The moisture content at the time of freeze-up can impact the effect of the freezing soil-water on the soil structure. This process can affect any portion of the wetted perimeter of a channel which becomes frozen, but would be most impactful near the water level where saturation is the highest.

2.7.1 Slaking

Slaking has been defined by Moriwaki & Mitchell (2009) as “a disintegration of unconfined soil or rock after exposure to the air and subsequent immersion in a fluid” and by Chan & Mullins (1994) as “the process of fragmentation that occurs when

aggregates are suddenly immersed in, or placed in contact with, water". According to Mitchell & Soga (2005), the three mechanisms responsible for slaking are dispersion, swelling, and the compression of entrapped air, as outlined below. These are the driving forces which work to separate soil particles and act against the resisting cohesive forces discussed in Chapter 2.5. In addition, vegetation and organic matter can greatly reduce the effects of slaking by binding mineral particles together and by slowing the rate of wetting (McMullen, 2000).

Dispersion and swelling can contribute to slaking, however they can occur whether or not a soil is initially unsaturated and are typically discussed as separate phenomenon.

Dispersion: Dispersion is the process of clay particles spontaneously detaching from one another and going into suspension when immersed in a fluid (Mitchell & Soga, 2005). Soils that deflocculate easily without mechanical assistance in water with a low salt concentration are referred to as dispersive clays (ASTM, 2021). Dispersion of an initially unsaturated dispersive clay is referred to by many authors as a slaking mechanism, however dispersion would occur even if the sample was fully saturated.

Dispersive clays can be identified using either a crumb test (ASTM, 2021) or a pinhole test (ASTM, 2013). The crumb test is a qualitative test in which a cube of remoulded soil or a crumb of intact soil is submerged in distilled water. In almost all cases the soil will slake or break apart into smaller pieces. Dispersive clays can be distinguished by colloidal suspension of clay particles which form a cloud of turbid water surrounding the slaked sample, which are a result of electrostatic forces (Mitchell & Soga, 2005). Highly dispersive clays will form a very large cloud such that it is difficult to distinguish between the original crumb and the colloidal suspension.

As previously noted, Exchangeable Sodium Percentage (ESP, concentration of sodium cations relative to other cations) is a strong indicator of dispersive behaviour. Clay particles are negatively charged and attract positively charged cations in the soil-water such as sodium (Na^{+}), calcium (Ca^{2+}) or aluminium (Al^{3+}). A triple charged aluminium will neutralize three negative charges while a single charged sodium will only neutralize one. The cations surrounding a clay particle form what is referred to as its shell (Mitchell & Soga, 2005) and the combined negatively charged surface layer and positively charged cation layer is referred to as the diffuse double layer. Without

sufficient attractive forces between particles, they diffuse from one another, separating soil particles until the concentration of the cations within each shell is equivalent to the concentration of cations in the soil-water. The tendency of the soil particles to separate in order to reach this equilibrium is referred to as the double layer repulsive force. If the soil solution has more cations (higher dissolved salts), the cation shell around clay particles can be smaller and still have the same concentration of cations as soil-water. However, since more sodium ions are required to neutralize the negative charge on a clay particle relative to other cations, a larger portion of sodium cations (larger ESP) present in the pore water results in a larger cation shell and increased dispersion.

Swelling: Swelling is the increase in volume of a soil resulting from osmotic pressure. This pressure is caused by the concentration of salts in the soil-water trying to equalize. The negative charges on clay particles restrict the flow of salts within the soil water but do not restrict the flow of water in the same way. As a result, only water flows past a restriction to equalize the concentration of salts, which causes pressure differentials within the soil structure and can cause slaking (Mitchell & Soga, 2005). Tests have shown that swelling slaking is frequently observed with dispersion slaking and can also occur in soils which are fully saturated prior to submergence (Lim, 2006).

Compression of Entrapped Air: Compression of entrapped air occurs when water rapidly enters an unsaturated soil. The rapidly entering water quickly fills larger soil pores, compressing air into smaller soil pores before it has a chance to escape. The compressed air exerts tensile stress on the soil structure, which can be strong enough to break whatever bonds exist between soil particles. This mechanism is sometimes distinguished from swelling and dispersion and used to more narrowly define slaking by some authors (Chan & Mullins, 1994), since it is the only mechanism that occurs only when a soil is slaked (i.e. rapidly wetted from an unsaturated condition, other mechanisms occur regardless of initial condition).

Compression of entrapped air can cause both body slaking and surface slaking, which are two of the four qualitative slaking classifications in addition to dispersion slaking and swelling slaking (Mitchell & Soga, 2005). Body slaking causes a material to split apart into large pieces, appearing to develop from the inside out. Surface slaking

causes clay particles to "spall of the exposed surface of a soil and accumulate as fine sediment in adjacent water" (Mitchell & Soga, 2005).

As noted, this slaking mechanism only occurs if a soil is unsaturated prior to rapid wetting. Experiments by Lim (2006) found that the amount of slaking resulting from this mechanism was a function the degree of saturation prior to immersion, and suggests that this is one of the most important factors affecting the erosion of unsaturated non-dispersive soils.

Similarly, Chan and Mullins (1994) immersed samples with varying antecedent matric suction, prepared by subjecting them to various moisture conditions. Matric suction is the negative pressure which develops in a soil due to capillary forces. Matric suction was measured by sealing samples with filter papers and then measuring the water content of the filter papers, in a method similar to ASTM D5298-16 (2016). With the ASTM method, suction can be determined for a soil sample by sandwiching three filter papers between two identical soil specimens and allowing the suction to equilibrate over seven days. The water content of the centre filter paper is determined, which can then be used to estimate matric suction using a calibrated suction-water content curve for the filter paper. Chan and Mullins found that the rate of water uptake and slaking increased with increased matric suction. Since this mechanism of slaking is caused by the pressure differentials within the soil structure during wetting, it can be reasoned that matric suction could be a more direct measure of the driving force behind particle separation compared to initial water content.

2.7.2 Freeze/Thaw Process

The formation and propagation of ice through a soil is a complex process involving the interrelationships between the phase change of water to ice at different temperatures and pressures, osmotic pressures due to dissolved ions in the pore water, and the interfacial tension at the ice-water interface (Mitchell & Soga, 2005). From its densest state at 4^{o}C, water can expand eight percent of its original volume, therefore a fully saturated soil increases in volume by eight percent of its porosity. This increase in volume can separate particles, breaking the bonds between them, which increases its erodibility. The impacts of the freeze-thaw process have shown to increase with increased clay content, organic matter, and exchangeable sodium percentage.

Kimiaghalam (2016) found that for intact clay soils collected along the Red River, critical shear stress decreased by up to 80% after the first freeze-thaw cycle, and reached approximately zero after the fifth cycle. After 5 cycles, the soil structure became brittle, and without confining pressure the soil samples fell apart.

2.8 Lime Stabilization of Soils

Lime stabilization is a technique widely used on road and rail construction projects to increase the strength and workability of silty and clayey soils (Herrier et al., 2018). However, the application of this technique to increase the erosion-resistance of hydraulic earthen structures remains limited, despite having proven to be a durable, safe, and economical alternative to the use of conventional erosion protection (riprap) on several dam and dyke projects in the United States (USBR, 2013). Most notably, lime stabilization can effectively prevent softening (slaking) of many clay/silt sediments (Herrier et al., 2018).

2.8.1 Stabilization Process and Construction Procedures

Lime can be used to treat soils in the form of either quicklime (calcium oxide – CaO) or hydrated lime (calcium hydroxide – $Ca[OH]_2$) (National Lime Association, 2004). Quicklime is produced by heating pure limestone to temperatures between 1100-1200 °C, while hydrated lime is produced from quicklime by allowing it to react with water prior to application (Boudaghpour & Majdzadeh, 2014). Quicklime has a greater effect in soil due to its more concentrated calcium content, however, working with hydrated lime is much safer and its application is more common in construction.

Both short-term and long-term reactions occur when lime is added to moist close-textured soil (Boudaghpour & Majdzadeh, 2014). In the short-term, calcium cations displace sodium cations in the cation shell of clay particles, reducing the size of the cation shell, bringing clay particles closer together and allowing them to flocculate, counter-acting the effects of dispersion. Carbonation reactions also occur in the short term, whereby lime reacts with carbon dioxide in the water or atmosphere, reverting lime back to it's inert chemical form of limestone.

Longer term reactions produce cementitious bonds between soil particles when calcuim hydroxide react with pozzolans (siliceous or aluminous materials) in the soil to produce cementitious gels known as calcium silicate hydrate (CSH) and calcium

aluminate hydrate (CAH) (Boudaghpour & Majdzadeh, 2014). The strength of the bonds depends in part on the concentration of pozzolans in the soil (National Lime Association, 2004). If pozzolan concentrations are not sufficient, fly ash or ground blast furnace slag can be added. Since pozzolanic reactions are prefered to carbonation reactions for increased bond strength, it is important to quickly combine the lime with soil.

Typically, soils are stabilized with lime by first scarifying or pulverizing the soil, spreading the lime, adding water, mixing, compacting to a maximum practical density, and allowing to cure (National Lime Association, 2004). The lime rate (soil-lime proportion requirement) varies depending on the application and soil composition. Bell (1996) found the optimum lime percentage is typically between 1% and 3%, while Jelisic (2006) suggests a rate of 1% lime for every 10% clay in the soil. The USBR design standard for embankment dams (USBR, 2013) recommends 22.5 to 30 cm soil-cement thickness for the bed and banks of channels. In general, silty soils are more suitable than clayey soils for lime stabilization since a lower lime rate is required and lime can more easily and uniformly be incorporated into the soil.

2.8.2 Safety Considerations

Lime is an alkaline material and reacts with moisture, including moisture on/in human skin, eyes, and lungs. As such, workers must be properly trained and wear proper protective equipment. Quicklime is especially reactive with water and can cause an excessive amount of heat to be released which can ignite combustible materials (National Lime Association, 2004). Hydrated lime is less reactive but is a very fine powder which can blow in the wind as dust, rendering its use unsuitable for populated areas given the noted dangers above.

2.8.3 Environmental Considerations

In addition to its use as a soil stabilizer for engineering applications, lime is widely used in agriculture to improve soil workability, trafficability, and to prevent surface crusting (Graymont, 2022). Lime is also used in environmental remediation for the treatment of soils contaminated with heavy metals and other hazardous waste. Since lime that has not reacted with pozzolans will eventually revert to the inert chemical form of limestone by reacting with carbon dioxide in the air or water, long term environmental

impacts are not anticipated. A temporary change in soil pH is considered the most significant toxic effect of hydrated lime (European Union, 2016).Tests have shown that soil pH returns to normal levels within one week of application at all concentrations up to 4.4 g/kg.

2.8.4 Economic Considerations

The use of lime stabilization for erosion protection applications should be weighed against conventional riprap erosion protection. In most cases, riprap remains the most economical alternative (USBR, 2013). However, since lime stabilization requires much less non-native material than riprap erosion protection, soil-cement may be a viable alternative depending on haul distance and project scale. The USBR Earth Manual (U.S. Department of the Interior, 1998) recommends that soil stabilization be considered as an alternative slope protection method to riprap if the haul distance to the rock source exceeds 32 km. Furthermore, lime-stabilized channel lining has a lower Manning's roughness compared to riprap or gravel lining, allowing for increased hydraulic capacity at the same cross-sectional area (Herrier et al., 2018).

2.8.5 Testimonials

While the principals of lime treatment are rarely applied for the purposes of erosion protection, several successful examples exist. The US Bureau of Reclamation chose to rehabilitate several areas of the Friant-Kern Canal in Fresno California by compacting native clayey soil treated with 4% quicklime (Herrier et al., 2013). This method was found to be significantly more economical and required less maintenance after 40 years of use than alternatives used in other sections of the channel. In fact, sheepfoot roller imprints were still visible along the channel banks both above and below the normal water level. Lime stabilization has also been used to repair more than 150 embankment failures along the Mississippi River levees by excavating the failed expansive clay, treating with 5% hydrated lime, and recompacting it in the failed area. Topsoil and fertilizer were then placed on top, completing the restoration and adding another layer of protection.

Lime stabilization has also been used for protecting the upstream face of dam embankments, including the Merritt, Palmetto Bend, Choke Canyon, and Virginia Smith Dams, as well as at the Warren H. Reservoir, all location in the United States (USBR,

2013). USBR also identified several other instances where it is anticipated that soil stabilization would have been more economical than the installed riprap protection, particularly at locations with long haul distances.

Chapter 3: Methodology

3.1 Introduction

To improve the understanding of glacial till erodibility and the impacts of slaking, intact glacial till samples were obtained from a quarry site near St. Laurent, Manitoba and along the banks of the Lake St. Martin Emergency Outlet Channel (LSMEOC). These samples were then subjected to various slaking and erosion tests at the University of Manitoba.

3.2 Field Reconnaissance

Two rounds of field reconnaissance were conducted in areas expected to have similar material to that through which the Lake Manitoba and Lake St. Martin outlet channels will be built. The first round of field reconnaissance was conducted at a quarry site located approximately 7 km southeast of St. Laurent. The second round was conducted along Reach 1 of the LSMEOC and a nearby quarry, as shown on Figure 10.

At both sites, the state of the glacial till encountered could generally be categorized as either intact (observed at various moisture contents), weathered and wet, or weathered and dry. Weathered wet till was easily identified since it was softened and in a fluid-like state. However, it was more difficult to differentiate between the intact (unweathered) till and the weathered, dry till. Weathered and dry till can appear as hard as intact till, since it is held together by apparent cohesion (caused by surface tension in unsaturated soils). However, when the weathered and dry till becomes saturated, it quickly softens and loses its structural integrity. To differentiate between the intact till and the weathered and dry till without needing to wet it, the till was broken up with a pickaxe and the crumbled material was observed. Material that broke up into very small pieces was assumed to be weathered, while material that maintained itself in larger aggregates or clasts (> 25 mm diameter) was assumed to be intact.

3.2.1 St. Laurent Quarry Site

The first round of field reconnaissance was conducted at a quarry site near St. Laurent on October 15th, October 16th, and November 3rd of 2020. The quarry site is located approximately 100 km southeast of the Lake Manitoba Outlet Channel and 160 km south of the Lake St. Martin Outlet Channel (LSMOC). The field reconnaissance

included sample collection and critical shear stress testing using a Cohesive Strength Meter (CSM).

3.2.1.1 Sample Collection

Both grab samples (loose earth) and intact samples (in-situ density and structure) were collected at this site. As noted in Chapter 2.6, erodibility testing using intact samples is far superior to testing using samples reconstituted (remoulded) from grab samples, because the remoulding process homogenizes the sample and eliminates the structural features present in glacial till (such as planes of weakness developed through glacial processes). However, grab samples are much easier to collect and can still be used to obtain various material properties which may be indicative of erodibility.

Typically, intact cohesive sediment samples are collected by pushing a cylindrical metal Shelby tube into undisturbed material using a geotechnical drill rig. Due to time and cost constraints, a geotechnical drill rig was not available for sample collection. As such, a manual Shelby tube hammer and guide (shown on Figure 7) was obtained from Maple Leaf Drilling and used to push the Shelby tubes. With this method, the guide is attached to the top (non-bevelled) end of the Shelby tube with bolts. The 32 kg hammer is then slid over top of the guide and hammered against the strike plate to push the tube into the dense till material until the steel begins to yield where it is attached to the bolts, at shown in Figure 7. The hammer is then removed and the Shelby tube and guide are extracted using a farm jack to push against the underside of the strike plate. Collecting samples this way takes approximately 15 minutes and requires two people.

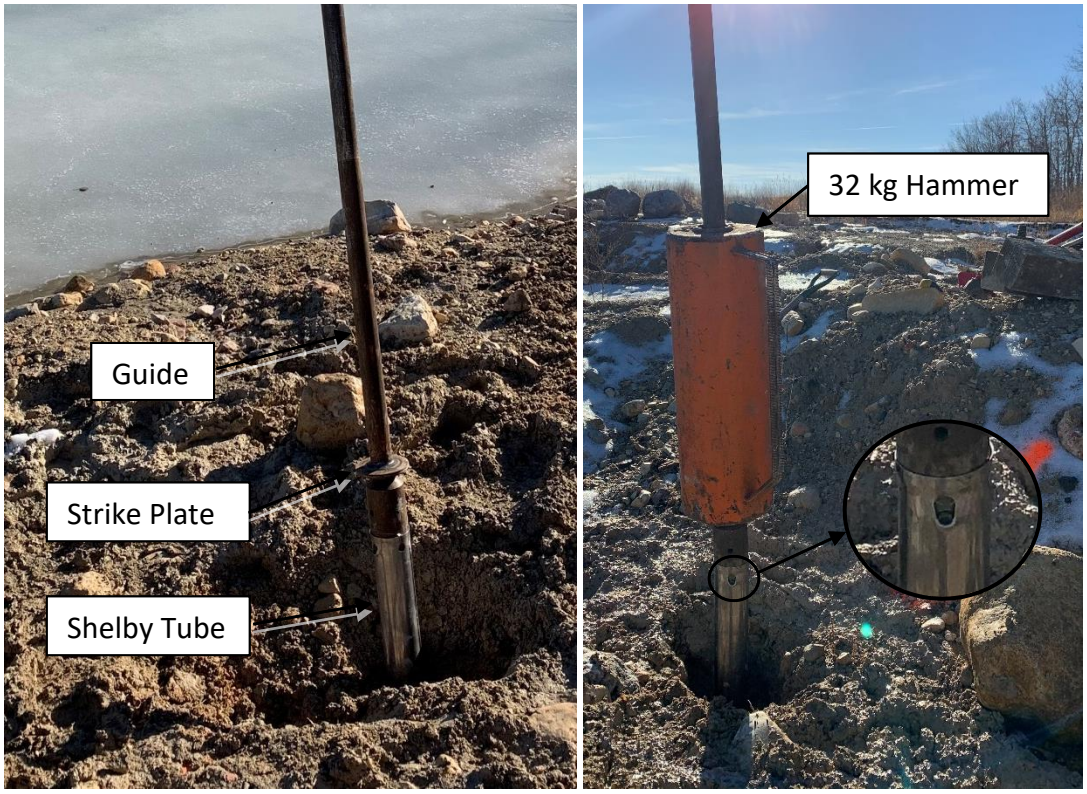

Figure 7: Shelby tube with guide attached (left) and Shelby tube with guide attached and hammer (right), showing yielded steel at holes

Since glacial till can contain gravel, cobbles or boulders in addition to finer cohesive material, when the bevelled edges of the cylinder are pushed into a large enough rock, the rock may cause the end of the tube to deform, stopping the tube from being pushed farther and compromising at least a portion of the sample, as shown in Figure 8. Yielding of the steel at the bolts provided a good indication of when the ends of the tube were becoming deformed and intact sample was no longer being pushed up into the Shelby tube. Since there was no way of knowing the depth at which the Shelby tube would encounter a rock at a given sample location, the depth of sample collected or, whether any intact sample was collected at all, was highly variable. For example, on the November 4th trip to the quarry site, only one of four attempts using this method resulted in an intact sample. In unsuccessful cases, the Shelby tube could be pushed to a reasonable d^{ep}th, but when the sample was extracted, the material inside had crumbled. It is anticipated that this could have resulted from a rock being pushed into the sample instead of stopping the tube from being pushed altogether, or from the vibration resulting from the hammer strikes. While some samples did not show any signs of crumbling and appeared to remain completely intact within the Shelby tube, it

is possible that the vibration of the hammer may still have exacerbated existing planes of weakness or caused new ones. Therefore, samples extracted in this way can be considered a conservative representation of the in-situ material when assessing its erodibility.

Figure 8: Deformed bevelled (bottom) edge of Shelby tube after sample extraction

Other methods of obtaining intact samples were attempted with limited success. A hammer drill was used to dislodge large irregular chunks of intact sample. However, without any confining pressure, these chunks would often crumble under their own weight either immediately or during handling and transport.

Additionally, the use of a concrete coring machine to collect cylindrical samples (similar to Shelby tube samples) was attempted. With this method, the cutting edge of the core barrel was able to cut through any rocks which may be encountered and a core of intact material could be collected within the core barrel, however it was not possible to remove the sample from the core barrel without destroying it.

3.2.1.2 Cohesive Strength Meter Testing

A Cohesive Strength Meter (CSM), a type of in-situ jet-tester (see Chapter 2.6.1), was used in an attempt to quantify the erodibility of the glacial till at the St. Laurent quarry site. The CSM was obtained by KGS Group from Université du Québec à Rimouski. It

works by applying a jet of water to in-situ material within a small test chamber which is filled with water prior to testing (Tolhurst et al., 1999). The test chamber contains infrared optics which measure the transmissivity of the water within the test chamber. The CSM is pre-programmed to apply increasing jet pressures while recording the transmissivity. Once the jet pressure is enough to cause sediment to go into suspension, the infrared optics detect a drop in transmissivity and the corresponding eroding jet pressure is recorded. The general components of the CSM are shown on Figure 9, while a more detailed overview of the device can be found in Tolhurst et al. (1999).

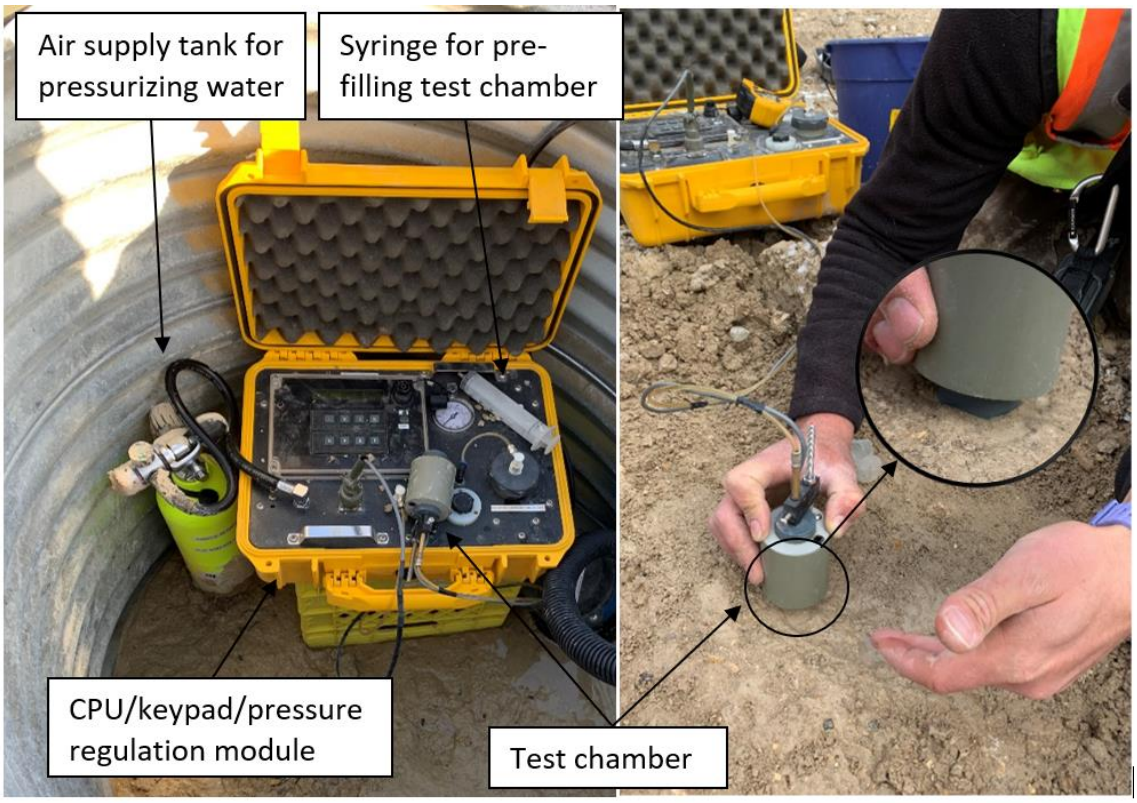

Figure 9: CSM used in dewatered area (left) and dry area (right) at St. Laurent quarry site

In addition to the general limitations of in-situ jet testers (see Chapter 2.6.1), the key limitation for this application was that the bottom/inner rim of the test chamber could not be inserted into either intact till or weathered and dry till, as it is intended. This prevents the test chamber from filling with water, such that a reduction in transmissivity cannot be observed by the infrared sensor, invalidating the test. Various methods of sealing the test chamber to the ground surface were attempted with no success. As such, the device was used to measure only the weathered and wet till.

Tolhurst et al (1999) determined an empirical relationship between the eroding jet pressure and the equivalent horizontal shear stress applied which takes the form of the following equation:

$$\tau_O = A1 \times \left[1 - e^{-x/t1}\right] + A2 \times \left[1 - e^{-x/t2}\right] \quad (3\text{-}1)$$

Where τ_O is the equivalent horizontal shear stress (Nm^{-2}), x is the eroding pressure (kPa), $A1$ is a constant (67), $A2$ is a constant (-195), $t1$ is a constant (310), and $t2$ is a constant (1623). This relationship was used to estimate the critical shear stress of the wet and weathered till.

3.2.2 Lake St. Martin Emergency Outlet Channel – Reach 1

A second round of field reconnaissance was conducted near the LSMOC alignment between November 1st and November 4thof 2021, mainly along Reach 1 of the Lake St. Martin Emergency Outlet Channel. This work included a more comprehensive series of sample collection, as well as some general site observations.

3.2.2.1 Sample Collection

Shelby tube samples were collected at seven locations along Reach 1 of the emergency channel and at a quarry site located approximately 4.5 km southeast of the channel, as shown in Figure 10 and summarized in Table 2. At each location, at least two duplicate Shelby tube samples were collected, along with several kilograms of grab sample. Shelby tube samples were collected using the same manual hammer method used at the St. Laurent quarry site, as described in Chapter 3.2.1.1. With this method, 20 of 28 attempts (71%) yielded at least some intact sample, a higher success rate than at the St. Laurent quarry site.

At most locations along Reach 1, a relatively distinct transition from the dry and weathered till to the intact till could be observed at some depth from the exposed channel banks (0.075 m to 0.450 m) based on how it crumbled (intact till maintained itself in clasts while weathered till broke up into individual aggregates). Unfortunately, it could not be concluded how much of the upper layer of material was weakened due to weathering, or due to construction activities (i.e. broken up during construction and left packed in place). The majority of samples were collected from the unexposed lower layer of till expected to be intact, however several samples were also collected without removing any overburden material.

In addition to Shelby tube samples, grab samples of material surrounding the extracted tubes were also collected at each sample location.

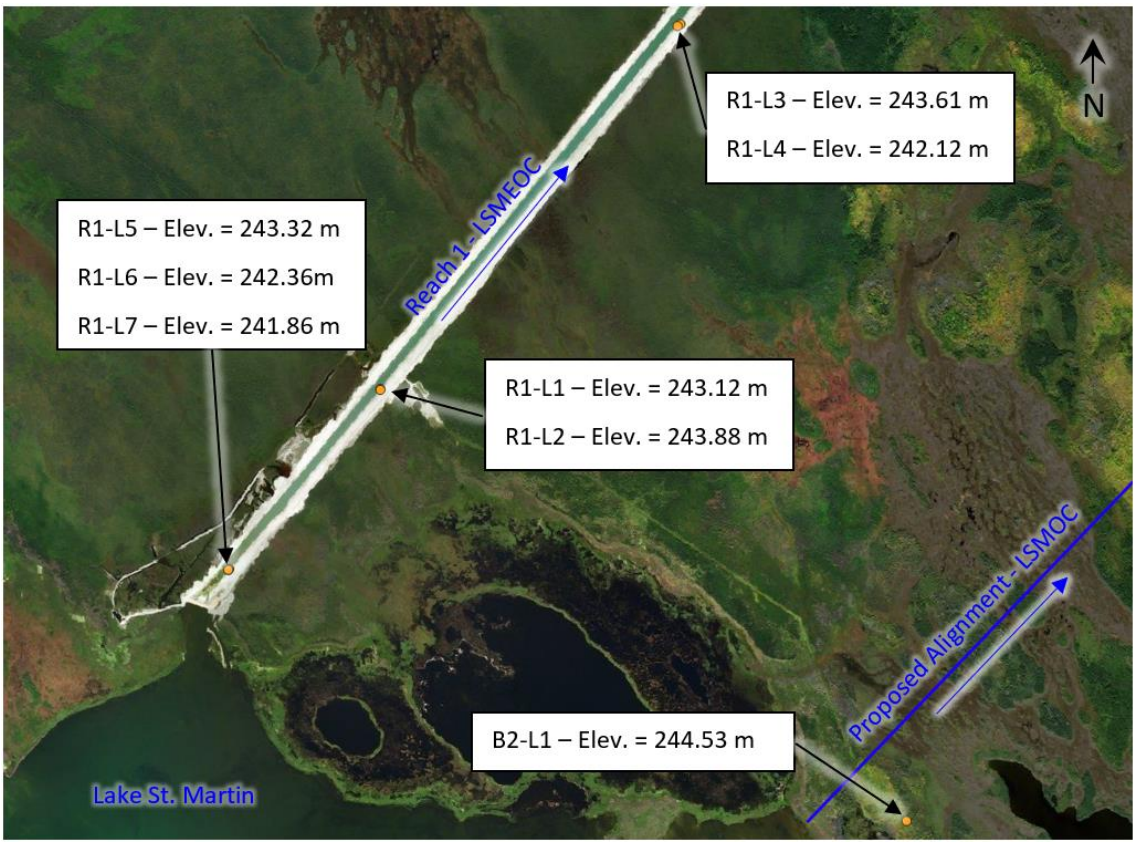

Figure 10: Phase 2 sample locations relative to existing and proposed channels

Table 2: Phase 2 sample summary

Sample Location ID	Location Description	Northing (m)	Easting (m)	Elevation (m)	Overburden (m)
B2-1	Borrow Pit near proposed channel	5738315	557741	244.53	0.35
R1-1*	Reach 1 - Near access road - lower/mid bank	5740992	554477	243.12	0.10
R1-2*	Reach 1 - Near access road - upper/mid bank	5740987	554478	243.88	0.15
R1-3	Reach 1 - Near Outlet - upper/mid bank	5743252	556337	243.61	0.05
R1-4	Reach 1 - Near Outlet - lower bank	5743242	556318	242.12	0.28
R1-5**	Reach 1 - Near Inlet - Upper Bank	5739875	553538	243.32	0.45
R1-6**	Reach 1 - Near Inlet - mid bank	5739868	553534	242.36	0.35
R1-7**	Reach 1 - Near Inlet- lower bank	5739868	553534	241.86	0.38

*Grab sample of overburden material collected in addition to grab sample at depth
**Shelby tube sample of overburden material collected in addition to Shelby tube sample at depth
Note: Reach 1 LSMEOC water surface elevation = 241.795 m

Figure 11: Shelby tube sample extraction near inlet of LSMEOC

3.2.2.2 Site Observations

As shown on Figure 10, the samples were collected at various locations and elevations within the vicinity of the proposed alignment of the LSMOC. It was immediately apparent from visiting Reach 1 of the LSMEOC that vegetation could not establish itself naturally on the exposed glacial till banks of the channel (Figure 12). It is understood that vegetation will be established on the banks of the proposed channel by mixing the existing till with locally sourced peat then seeding with native grasses. As previously noted, plant root systems are known to reduce the effects of slaking and a successfully established vegetation layer could help reduce the erodibility of the channel banks.

Furthermore, very large rills and gullies were observed along the banks of the emergency channel. These are formed as a result of local rainfall and runoff as it drains towards the channel, particularly at locations where a relatively large top-of-bank area flows toward a single point (overbank consists of a large flat area, sloped gradually toward the channel). Since slaking can be very dependent on the rate of wetting; which would likely be more rapid if resulting from rainfall-induced overland flow channelized into rills than from a rising water level within the channel, it is reasonable to expect that unvegetated channel slopes would be very susceptible to this form of erosion. Rill and gully erosion are not a focus of this paper, but are important considerations for channel design, particularly if the channel banks will not be

vegetated for a period of time. Photos of the rills and gullies observed during the field reconnaissance are provided on Figure 13.

Figure 12: Rill erosion along banks of LSMEOC (person is 1.94 m tall)

3.3 Preparation of Intact Shelby Tube "Puck" Samples

Of the various methods attempted, the manual Shelby tube hammer was most successful in obtaining intact samples. In order to fit the samples into the experimental apparatus (discussed later in Chapter 3.8.2), Shelby tubes were cut into 50 mm lengths referred to as "puck" samples. The "puck" samples were cut from the extracted Shelby tubes using a chop saw with a masonry blade, as shown in Figure 13. Sharp edges of the puck samples were smoothened using a bench grinder and the samples were sealed using Shelby tube caps to prevent moisture loss prior to testing. Cutting the Shelby tube samples to length without extruding them from the Shelby tube preserved the in-situ lateral confining pressure acting on the samples. It was anticipated that the heat from the masonry blade caused some moisture loss of each sample due to evaporation, however this was not quantified. These samples were used for the majority of erosion and slaking tests.

Figure 13: Shelby tube being cut by chop saw with masonry blade and jig for cutting 50 mm lengths

3.4 Slaking Observation Procedure

Slaking, defined as "a disintegration of unconfined rock or soil after exposure to the air and subsequent immersion in a fluid" (Moriwaki & Mitchell, 2009), is an easily observable phenomenon, but can be challenging to quantify. The following methods were used to assess the degree of slaking having occurred to a given Shelby tube puck sample immersed in water:

1. A ruler or point gauge was used to measure the height of sample expansion, as shown in Figure 32. In general, samples which were more thoroughly disintegrated tended to have an increased expansion height.
2. A pocket penetrometer was used to the measure compressive strength of slaked sample surfaces. The pocket penetrometer used indicates the compression being applied to a sample in kg/cm^2 (from 0 to 4.5) and is to be recorded when the probe end of the device is inserted by 6 mm (shown as a line on the device). For most slaked samples, the device could be inserted by 6 mm without registering any compressive force being applied to the sample. Conversely, for most samples which were not slaked, the maximum compressive force of 4.5 kg/cm^2 could be applied with minor or no observable indentation (less than 6 mm).

3. Slaked material was removed by “hand brushing” loose material from the sample. In most cases, a distinct transition was observed between the loose and relatively hard material. The maximum depth of loose material removed was measured with a point gauge or ruler.
4. Finally, in some cases a pocket penetrometer was also used to measure the compressive strength of the remaining, relatively unslaked sample after the loose material was removed.

3.5 Increasing and Decreasing Initial Moisture Content of Puck Samples

Since initial observations and previous experiments conducted by others suggest that the amount of slaking due to the compression of entrapped air is a function of moisture content prior to immersion in water, it was necessary to increase and decrease sample moisture content prior to slaking tests. To increase their moisture content, samples were saturated through capillary rise.. To do this, samples were placed on a tray which maintained a water level equivalent to the height of the tray sides. A submersible electric pump continuously supplied a low flow rate to the tray, where water then either evaporated, entered the sample, or spilled over the edges of the tray into the basin below and was allowed to recirculate through the pump. Due to the reduced rate of water intake, this method did not cause the samples to slake as they often would have if submerged directly in water.

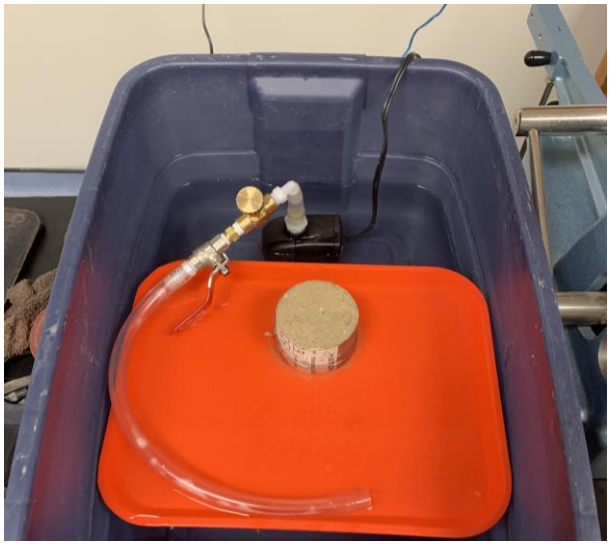

Figure 14: Tray with constant water level for saturating samples via capillary rise

To decrease the initial moisture content of puck samples, samples were exposed to the air and allowed to dry for various periods of time. Samples were repeatedly weighed over time to determine the mass of moisture lost. Once the desired moisture loss was reached, samples were sealed for a minimum of one week to allow the moisture content to equilibrate throughout the sample. Figure 15 shows the weight of an air-drying sample (one side sealed) over time, which was used for planning subsequent tests.

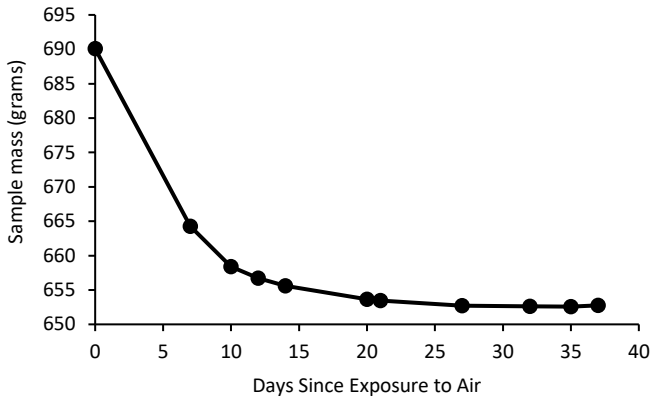

Figure 15: Shelby tube puck sample weight over time (one side sealed)

3.6 Reconstituting Puck Samples

Several puck samples were reconstituted (remoulded) to observe the effects of the in-situ soil structure and long-term bond development within the in-situ soil matrix, as the reconstituted samples would be homogenized and long-term bonds would not be present. Reconstituted samples were prepared by oven-drying grab sample material, breaking it up into individual particles, combining with water (consistent with the in-situ moisture content), then compressed using a hydraulic press until the in-situ density was reached. Samples were left in the press for a minimum of five minutes to allow pore water pressure to dissipate (pressure gauge on hydraulic press read significantly less after five minutes).

3.7 Reconstituting Puck Samples with Hydrated Lime

A total of four Shelby tube puck samples were reconstituted with hydrated lime added to investigate the effectiveness of lime stabilization. As previously discussed, hydrated lime stabilizes soils by forming cementitious bonds between soil particles similar to those that exist naturally, but to a greater degree. Grab samples of till obtained from

the St. Laurent Quarry and from along the proposed LSMOC alignment (3.6 m depth, obtained from KGS Group) were reconstituted to form Shelby tube puck samples at both a 2% and 4% lime content. The lime reconstitution and stabilization procedure was based in part on that described in National Lime Association (2006). This procedure recommends that the optimum lime content be determined using ASTM D627 (ASTM, 2019) 6. Instead, 2% and 4% lime content were selected since they are values typically used in practice (Bell, 1996; Herrier et al., 2013). The procedure also recommends that samples be compacted at 2%-3% above their optimum moisture content, as determined using ASTM D698 (ASTM, 2021). Samples were instead compacted to a target dry density of 2125 kg/m^3 (consistent with typical in-situ dry densities determined for St. Laurent and LSMEOC till) and at a moisture content of 10% (approximately 2% greater than moisture content known to provide good compaction based on previous tests). Samples were then sealed and allowed to cure for seven days before being saturated using the capillary tray for two weeks, consistent with the outlined procedures. It is anticipated that more strictly adhering to the procedures outlined by the National Lime Association would have resulted in a further increase to stability.

3.8 Hydraulic Flume Testing

3.8.1 Variable Slope Flume Overview

A variable slope flume, located in the University of Manitoba's Hydraulic Research & Testing Facility (HRTF), was used to apply increasing hydraulic shear stresses to sediment samples in order to determine their critical shear stress. The HRTF has a recirculating flow system which draws water from an underground cistern using one or two electric pumps (only the 75-horsepower pump was operational for these experiments) to a constant head tank. The constant head tank maintains its constant hydraulic head with a series of weirs which continuously return water exceeding this constant level to the underground cistern. Water is distributed to the various flumes in the lab through 350 mm diameter PVC pipes and eventually returns to the cistern through the lab's collection channels.

The flume's base and structural components are of steel construction, while the channel side walls are made of glass to allow observation of flow and erosion within

the flume. The base width of the flume is 0.94 m and its total length (from headwater tank to downstream gate) is 13 m. Flow through the distribution pipe from the constant head tank is regulated using a manually operated gate valve and measured using a digital flow gauge. Pipe flow from the distribution pipe transitions to open channel flow in the headwater box located at the upstream end of the flume. A vertical curtain style tailwater gate is located at the downstream end of the flume and allows the downstream water level to be adjusted to a desired level. A hydraulic jack located at the upstream end of the flume, and a fulcrum located near the downstream end of the flume, allow the flume slope to be adjusted between 0.2% and 2.0%. The basic components of the flume are labelled in Figure 16, while the headwater box and tailwater gate are shown in more detail in Figure 17.

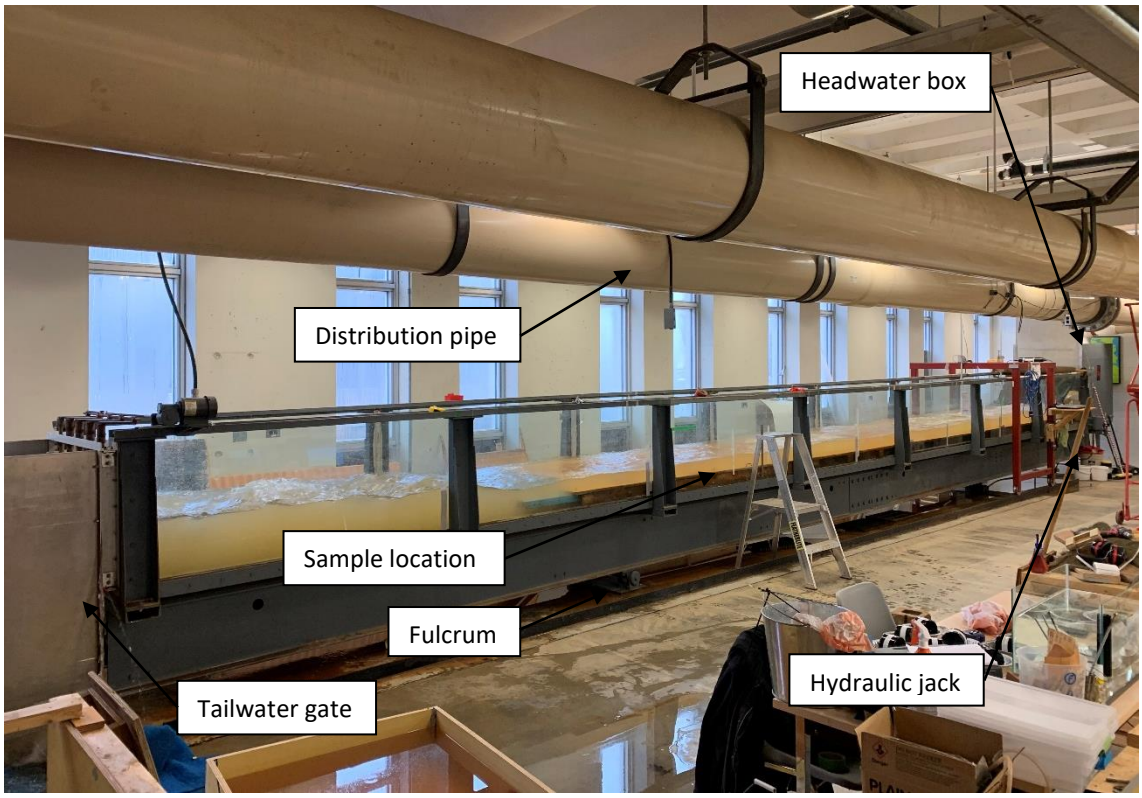

Figure 16: Variable slope flume located in the University of Manitoba Hydraulic Research and Testing Facility

Figure 17: Variable slope flume headwater box (left) and tailwater gate (right)

3.8.2 Design and Construction of Modifications to Variable Slope Flume

Applying a hydraulic shear stress test to a soil sample in a similar manner to how it would be applied to a channel bed requires that the eroding surface of the sample be flush with the bed of the flume. This allows a consistent vertical velocity profile to develop along the flume bed and persist through the samples. To avoid having to permanently modify the variable slope flume bed, a sub-floor was constructed and installed through most of the flume such that a sample could be inset and situated flush with its surface.

The subfloor consists of High Density Overlay (HDO) plywood and is supported by short segments of 37.5 mm by 87.5 mm dimensional lumber. Attaching the subfloor to the flume would require permanent modifications to the flume bed which could cause leaking. Therefore, a combination of C-channel girders affixed to the underside of the subfloor and steel plates placed on top of the subfloor were used to resist the buoyancy and lift forces acting on the subfloor, thereby keeping it stationary.

Figure 18: Subfloor HDO panels and C-channel girders (attached for weight) pictured during construction

A 0.74 m long segment of the subfloor located 7.75 m downstream of the headwater box was constructed as a removable and interchangeable panel. Two panels were constructed, one capable of housing a 300 mm by 300 mm by 50 mm reconstituted block sample and one capable of housing twelve 75 mm by 55 mm Shelby tube "puck" samples, described in the following Chapter. The panels are shown in Figure 19.

Figure 19: Reconstituted block sample panel (left) and Shelby tube "puck" sample panel (right)

3.8.3 Varying the Applied Shear Stress

Incrementally increasing shear stresses were applied to the samples at integer values between 2 Pa and 17 Pa for a duration of one hour by changing the discharge, slope, and tailwater gate setting. For simplicity, the discharge/slope/tailwater gate configurations selected aimed to establish uniform flow such that equation (*2-1*) could be used to determine the basic flow characteristics, and equation (*2-3*) could be used to determine the average shear stress applied to the wetted perimeter of the flume. The shear stresses applied to the central 70% of the flume bed (where samples were situated) was approximated as 1.1 times the average shear stressed, based on the review of experimental data conducted by Mirauda & Russo (2020), discussed in Chapter 2.2.2. Table 3 describes the discharge and slope combinations used to apply the various shear stresses to the flume bed for the majority of experiments. The flume slope was set such that flow depths were greater than 8 cm and discharges did not exceed the 250 l/s, which is the maximum output of the 75-horsepower pump. Once these were established, the tailwater gate was adjusted until the flow depth throughout the flume was approximately equal to normal depth and the uniform flow assumption was valid. Samples were covered with a thin acrylic sheet while the desired conditions were being established which was then removed to initiate the test.

Table 3: Applied shear stress conditions

Shear Stress Applied to Central 70% of Flume Bed (Pa)	Average Shear Stress Applied to Wetted Perimeter (Pa)	Flume Slope	Discharge (l/s)	Normal Depth (m)
2.0	1.8	0.2%	83	0.116
4.0	3.6	0.5%	86	0.088
6.0	5.4	0.5%	183	0.145
8.0	7.3	1.0%	122	0.088
9.0	8.2	1.0%	153	0.102
10.0	9.1	1.0%	184	0.115
11.0	10.0	1.0%	222	0.130
12.0	10.9	1.5%	149	0.088
13.0	11.8	1.5%	173	0.097
14.0	12.7	1.5%	199	0.106
15.0	13.6	1.5%	229	0.116
16.0	14.5	2.0%	172	0.088
17.0	15.4	2.0%	194	0.097

A Manning's roughness coefficient of 0.012 was used to represent the smooth bed and side walls of the flume for the normal depth calculations, which is consistent with that used by Peters (2015) at the University of Manitoba HRTF with a similar physical model configuration.

3.8.4 Validation of Applied Shear Stress Using ADV

Eleven applied shear stress conditions between 3 Pa and 13 Pa were validated using a Nortek Vectrino II profiling acoustic Doppler velocimeter (ADV). The ADV was used to measure the vertical profile of streamwise velocity near the flume bed at the sample location. The ADV was mounted to a point gauge allowing it to be positioned at varying distances to the flume subfloor, and attached to a rigid frame, as shown in Figure 20 below. Matlab programs adapted from those used in Durand (2014) were used for post-processing by removing bad cells and de-spiking and compiling the data.

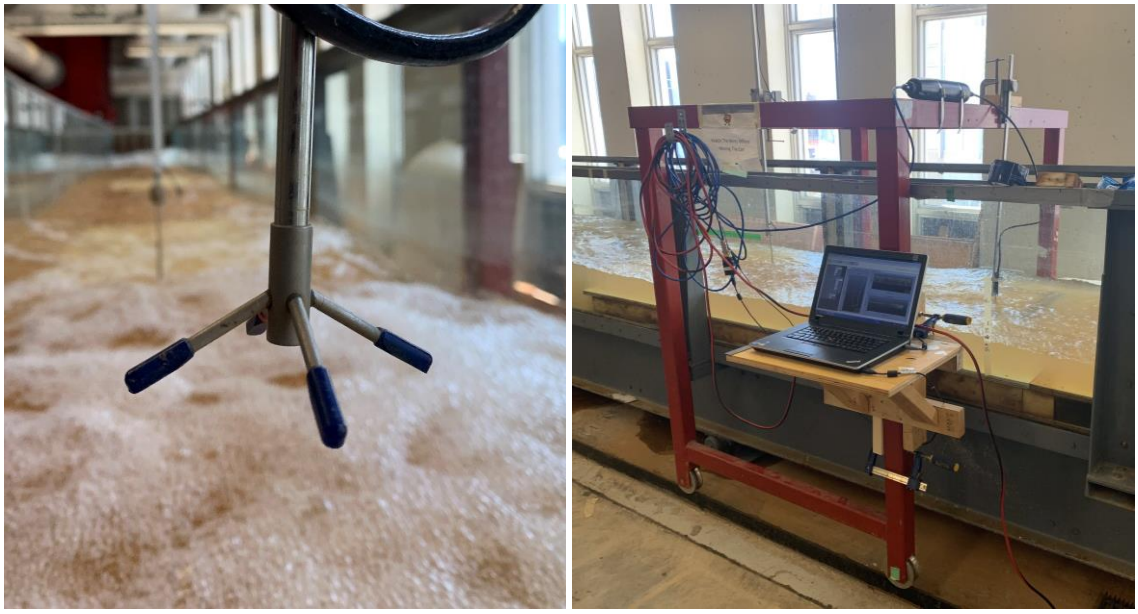

Figure 20: ADV transducer (left) and transducer mounted to point gauge and movable frame with laptop for recording data (right)

The velocity profile was measured in terms of average streamwise velocity at a point ($\bar{u}$) and the corresponding distance from the flume bed (y), which were then converted to a dimensionless velocity (u_+) and dimensionless distance from bed (y_+) using equations (*3-2*) and (*3-3*), respectively.

$$u_+ = \frac{\bar{u}}{u_*} \tag{3-2}$$

$$y_+ = \frac{y u_*}{v} \tag{3-3}$$

Where u_* is the shear velocity and v is the kinematic viscosity.

The log-law (equation (*2-2*)) can also be expressed in terms of u_+ and y_+ as follows:

$$u_+ = \frac{1}{\kappa}\ln(y_+) + 5 - \Delta B \tag{3-4}$$

Where κ is the von Karman constant (0.41) and ΔB is the roughness shift.

The measured dimensionless velocity data and the theoretical log-law (equation (*4-4)*) were then plotted in semi-log space and values for u_* and ΔB (fitting parameters) which result in a good fit between the measured data and the theoretical relationship were determined. The applied shear stress was then calculated based on the fitted value for u_* using equation (*2-4*). It was found that velocity measurements taken

between 7% and 25% of the total depth from the bed provided a reasonable fit to the theoretical log-law once the appropriate fitting parameters were determined.

Figure 21 provides an example of the measured and theoretical relationships between y_+ and u_+ for one of the validated shear stress conditions. For this example, the shear stress applied to the centre 70% of the bed was approximated as 9.3 Pa (determined by multiplying the average shear stress by 1.1, per Mirauda & Russo (2020)). Fitting parameters u_* and ΔB were optimized using Excel Solver by minimizing the sum of the squared differences between measured and theoretical values for u_+ between 7% and 25% of the total depth from the bed. The resulting applied shear stress at the sample location was then determined using equation (2-4) to be 9.4 Pa . This close agreement suggests that bed shear stresses determined by multiplying the average shear stresses by 1.1 provide a reasonable approximation of the actual applied shear stress.

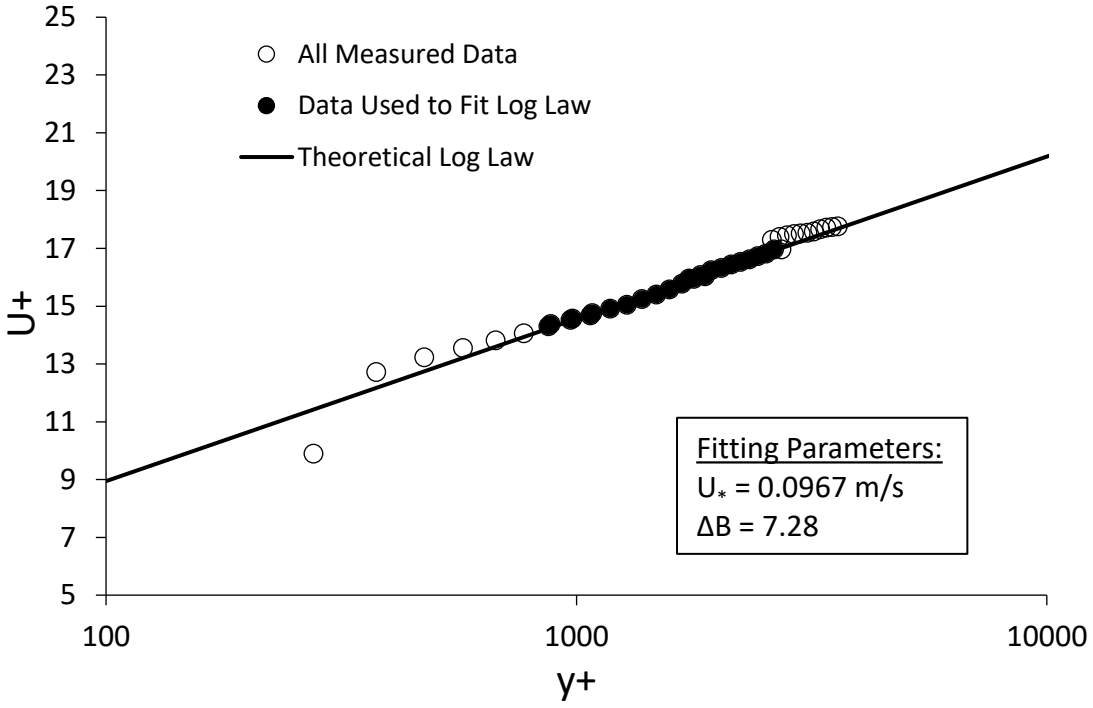

Figure 21: Measured and theoretical relationship between dimensionless velocity (u^+) and dimensionless distance from bed (y^+) under 9.3 Pa applied shear stress condition

3.8.5 Quantifying Erosion

Typically, erosion is quantified as either mass or volume of sediment over time, referred to as the erosion rate. A recirculating unidirectional flume known as the Erosion Measurement Device (EMD) was designed and built at the University of Manitoba and used by Kimiaghalam (2016) and Jianfar (2014) to define a relationship

between applied shear stress and erosion rate. This device used a screw jack system to extrude a Shelby tube sample up through the bottom of the flume such that it could continuously be made flush with the flume bed as the sample eroded. The rate that the top of the sample eroded, expressed in terms of distance over time, was converted to a volume or mass over time.

For several reasons, it was anticipated that this device would not be as effective for quantifying glacial till erosion. Firstly, it was predicted that the screw jack system would be unable to extrude the till samples due to their high density and the resulting side wall friction. Without being able to extrude the sample, as the sample erodes its exposed surface becomes lower than the flume bed and the shear stress being applied to the depressed soil surface would no longer be equivalent to the shear stress applied to the flume bed (the desired, known shear stress). Additionally, glacial till is known to erode in larger clasts along planes of weakness, which would result in an irregular eroding surface and would make quantifying erosion in terms of distance over time less practical.

Instead, erosion was quantified based on the area of the sample surface eroded after each applied shear stress increment. This ensures that only erosion occurring along the plane flush with the flume bed (where applied shear stresses are known) is quantified. Since the till contains large, visible aggregates and often erodes as larger clasts, the eroded areas could usually be easily identified in photographs.

Photographs were taken prior to testing and after each applied shear stress increment using a smartphone. For most tests (all LSMOC till), the smartphone was situated on a mount which allowed photos to be taken at a consistent height and angle (normal to surface). Mount locations were traced onto the sample panel (Figure 19) which allowed for a relatively consistent frame for each photo. For most tests, a second series of photos was taken at each shear stress increment after a diluted water-based paint was sprayed on each sample surface, as shown in Figure 22. This effectively highlighted any depressions/pitting in the sample surface which may not have been obvious in the unpainted photos. Ultimately, both sets of photos (painted and unpainted), were used to determine the eroded areas after each shear stress increment. The eroded areas were delineated in QGIS along with the total area of the

specimen (excluding the area covered by the smudged metal Shelby tube side wall which sometimes occurred) and the eroded area as a portion of the total area was then calculated for each shear stress increment. Figure 23 provides an example of the painted and unpainted photos taken at various shear stress increments and the corresponding eroded areas determined.

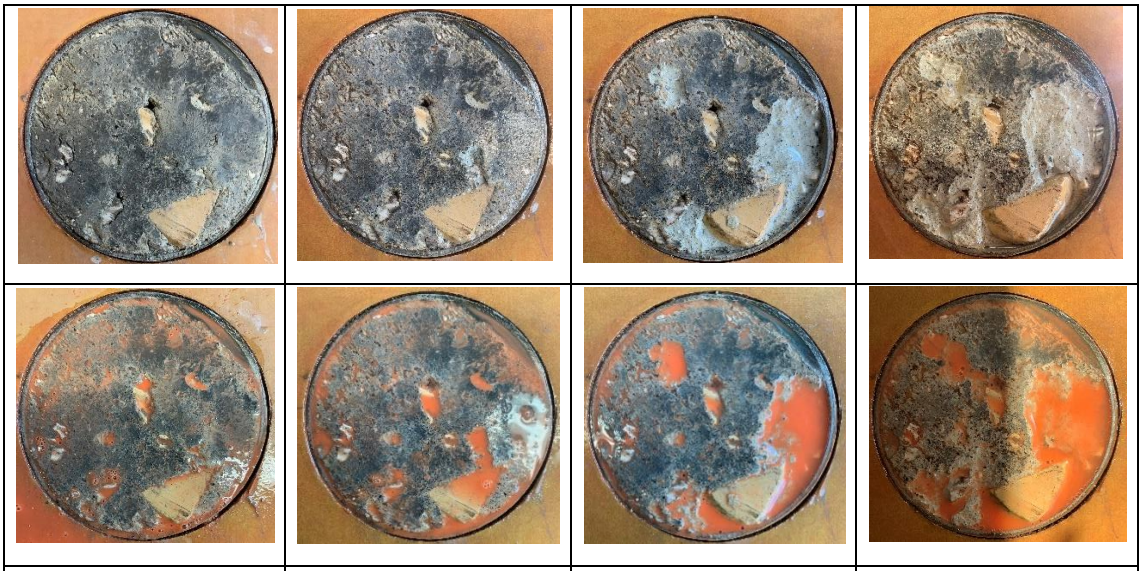

0 Pa – 2% Pitted	2 Pa – 4% Pitted	4 Pa – 27% Pitted	17 Pa – 38% Pitted

Figure 22: Example of erosion progression and calculated pitted areas (shown with and without paint to highlight depressions) – Sample R1-L6-D1

For many of the tested specimens, the scour depth was documented after the final 17 Pa shear stress test to give a sense of the material volume being eroded. However, this depth should not be directly interpreted as an erosion rate since the shear stress applied below the flume bed is not known.

3.8.6 Comparison to Previous Experiments Using Buffstone Clay

Previous unpublished work conducted at the University of Manitoba by Jianfar (2014) was used to compare the erosion of Buffstone Clay (a commercially available pottery clay) observed using the Erosion Measurement Device (EMD) to that observed using the modified variable slope flume. Firstly, it was noted that the buffstone clay did not erode in large clasts as the glacial till did. As such, it was more difficult to estimate the portion of the area eroded, but still possible due to an observable texture change. Also, unlike the glacial till, the buffstone clay was observed to swell and soften over time, changing its erodibility - which is anticipated to result in continued erosion for longer test durations even at low applied shear stresses. This more gradual and time

dependant form of erosion requires a means of quantifying erosion as a rate which can be converted to a mass or volume over time. For these reasons, the EMD would likely be the preferred method for determining the erodibility of this type of homogenous cohesive sediment (without the presence of planes of weakness) which erodes on a particle-by-particle basis.

Regardless of the above limitations, erosion observed using the variable slope flume (expressed as a portion of sample area eroded, as shown on the left y-axis) was compared to erosion observed using the EMD (expressed as a distance over time, as shown on the right y-axis), shown as Figure 23. As shown, experiments conducted using the variable slope flume indicate that the entire sample area becomes eroded and therefore the maximum elevation of the sample surface begins to recede below the flume bed at approximately 10 Pa. This is consistent with results from the EMD which shows a measurable change in sample height (expressed as an erosion rate in mm/hr) at 9.4 Pa.

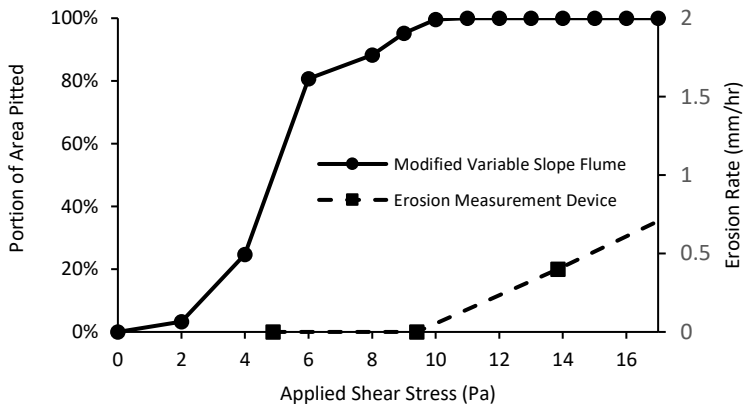

Figure 23: Erosion of Buffstone clay observed using modified variable slope flume and EMD (unpublished data from Jianfar, 2014)

Chapter 4: Results and Analysis

This Chapter summarizes the measurements and results from the various erosion, slaking, and material properties tests conducted as part of this study. Comparisons of these results with results from previous studies are also provided.

4.1 Material Properties

A wide range of physical, mechanical, and electro-chemical soil properties expected to influence erosion and slaking (Chapter 2.5) were determined for each sample location. In-situ density, moisture contents (MC), and degree of saturation (DOS) were determined using Shelby tube puck samples. In-situ matric suction was also determined from Shelby tube puck samples, based on the procedures and Whatman No. 42 filter paper moisture content / suction relationship outlined in ASTM D5298 (ASTM, 2016). The grain size distributions for each sample location were determined from sieve analysis (ASTM, 2017) and hydrometer analysis (ASTM, 2017) of grab samples obtained from around the extracted Shelby tubes. The median grain size (d_{50}) and the gravel, sand, silt, and clay fractions were determined from the grain size distribution for each sample location. The liquid limit (LL), plastic limit (PL), and plasticity index (PI) (Atterberg limits) were also determined using ASTM D 4318 (ASTM, 1998) from grab samples. Finally, the cation exchange capacity (CEC) for each sample location was determined using the Ammonium Acetate Method (Carter & Gregorich, 2007) from grab samples tested by ALS Laboratories. The soil properties determined for each sample location are summarized in Table 4. The exchangeable sodium percentage (ESP) could not be determined since the sodium concentration was found to be below its detection limit. However, based on this detection limit and the CEC values summarized in the table below, it can be concluded that ESP is less than 24% in all cases and in most cases, less than 12%. This suggests that clay dispersion is unlikely to occur (Laker & Nortjé, 2019). The crumb tests conducted on a few intact chunks of till from various sample locations also suggest that these materials are non-dispersive.

Table 4: Soil Sample Properties

ID	Dry Density (kg/m³)	MC (%)	DOS (%)	Suction (kPa)	d_{50} (mm)	Gravel (%)	Sand (%)	Silt (%)	Clay (%)	PI (%)	CEC (meq/100g)
SL-L1	-	-	-	-	0.116	24	29	35	11	6	2.74
B2-L1	2113	10.2	96.2	12.3	0.020	23	17	34	26	17	2.43
R1-L1	2167	8.4	84.2	43.6	0.023	15	27	40	18	7	4.29
R1-L2	2169	7.4	80.3	56.5	0.002	11	9	31	49	36	18.4
R1-L3	1981	11.0	85.5	28.8	0.012	13	21	36	30	18	7.73
R1-L4	2043	12.4	90.3	3.9	0.003	9	16	31	44	24	15.4
R1-L5	2187	9.3	94.4	17.9	0.035	15	28	41	15	8	3.43
R1-L6	2198	8.1	97.0	13.2	0.025	19	22	39	21	13	5.42
R1-L7	2085	10.4	97.0	5.5	0.026	10	28	47	14	6	2.11

The liquid limits and plasticity indexes determined were plotted on a plasticity chart (Figure 24) and used to classify the fine-grained fraction of collected soil samples.

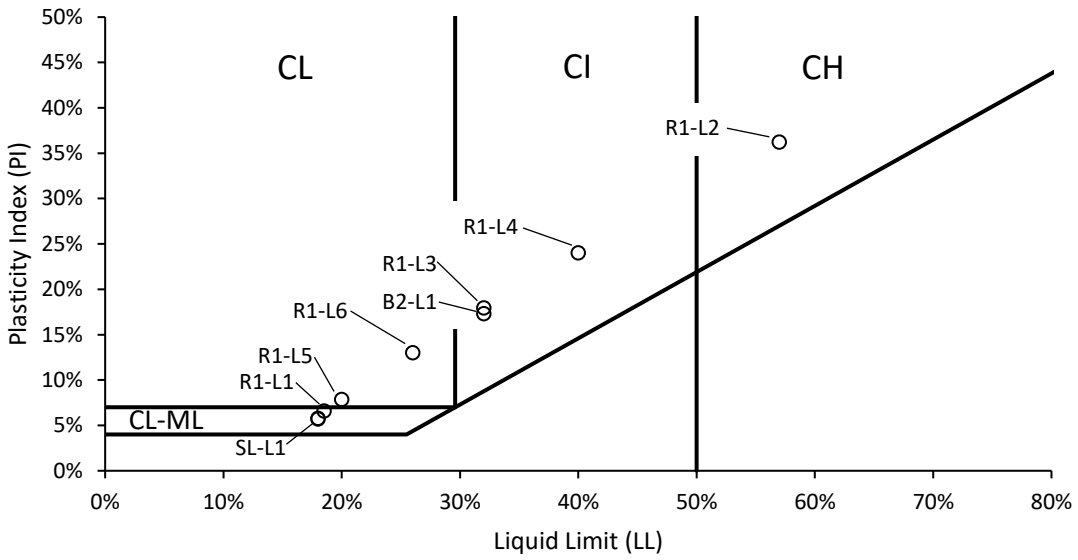

Figure 24: Plasticity chart for till samples used in this study

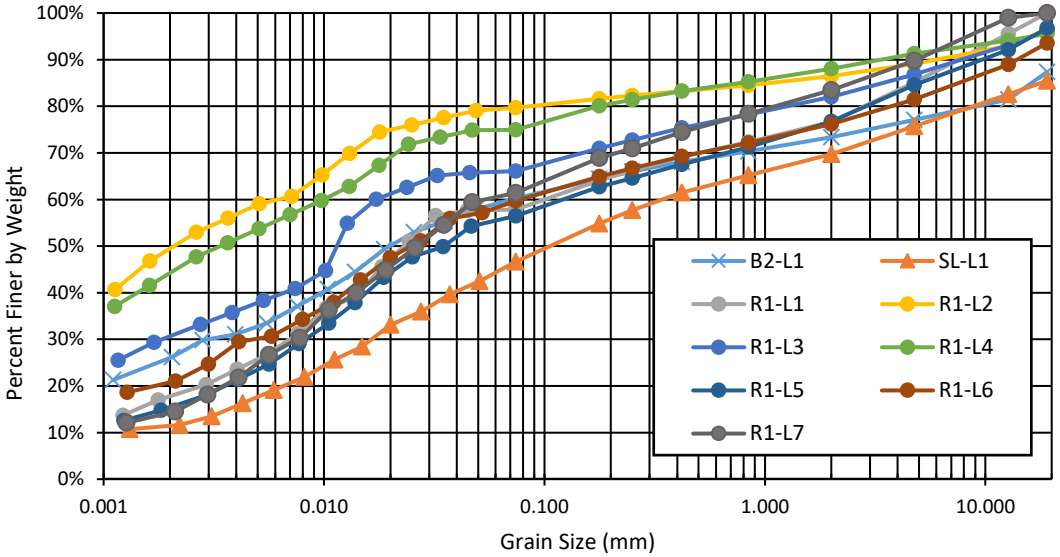

Figure 25: Grain size distribution of till samples used in this study

As shown, the samples collected represent a relatively wide range of soil properties. Relationships observed between these properties and erosion/slaking characteristics are discussed in Chapter 4.6.

The in-situ degree of saturation and matric suction of samples collected along Reach 1 of the LSMEOC (samples R1-L1 through R1-L7) were expected to be dependent on their relative proximity to a groundwater boundary condition (approximated by the water level in the channel) and an evaporation boundary condition (i.e. the exposed channel surface). Figure 26 through Figure 28 show how the in-situ degree of saturation and matric suction of these samples varies with distance from these assumed boundary conditions.

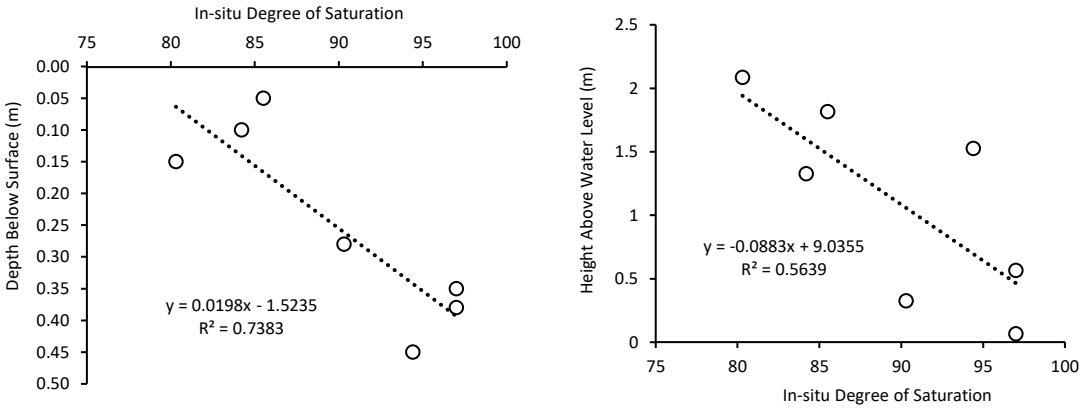

Figure 26: In-situ degree of saturation variation of Reach 1 samples with overburden material depth and height above channel water level.

As shown, a relationship can be observed between in-situ degree of saturation and both overburden material depth and the height above the water table. As would be expected, degree of saturation increases at increasing depths from the ground surface and decreases with increasing height above the water table.

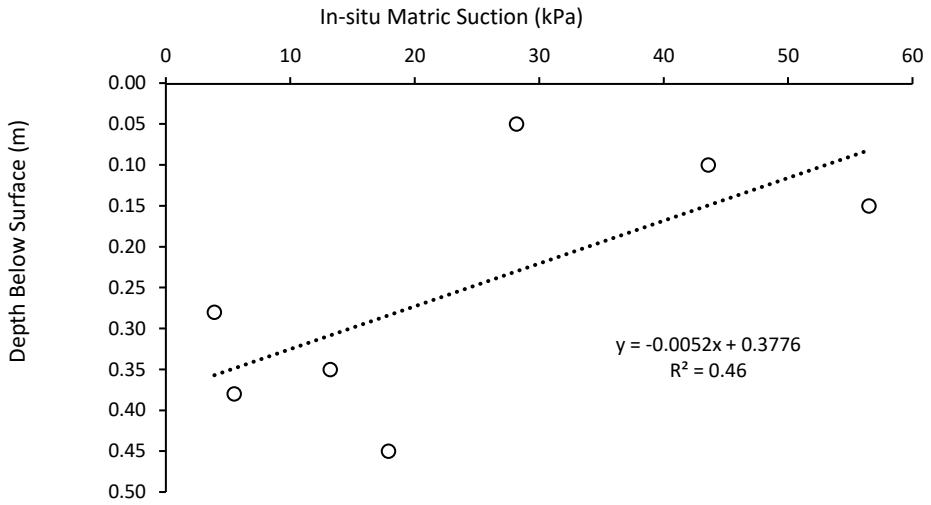

Figure 27: In-situ matric suction variation of Reach 1 samples with overburden material depth

Similar to Figure 26, Figure 27 shows how the in-situ matric suction varies with the overburden material depth. Matric suction is shown to increase with decreasing overburden material depth as would be expected, however the relationship is weak.

Finally, the variation of matric suction with height above the assumed groundwater level was assessed and is presented on Figure 28. The equilibrium hydrostatic matric

suction (hydrostatic line), defined as the matric suction which would be present without any evaporation, evapotranspiration, or infiltration effects (Fredlund et al., 2012), is also shown (matric suction equals the product of the height above the water table and the unit weight of water). This figure also includes labels for each sample point along with their depth below surface shown in brackets.

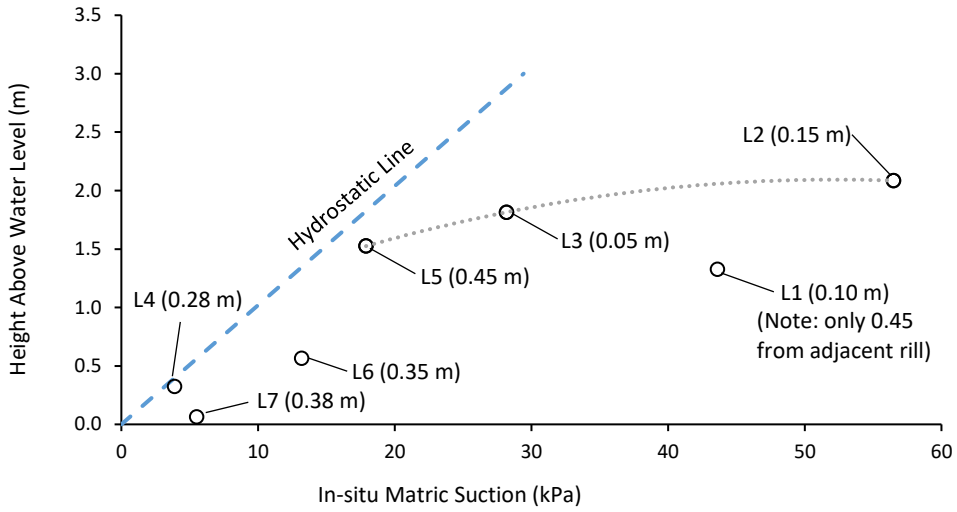

Figure 28: In-situ matric suction variation of Reach 1 samples with height above water level

As shown, samples collected between 0 and 1.5 m from the assumed groundwater boundary condition (L4, L7, L6, and L5) lie closely below the hydrostatic line. It is anticipated that within this distance, matric suction is governed mostly by distance to the groundwater level and that the overestimation of suction is due to measurement error (sample moisture content reduction from heat of chop saw blade and filter paper moisture content reduction due to exposure longer than three seconds). However, the increased suction recorded for these samples could also be due to the evaporation boundary condition.

Samples L1, L2, and L3 were shown to plot considerably lower than the hydrostatic line. It is expected that at this greater distance from the groundwater level, evaporation begins to have a greater impact. Figure 29 provides a conceptual representation of how matric suction varies relative to groundwater, evaporation, and infiltration boundary conditions. A best-fit polynomial line which includes L2, L3, and L5 was drawn on Figure 28 to provide a rough approximation of the excessive evaporation line shown conceptually on Figure 29. L1 was excluded since this sample

was collected only 0.45 m from the large rill shown on Figure 12, which is expected to have increased matric suction at this location (all other samples were collected at least 1.4 m from adjacent rills). It should be noted that Figure 28 and Figure 29 are not directly comparable since Figure 29 shows a single vertical column where distance to the ground surface increases equal to decreasing distance from the groundwater level. However, a reasonable linear trend (similar to the hydrostatic line) is observed within 1.5 m of the groundwater level, beyond which evaporation seems to have a greater effect and the elevation/matric suction line more closely resembles the excessive evaporation line shown in Figure 29. While these suction measurements were prone to some error (as noted) and cannot be perfectly represented by theory, based on Figure 26 through Figure 28, it is anticipated that the vertical matric suction gradient could be predicted through more extensive modelling efforts.

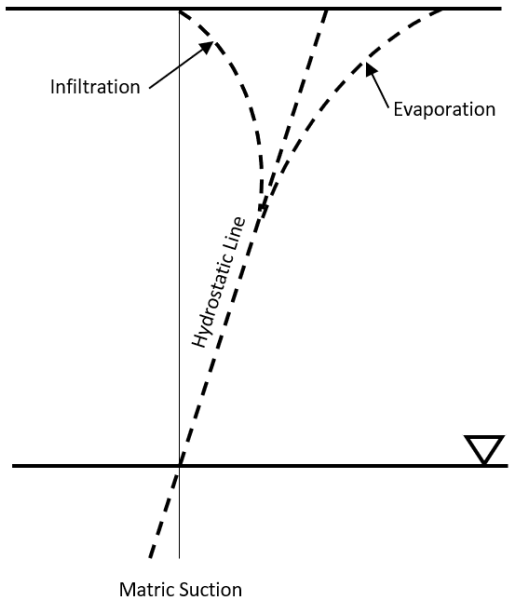

Figure 29: Conceptual representation of matric suction relative to different boundary conditions (adapted from Fredlund et al., 2012)

4.2 Slaking Experiments

Slaking experiments were conducted in two phases. Phase 1 was conducted using grab samples and limited Shelby tube samples obtained from the St. Laurent quarry. The first phase consisted of a series of qualitative and quantitative experiments aimed at gaining a general understanding of the impacts of slaking on glacial till. Phase two was

conducted using Shelby tube samples collected from eight locations along and near the Lake St. Martin Emergency Outlet Channel (LSMEOC). The second phase included a systematic procedure for approximating a threshold moisture content below which slaking occurs, for each of the samples collected.

4.2.1 St. Laurent Quarry Till (Phase 1)

Although the St. Laurent quarry location is not within the immediate vicinity of either of the proposed channels, its material is expected to be similar to the silt-till found along the proposed channel alignments and is nonetheless an additional till studied for comparison.

4.2.1.1 Slaking of Intact Till at In-Situ Moisture Content

Since the bed of the Lake St. Martin Outlet Channel is likely to remain permanently under water throughout its operation, it is useful to understand whether softening (resulting in an increase in erodibility) of glacial till would occur without being subject to a wetting and drying cycle. A Shelby tube puck sample from the St. Laurent quarry site was submerged at its in-situ moisture content and the vertical displacement of its exposed surface was continuously measured using an LDVT (linear variable differential transformer). Displacement of the exposed surface (i.e. a volume change of the sample) would indicate softening resulting from dispersion or swelling. After 22 days of submergence, the LDVT (accurate to 0.001 mm) did not register any vertical displacement of the sample. Furthermore, the post-submergence compressive strength of the sample surface was measured using a pocket penetrometer which registered the maximum applied pressure of 4.5 kg/cm^2 without creating any observable indent in the sample. This suggests that for this particular till, swelling and dispersive forces (slaking mechanisms) alone are not enough to overcome the attractive forces between particles and softening is not likely to occur if the till remains permanently submerged. Furthermore, the addition of internal tensile stresses caused by the compression of entrapped air (third mechanism of slaking which develops when an unsaturated soil is immersed in water) are also not enough to overcome the attractive forces between particles when the sample is initially at its in-situ moisture content.

Figure 30: Submerged Shelby tube puck sample with LVDT to measure vertical displacement

4.2.1.2 Slaking of Reconstituted Till at In-situ Moisture Content.

A reconstituted till sample was submerged for 18 days in approximately 1 m of water and its slaking was observed. Unlike an intact sample which was subjected to the same test, the reconstituted sample exhibited some visible swelling and the top surface of the sample could easily be indenting with a finger. This suggests that the reconstituted sample did not have the same bond strength between particles as the intact sample. It should be noted that the reconstituted sample was submerged shortly after it was moulded (within the same day) and it is possible that there are some time-dependant processes which would have increased the bond strength between particles if it was left longer.

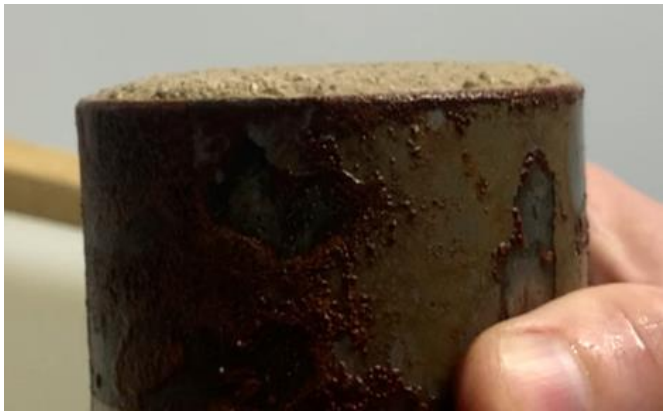

Figure 31: Swelling of reconstituted St. Laurent till sample submerged at in-situ moisture content

4.2.1.3 Slaking at Air-Dried Moisture Content

It was first observed that dried and relatively intact "chunks" of St. Laurent till quickly broke down into individual particles when submerged. A pair of intact and reconstituted Shelby tube puck samples were left to air dry for 15 days. They were then submerged and their vertical displacement (swelling) was measured with a point gauge, as shown in Figure 32.

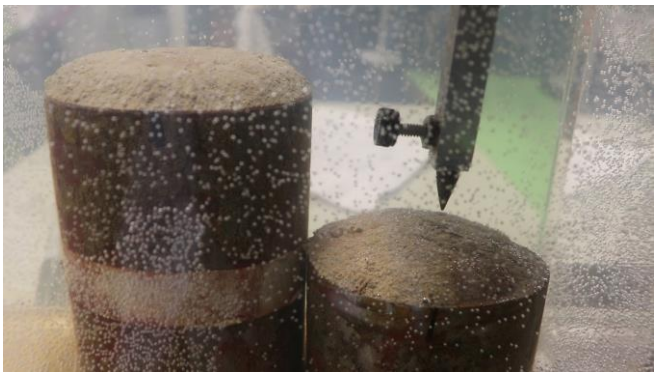

Figure 32: Point gauge used to measure vertical displacement (swelling) of air-dried reconstituted (left) and intact (right) St. Laurent till samples.

In both cases, significant vertical displacement was observed compared to similar samples which were not air-dried. The slaked material had a fluid-like consistency, and it was clear that this material would easily erode under a small applied shear stress. Regular measurements of vertical displacement of the sample surfaces were recorded over time and are presented in Figure 33.

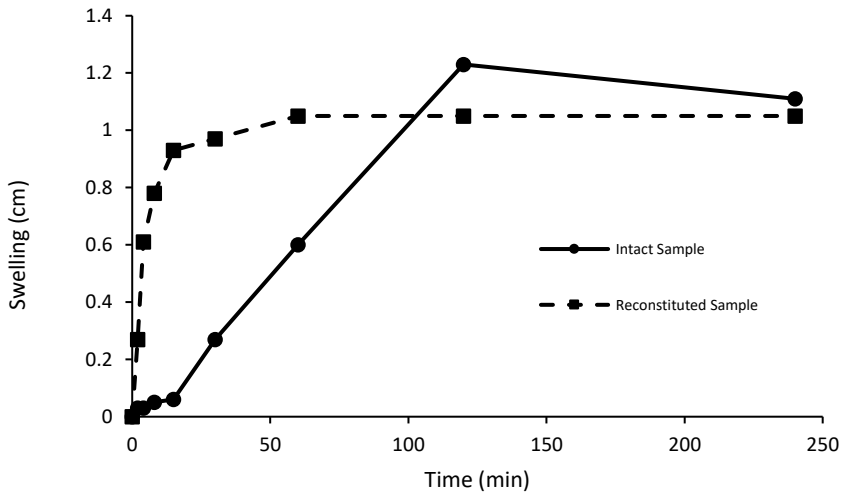

Figure 33: Swelling of Air-dried Intact and Reconstituted St. Laurent Till Samples

As shown in Figure 33, the swelling process occured over approximately 60 minutes for the reconstituted till and 120 minutes for the intact till, however the vertical displacement was observed to be approximately the same between the two. The increased swelling rate of the reconstituted sample supports the conclusion that remoulding reduces the bond strength between particles. Furthermore, this test also supports the conclusion that the degree of slaking and resulting increased erodibility is critically dependant on the initial moisture content prior to submergence and suggests that the compression of entrapped air is the governing slaking mechanism.

4.2.1.4 Effects of a Groundwater Boundary Condition

From the above tests, it is clear that reducing the moisture content (increasing the matric suction) of reconstituted and intact till followed by submergence can significantly increase its erodibility through slaking. However, it is unclear what degree of drying would occur along the exposed banks of a channel with the presence of a groundwater boundary condition, particularly within 5 cm of the exposed bank where evaporation effects would be more significant. In-situ moisture content and suction values are provided in Chapter 4.1.

To test the effects of a groundwater boundary condition on drying, intact and reconstituted samples (reconstituted to the same moisture content and density as the in-situ till) were placed on the capillary tray (described in Chapter 3.5) for approximately 45 days. The samples could be considered representative of material situated just above the stagnant channel water level. A reconstituted sample was also left sealed over the 45-day period as a control. All three samples were then submerged and their swelling was measured using a point gauge (error = ±0.2 mm) after a six-day period (Figure 34). The intact sample did not exhibit any observable swelling or softening, confirming that a groundwater boundary can prevent drying and resultant slaking. The reconstituted and sealed sample exhibited approximately 5 mm of swelling, appearing to be consistent with the reconstituted sample described in Chapter 4.2.1.2. Interestingly, the reconstituted sample which was left on the capillary tray exhibited only minor swelling (0.6 mm) after submergence. This suggests that not only can a groundwater boundary prevent drying (and resultant slaking in the case of the intact sample), but can also increase the moisture content in a way that does not

induce slaking, unlike the reconstituted sample held at a constant moisture content (sealed) which exhibited significant slaking when immersed in water.

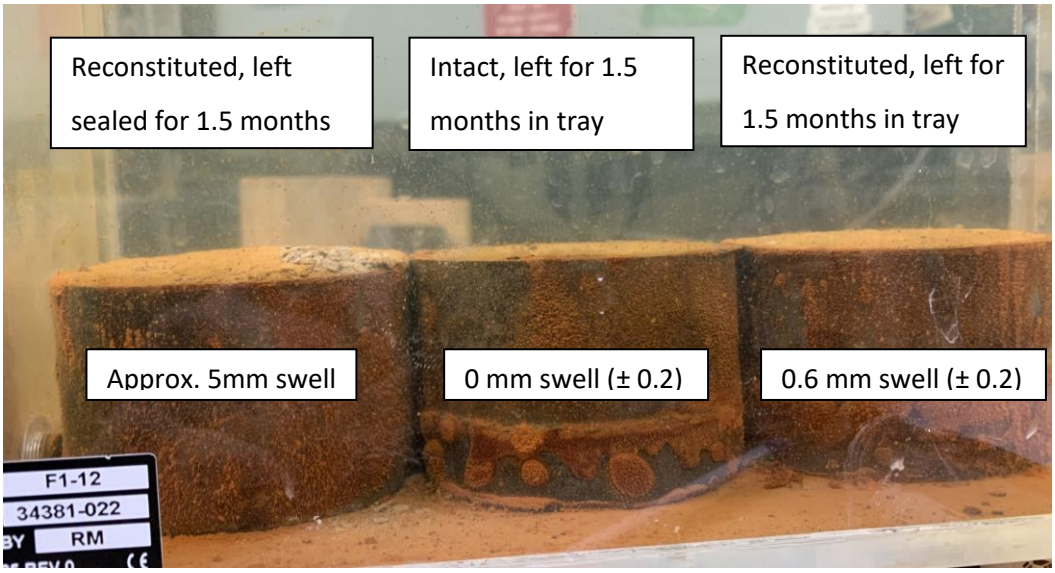

Figure 34: Effect of groundwater boundary condition on swelling/slaking

Subsequent tests on intact St. Laurent till samples showed that air-dried samples which would slake significantly if immersed in water, could instead be saturated using the capillary tray, increasing their moisture content past a slaking threshold such that they would not exhibit any slaking when submerged. These tests, along with Phase 2 slaking tests on the LSMEOC till described in the following section, further support the conclusion that the compression of entrapped air a governing slaking mechanism and that saturating the till more slowly through capillary rise reduces this compression of entrapped air, preventing slaking.

4.2.2 LSMEOC Till (Phase 2)

Phase two slaking testing was conducted using intact Shelby tube samples collected from eight locations along and near the LSMEOC. This phase consisted of implementing a systematic procedure for approximating a threshold moisture content and matric suction below which slaking occurs using Shelby tube puck samples. The procedure is outlined as follows.

1. Mass, height (approximately 50 mm), and matric suction (ASTM D5298-16, seven days required for filter paper and sample to equilibrate) of each Shelby tube puck sample measured and recorded.

2. Samples immersed in water and slaking observed (first at in situ moisture content). Saturated mass of samples recorded.

3.a For samples which did not slake, moisture content decreased (air-dried) for further testing

3.b For samples which slaked, sample oven-dried and soil dry mass / tube weight determined. Moisture content of identical intact (un-slaked) puck sample increased (via capillary tray) for further testing.

4. Steps 1-3 repeated until all samples slaked and slaking threshold suction determined to be within a range between a known slaked and unslaked condition.

Ultimately, up to five pre-submergence moisture content / suction conditions were tested for each sample location, as summarized in Table 5. The table also indicates whether major, minor, or no slaking occurred, as well as the amount of swelling of the sample surface associated with slaking. Slaking resulting in more than 2 mm of swelling was defined as major slaking, while slaking resulting in less than 2 mm of swelling was defined as minor slaking. Figure 35 shows the difference between minor and major slaking for two samples obtained from location R1-L7.

Figure 35: Minor (top) and major (bottom) slaking – Sample Location R1-L7

Table 5: Suction and slaking determined for various initial moisture conditions

Moisture Condition (sample used)		B2-L1	R1-L1	R1-L2	R1-L3	R1-L4	R1-L5	R1-L6	R1-L7
Saturated (A)	MC%	10.3%	8.9%	9.3%	13.2%	13.7%	7.9%	9.8%	10.4%
	Suction (kPa)	Assumed to be approximately zero							
	Slaking?	no	no	no	no	no	no	no	no
In-situ MC% (F*)	MC%	10.2%	8.4%	7.4%	11.0%	12.4%	9.3%	8.1%	10.4%
	Suction (kPa)	12.3	43.6	56.5	28.2	3.9	17.9	13.2	5.5
	Slaking? (swelling, mm)	no	no	minor (<1)	major (4)	minor (<1)	no	no	no
3.5 hrs Air-Dry (F)	MC%	9.5%	7.6%				8.7%	7.5%	9.6%
	Suction (kPa)	27.5** (7.7)	120.8				62.4	33.1** (198.4)	37.3
	Slaking?	no	no				no	no	no
6 hrs Air-Dry (F)	MC%	8.5%	7.1%				7.6%	6.4%	8.3%
	Suction (kPa)	91.1	399.5				292.5	171.7	77.4
	Slaking? (swelling, mm)	minor (1.0)	minor (1.6)				minor (2.0)	major (3.2)	minor (1.6)
22 hrs Air-Dry (A)	MC%	6.4%	5.6%	5.7%		9.8%	4.4%	6.1%	6.7%
	Suction (kPa)	1100	1049	1673		1688	343.6** (44.8)	322.5	412.7
	Slaking? (swelling, mm)	major (10)	major (10)	major (8)		major (3)	major (6)	major (10)	major (6)

*Sample A used to determine moisture content of R1-L2, R1-L3, and R1-L4

**Measured value (shown in brackets) identified as outlier, corrected value calculated based on best-fit logarithmic relationship of other moisture content/suction values

Some potential for error/misrepresentation should be noted with the method for both the suction and moisture content determination. The method of weighing the filter papers to determine matric suction requires transferring the papers from puck samples to the scale within 3-5 seconds to avoid significant error due to evaporation. While most papers were transferred quickly, the exact time was not measured, and some error is possible. For quality control purposes, the semi-log relationship between matric suction and moisture content (known as the soil-water characteristic curve) was plotted for sample locations where at least three pairs of moisture content / suction measurements were recorded (shown in Appendix A). Single outliers were identified for sample locations B2-L1, R1-L5, and R1-L6 (indicated in Table 5 and Appendix A) and were assumed to be erroneous due to measurement error. With the erroneous values

removed, very strong logarithmic relationships were observed between moisture content and suction for all sample locations with at least three pairs of moisture content / suction measurements recorded (R^2>0.98), as shown in Appendix A. This relationship is consistent with what would be expected through what is referred to as the transition zone, described in Figure 36. Corrected suction values were determined for the erroneous values identified at sample locations B2-L1, R1-L5, and R1-L6 and are provided in Table 5.

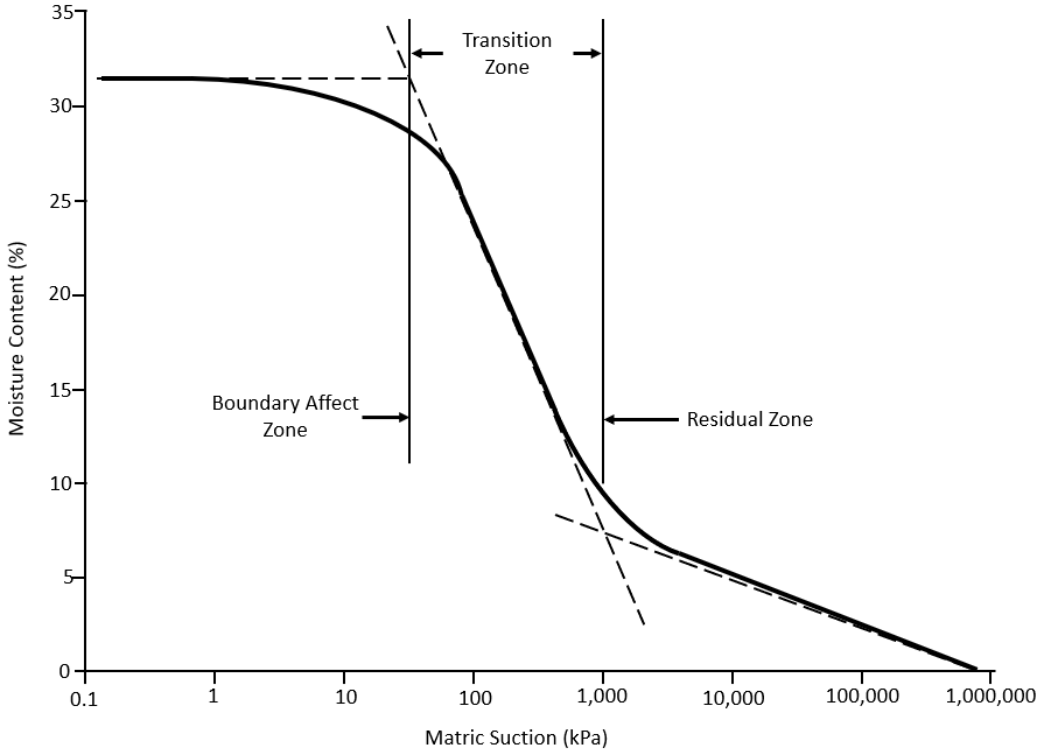

Figure 36: Example soil-water characteristic curve (adapted from Fredlund et al., 2012)

It should also be noted that the moisture contents determined for each sample may not accurately represent the moisture content within the fine-grained soil matrix since samples contained varied amounts of coarse aggregate. This coarse aggregate would contribute to the dry soil mass but would adsorb only minimal moisture, therefore the amount of coarse aggregate in a given sample could skew its measured moisture content relative to other samples cut from the same Shelby tube. This should be considered when comparing moisture contents determined using "A" samples to those determined using "F" samples.

Based on the slaking observed at varied initial moisture / suction conditions, the range of possible threshold moisture content / suction conditions for slaking of samples from each sample location were defined and are presented in Table 6.

Table 6: Ranges Determined for Slaking Thresholds – Initial Suction and Moisture Content

	B2-L1	R1-L1	R1-L2	R1-L3	R1-L4	R1-L5	R1-L6	R1-L7
Min MC% without Slaking	9.5%	7.6%	9.3%	13.2%	13.7%	8.7%	7.5%	9.6%
Max MC% with Slaking	8.5%	7.1%	7.4%	11.0%	12.4%	7.6%	6.4%	8.3%
Max Suction without Slaking (kPa)	27.5	120.8	0	0	0	62.4	33.1	37.3
Min Suction with Slaking (kPa)	91.1	399.5	56.5	28.2	3.9	292.5	171.7	77.4

4.3 Cohesive Strength Meter (CSM) Testing

A total of 28 CSM tests were conducted on October 15th and 16th on the weathered and wet till at the St. Laurent quarry site. The average critical eroding pressure determined for the valid tests was 23.8 kPa and the average critical horizontal shear stress was 1.91 Pa. This helps confirm that the weathered till is very erodible, and unlikely to be able to resist the shear stresses that would be applied during channel operation.

4.4 Hydraulic Flume Tests

Hydraulic flume tests were conducted to assess the erodibility of Shelby tube puck samples of material obtained from one location at the quarry near St. Laurent and eight locations along or near the LSMEOC. Test results for each of the nine locations are summarized in Table 7 and Figure 37. The specific test conditions are discussed in the following subsections.

4.4.1 St. Laurent Quarry Till

A total of three rounds of hydraulic flume testing (consisting of increasing increments of applied shear stress) was conducted on till samples obtained from the St. Laurent quarry location. At this stage of testing, the sample panel was only fitted with a single Shelby tube puck sample slot and only a single intact puck sample was available for erosion tests. The first round of testing consisted of applying shear stresses of 6, 8.5,

10, and 11.5 Pa to the intact sample for durations of 5 minutes. The second round of testing consisted of applying shear stresses of 6, 8.5, and 10 Pa to the same intact sample for durations of two hours each. The third round of testing consisted of applying shear stresses of 4.6 to 15.4 Pa in increments of approximately 2 Pa to a reconstituted sample (prepared as described in Chapter 3.6) for thirty-minute durations.

4.4.2 Lake St. Martin Emergency Outlet Channel Till

A total of 5 rounds of hydraulic flume testing was conducted on intact Shelby tube puck samples obtained from 8 locations along or near the LSMEOC. At this stage of testing, the sample panel was fitted with 12 Shelby tube puck sample slots such that 12 samples could be tested simultaneously. Each round of testing consisted of applying shear stresses of 2 Pa to 8 Pa in 2 Pa increments and then 9 Pa to 17 Pa in 1 Pa increments (or until all samples had eroded completely). Each shear stress increment was applied for a duration of one hour. The duration was assumed to be sufficient since almost all erosion of the St. Laurent till samples occurred within the first fifteen minutes, and very little additional erosion would be expected after the one-hour period. The one-hour duration used for each applied shear stress is significantly greater than the one minute duration used by Mier & Garcia (2011) and the fifteen minute duration used by Pike (2014) for most of their tests. A total of 45 tests (defined as applying the range of shear stress increments to a sample) were conducted on a total of 28 Shelby tube puck samples. Samples which did not erode were sometimes tested again with a different initial condition. The initial conditions for the various tests are as follows:

In-situ Moisture Content: Three samples from each of the eight sample locations were tested at their in-situ moisture content. Samples were submerged in water for a minimum of 24 hours prior to flume testing. The in-situ moisture content and matric suction present in these samples prior to submergence can be expected to be relatively consistent with samples collected from the same sample locations (cut from the same Shelby tube) as shown in Table 7.

Increased Moisture Content (IM): For sample locations where samples eroded at their in-situ moisture content, an additional sample was prepared with an increased

moisture content prior to submergence. The moisture content of these samples was increased using the capillary tray as described in Chapter 3.5. Samples were left on the capillary tray until their mass was no longer increasing (no longer taking in water).

Decreased Moisture Content (DM): For sample locations where samples did not erode at their in-situ moisture content, a previously uneroded sample was subjected to 48 hours of air-drying prior to pre-test submergence.

Subjected to Freeze / Thaw Cycle (F/T): Several previously uneroded samples were subjected to 24 hours of freezing (-15°C to -18°C) prior to a 24-hour period of thawing during pre-test submergence. These samples were frozen from a saturated condition (saturated via capillary rise) to maximize the effects of freezing.

Centre Pit Initiated (CP): Previous tests had shown that erosion observed on the surface of a given puck samples tends to be localized and not consistent across the whole sample. It was then theorized that erosion may more easily occur if an initial pit in the sample surface is present from which erosion would propagate. This could represent an irregularity in a channel bed resulting from channel construction (e.g. a rock plucked by machinery excavating the channel bed resulting in a depression). A centre pit was formed in several previously uneroded samples by drilling a 12.5 mm deep hole using a 11 mm diameter drill bit.

4.4.3 Hydraulic Flume Test Results Summary

The results of the hydraulic flume testing, expressed primarily as eroded area at increasing shear stress increments, are described in Table 7 and in Figure 37. The reader should note that the first character in the puck / test ID in column two of Table 7 and the legends in Figure 37 is simply a unique identifier for each individual puck sample from their respective sample locations. The second character indicates whether it is the first, second, or third time the puck sample has been tested (e.g. puck/test ID = A2 could have an initial pitted area equivalent to ending pitted area of puck/test ID = A1 which would have been a result of some erosion during the first test of A). Finally, the bracketed characters indicate whether the initial condition of the sample has been modified by increasing its moisture content (IM), decreasing its moisture content (DM), subjecting it to a freeze/thaw cycle (F/T), or initiating a centre pit (CP).

Table 7: Hydraulic Flume Testing Summary

Sample Location ID	Puck / Test ID	Puck/Test Description	Pre-test Slaking?	Pitted Area Before Test	Pitted Area After Test	Scour Depth (mm)
SL-L1	I1	Intact, in-situ MC%, 5 min test duration	none	5%	30%	N/A
	I2	Intact, in-situ MC%, 120 min test duration	none	30%	50%	N/A
	R1	Reconstituted, in-situ MC%, 30 min test duration	none	2%	22%	N/A
B2-L1	C1	In-situ MC%	none	0%	0%	0
	D1	In-situ MC%	none	0%	4%	N/A
	E1	In-situ MC%	none	0%	0%	N/A
	C2 (CP)	Centre pit drilled	none	5%	5%	N/A
	D2 (F/T)	Freeze/thaw cycle	N/A*	8%	47%	3
	E2 (CP)	Centre pit drilled	none	19%	34%	N/A
	C3 (DM)	Decreased MC%	yes	0%	100%	11
R1-L1	B1	In-situ MC%	none	17%	17%	< 1 mm
	C1	In-situ MC%	none	25%	30%	< 1 mm
	D1	In-situ MC%	none	6%	34%	N/A
	B2 (CP)	Centre pit drilled	none	25%	25%	N/A
	C2 (F/T)	Freeze/thaw cycle	N/A*	25%	75%	3
	D2 (DM)	Decreased MC%	yes	0%	100%	10
R1-L2	C1	In-situ MC%	slight	10%	100%	6
	D1	In-situ MC%	none	8%	88%	10
	E1	In-situ MC%	none	0%	99%	10
	B1 (IM)	Increased MC%	none	0%	0%	0
R1-L3	B1	In-situ MC%	slight	0%	90%	19
	C1	In-situ MC%	slight	0%	87%	10
	D1	In-situ MC%	slight	0%	100%	50
	E1 (IM)	Increased MC%	none	3%	19%	3
R1-L4	C1	In-situ MC%	slight	14%	100%	5
	D1	In-situ MC%	slight	1%	89%	16
	E1	In-situ MC%	slight	20%	94%	4
	B1 (IM)	Increased MC%	none	14%	70%	5
R1-L5	B1	In-situ MC%	none	0%	0%	0
	C1	In-situ MC%	none	0%	1%	< 1 mm
	D1	In-situ MC%	none	0%	0%	0

Sample Location ID	Puck / Test ID	Puck/Test Description	Pre-test Slaking?	Pitted Area Before Test	Pitted Area After Test	Scour Depth (mm)
	B2 (CP)	Centre pit drilled	none	8%	8%	N/A
	C2 (CP)	Centre pit drilled	none	7%	8%	N/A
	C3 (DM)	Decreased MC%	yes	0%	100%	13
R1-L6	C1	In-situ MC%	none	0%	0%	< 1 mm
	D1	In-situ MC%	none	0%	37%	4
	E1	In-situ MC%	none	0%	55%	5
	B1 (IM)	Increased MC%	none	0%	3%	< 1 mm
	B2 (F/T)	Freeze/thaw cycle	N/A*	5%	70%	14
	C2 (CP)	Centre pit drilled	none	5%	6%	N/A
	C3 (DM)	Decreased MC%	yes	0%	100%	10
R1-L7	B1	In-situ MC%	none	0%	1%	< 1 mm
	C1	In-situ MC%	none	0%	4%	N/A
	D1	In-situ MC%	none	0%	0%	0
	B2 (F/T)	Freeze/thaw cycle	N/A*	1%	80%	15
	C2 (CP)	Centre pit drilled	none	13%	22%	N/A
	D2 (CP)	Centre pit drilled	none	5%	5%	N/A
	D3 (DM)	Decreased MC%	yes	0%	100%	12

*Surface softening/flaking observed due to freeze/thaw cycle, not referred to as slaking

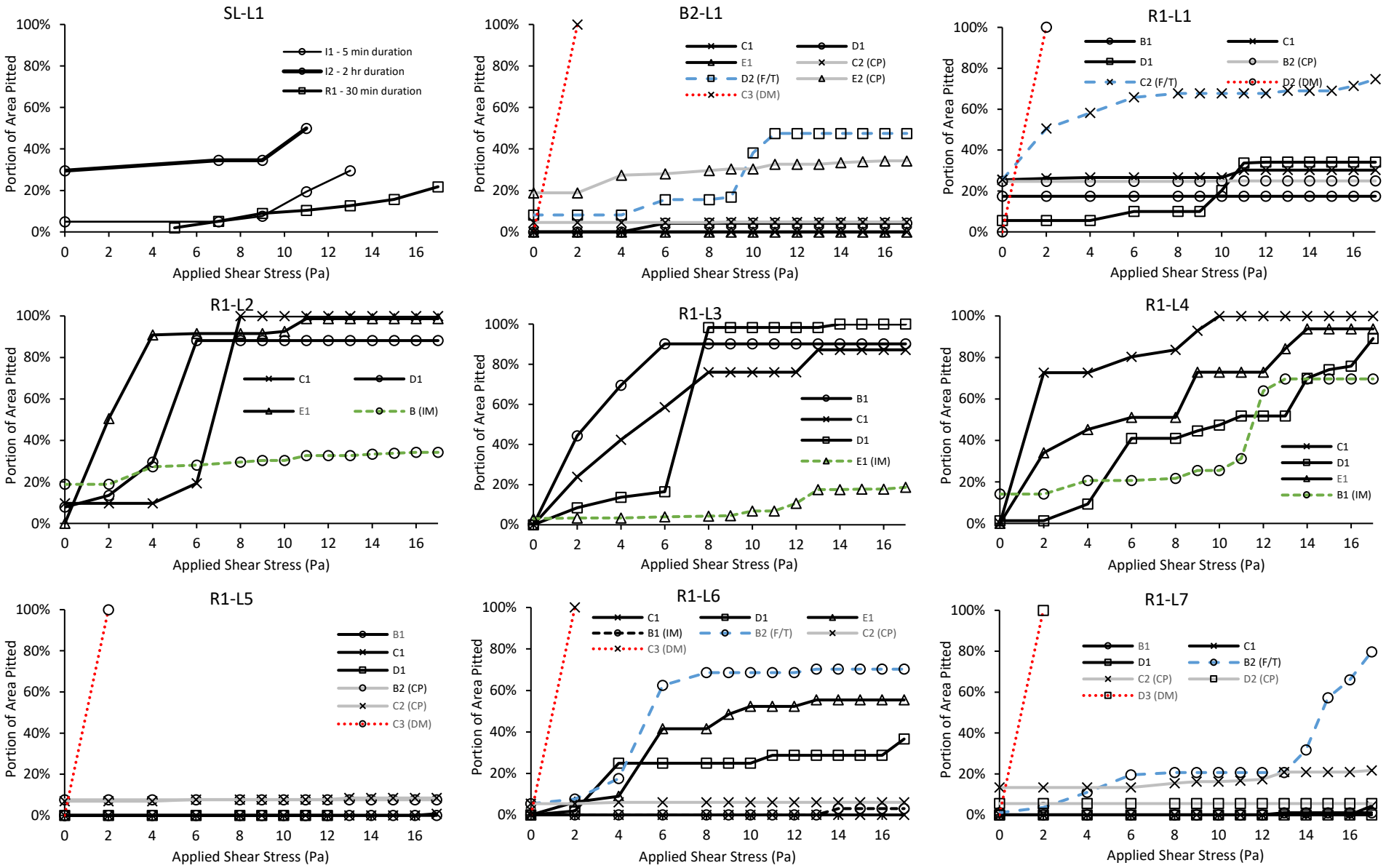

Figure 37: Portion of sample area pitted at increasing increments of applied shear stress

4.4.4 General Observations

Videos of the sample surface were recorded during the testing of the intact St. Laurent quarry till to observe how and when erosion occurred. The videos clearly showed that material eroded as intact clasts or chunks (referred to as mass erosion), separating along planes of weakness. This is consistent with observation by Kamphuis et al. (1990), Mier & Garcia (2011), and Pike (2014). Furthermore, at a given applied shear stress, most eroded clasts were ejected from the sample surface within the first minute of testing and almost all were ejected within the first 15 minutes. This is consistent with observations by Mier & Garcia (2011) and Kamphuis et al. (1990), however Pike (2014) observed a gradual propagation of cracks leading to mass erosion over time. One possible explanation for this difference observed by Pike (2014) could be that slaking had occurred during the test since samples were noted to have dried slightly during storage and were only submerged for twelve hours prior to testing (samples tested by Kamphuis et al. (1990) were noted to be saturated while samples tested by Mier & Garcia (2011) were submerged for at least 48 hours prior to testing).

To further verify whether continued erosion would be expected, particularly after the one-hour duration used for the majority of tests, eleven of the LSMEOC samples were subjected to an additional 17 Pa applied shear stress for a four-hour duration after the one-hour, 17 Pa test had been completed and documented. Of the eleven samples, additional erosion during the four-hour period was only observed for one sample, and the clast ejected accounted for less than 1% of the sample area. This helps confirm that most erosion occurs when a given shear stress is first applied, and that the one-hour duration used was sufficient.

Previous tests had shown that erosion observed on the surface of a given puck sample tends to be localized and not consistent across the whole sample. It was then theorized that erosion may more easily occur if an initial pit in the sample surface is present from which erosion would propagate. It was thought that an initial pit might have the potential to locally reduce aggregate stability (reduced lateral confining pressure) and potentially change local flow patterns (flow separation, local eddies) such that applied shear stresses on the pitted surface would be higher than the validated bed shear stresses on a flat surface. If this was true, one could then question

whether the critical shear stress determined from lab tests on flat soil samples would be relevant to a large-scale construction project that would have a more irregular channel bed surface.

To test this, a centre pit was formed in several previously uneroded samples by drilling a 12.5 mm deep hole using a 11 mm diameter drill bit, as shown in Figure 38. This artificial pit could represent an irregularity in the channel bed resulting from channel construction (e.g. a rock plucked by machinery excavating the channel bed resulting in a depression). As shown in Figure 37, little to no erosion occurred to the previously uneroded and artificially pitted samples throughout the application of the full range of applied shear stresses. This suggests that erosion is not dependant on an irregularly in the sample surface and helps validate the results from tests conducted without an artificial pit.

Figure 38: Intact till sample with centre pit drilled prior to testing

4.4.5 Defining the Critical Shear Stress

As discussed in Chapter 2.4, defining the critical shear stress can be challenging since in theory, there will be at least some particle movement at any applied shear stress. Some researchers have defined the critical shear stress as the lowest shear stress which results in erosion that is “visible to the eye” (Mier and Garcia, 2011). However, since glacial till tends to erode as large clasts which are easily visible to the eye, and since often times a small clast may be ejected at a very low shear stress while the

remaining exposed material surface remains completely intact throughout the application of much larger shear stresses, this definition would result in very conservative estimates of critical shear stress. The buffstone clay validation exercise discussed in Chapter 3.8.6 suggests that the critical shear stress defined by Jianfar (2014) corresponds to the shear stress which begins to erode the entire area of a sample such that erosion can be measured as a reduction in sample height. However, since glacial till is a very heterogeneous material with a wide range of aggregate size and bond strengths within its matrix, a particular large aggregate or small area lacking planes of weakness could result in an unreasonably high critical shear stress value if its definition required that the entire sample surface be eroded.

This study will adopt the definition proposed by Paintal (1971), which states that the critical shear stress is the applied shear stress "below which erosion is of no practical importance". Of course, this definition of critical shear stress requires an understanding of its application and in this way, puts the onus of defining its value on the designer. In this study, it was decided that the critical shear stress is defined as the shear stress required to erode 60% of the pre-test sample surface. This definition considers the objective of designing a non-eroding channel, with the caveat that some erosion resulting from its initial operation (the first "flush") would be expected and acceptable, while also considering the measured scour depths and the progression of erosion (or lack thereof) at increasing shear stresses. It is suggested that this threshold provides a practical balance of the various shear stress definitions for the purpose of stable channel design. Based on this definition, the critical shear stress for the various materials tested were determined and are summarized in Table 8.

Table 8: Critical Shear Stresses for Glacial Till Material

Sample Location ID	Puck / Test ID Critical Shear Stress (Pa)			
	In-Situ MC%*	Increased MC%	Decreased MC%	Freeze/Thaw
SL-L1	>17	>17**	< 2**	-
B2-L1	>17	>17**	< 2	>17
R1-L1	>17	>17**	< 2	16
R1-L2	4.0	>17	< 2**	-
R1-L3	6.7	>17	< 2**	-
R1-L4	8.3	13	< 2**	-
R1-L5	>17	>17**	< 2	-
R1-L6	>17	>17**	< 2	8
R1-L7	>17	>17**	< 2	16

*Taken as average of three erosion tests

**Value assumed based on results of slaking tests

4.5 Effects of Slaking on Erosion

It is clear from the results of this investigation that slaking has a significant impact on erosion. Samples (or identical sample groups) that did not exhibit any slaking prior to erosion tests appear to maintain a critical shear stress above 17 Pa, with the exception of sample R1-L4 which still maintained a relatively high critical shear stress of 13 Pa. Samples which exhibited slight slaking prior to erosion tests (i.e. samples R1-L2, R1-L3, and R1-L4 at their in-situ moisture content) had significantly lower critical shear stresses and in each case, at least one of the three samples tested exceeded the 60% eroded area threshold after the application of only 4 Pa. Finally, all samples which exhibited major slaking prior to erosion tests eroded completely (i.e. 100% of surface area eroded) after the application of only 2 Pa.

4.6 Effect of Material Properties on Erosion and the Slaking Threshold

The results of this investigation have shown that in most cases, only weathered till (i.e. subjected to wetting and drying or freezing and thawing cycles) erodes from the application of shear stresses up to 17 Pa. This investigation focuses primarily on the effects of slaking since these effects seemed to have the most significant impact on erodibility. Since a material with a 17 Pa critical shear stress would be sufficient in resisting erosion for many engineering applications, it is anticipated that slaking may

be more likely to govern erosion than the critical shear stress of unslaked material. As such, the slaking threshold, which has shown to vary significantly for different materials, may be an important parameter for predicting erosion.

The following subsections evaluate the relationships between the slaking threshold and various material properties using linear regression. Since matric suction is considered a more direct measure of the driving force behind slaking (i.e. the particle separation forces caused by pressure differentials within the soil matrix which results from the compression of entrapped air during wetting), and since the moisture contents determined may be skewed due to coarse aggregate present in the Shelby tube puck samples (discussed in Chapter 4.2.2), matric suction was used to define the slaking threshold. In Table 6, the slaking threshold was defined as a range between unslaked and slaked conditions. Regression was conducted using both the minimum suction with which each sample slaked (note only "slight" slaking was observed in each case except sample R1-L3) as well as the average of the upper and lower suction bounds of the slaking threshold. Matric suction is expressed as its logarithm (log kPa) since matric suction tends to vary logarithmically with other factors and is most often presented in this way. Finally, the goodness-of-fit of the regression models were assessed based on their coefficients of determination (R^2 values) as well as their p-value. Models with a p-value less than 0.05 (i.e. $\alpha = 0.05$) were considered to be statistically significant. A similar regression analysis was conducted using moisture content instead of matric suction, and in general, this resulted in considerably worse (poorer fitting) regression models. Unfortunately, the degree of saturation could not be determined for all samples used in this analysis since not all were weighed under their saturated condition.

4.6.1 Effect of Dry Density

Dry density was found to have a statistically significant effect on the slaking threshold (P>0.05) based on the regression analysis conducted. It was found that the slaking threshold increases with increasing dry density. Mier and Garcia (2011) found that critical shear stress of till increases with increasing density, suggesting that the attractive force between particles is stronger for denser material, which is consistent with these findings. Electromagnetic attraction forces (Van der Waals forces) are said to increase inversely proportionally to the cube of the distance between particles

(equation (*2-3*)), while preliminary valence bonding occurs at only very short particle distances. As such, it is suggested that these cohesive forces increase with increasing density. The critical shear stress of non-till cohesive sediments have also been found to increase with increasing density, as discussed in Chapter 2.5. Seedsman (1986) also found material with a higher density to be more resistant to slaking.

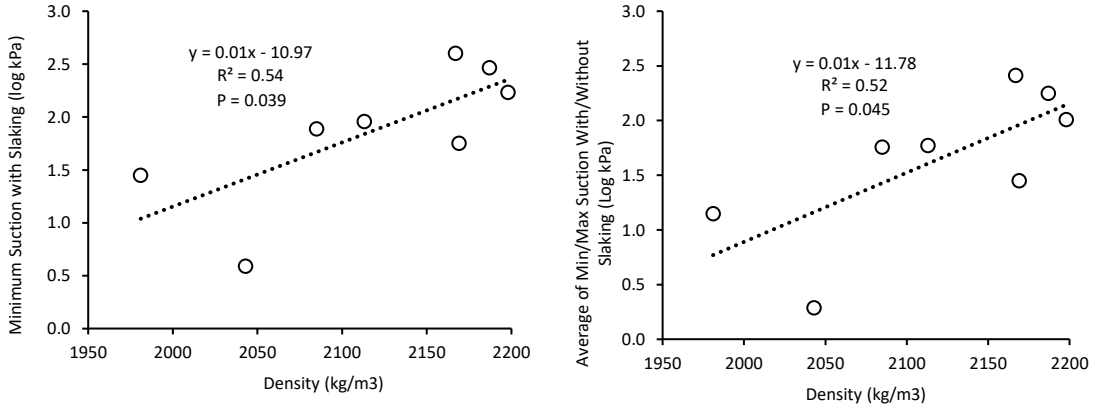

Figure 39: Effect of dry density on slaking threshold

4.6.2 Effect of Grain Size Distribution

Both median particle diameter and clay fraction were found to have a statistically significant effect on the slaking threshold. These variables were highly correlated with one another (correlation coefficient = -0.95) and the clay fraction was highly correlated with the plasticity index (correlation coefficient = 0.97) and the cation exchange capacity (correlation coefficient = 0.95). The slaking threshold was found to increase with increasing median particle diameter and decrease with increasing clay fraction. Assuming that critical shear stress and the slaking threshold are dependent on the same interparticle attraction and repulsion forces, these results are inconsistent with Mier and Garcia (2011), which suggests that for cohesive sediments, critical shear stress decreases with increasing particle size. This suggests that during the application of a shear stress the clay fraction may have a different impact on aggregate stability through the wetting process than after the wetting process. As such, the adsorption of water by clay particles during wetting (i.e. the cause of swelling slaking) may also contribute to the particle separating forces.

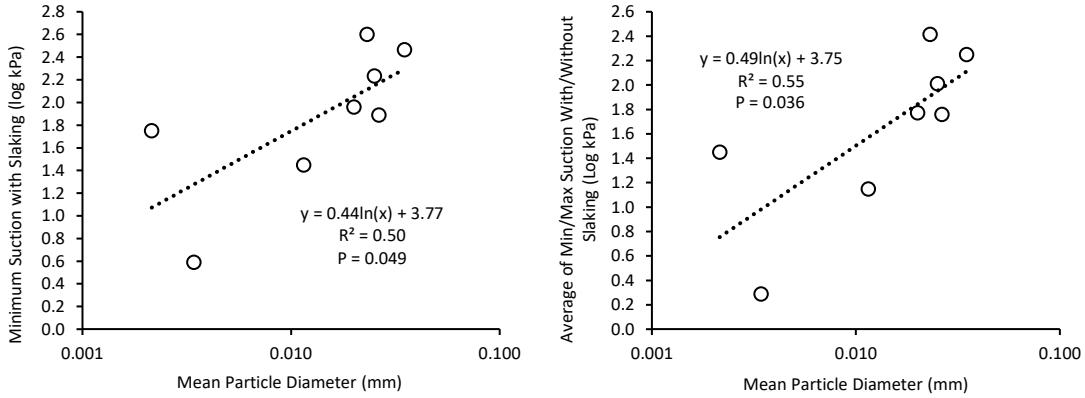

Figure 40: Effect of median particle diameter on slaking threshold

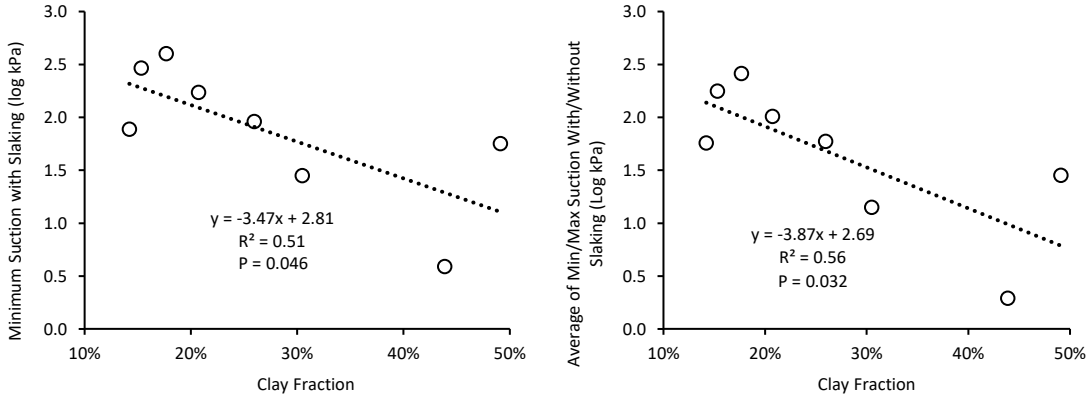

Figure 41: Effect of clay fraction on slaking threshold

4.6.3 Effect of Atterberg Limits

Plasticity Index was not found to have a statistically significant effect on the slaking threshold based on the regression analysis conducted, however it was found that the slaking threshold increases with decreasing plasticity index. Unsurprisingly, plasticity index and clay content are strongly correlated (correlation coefficient = 0.97).

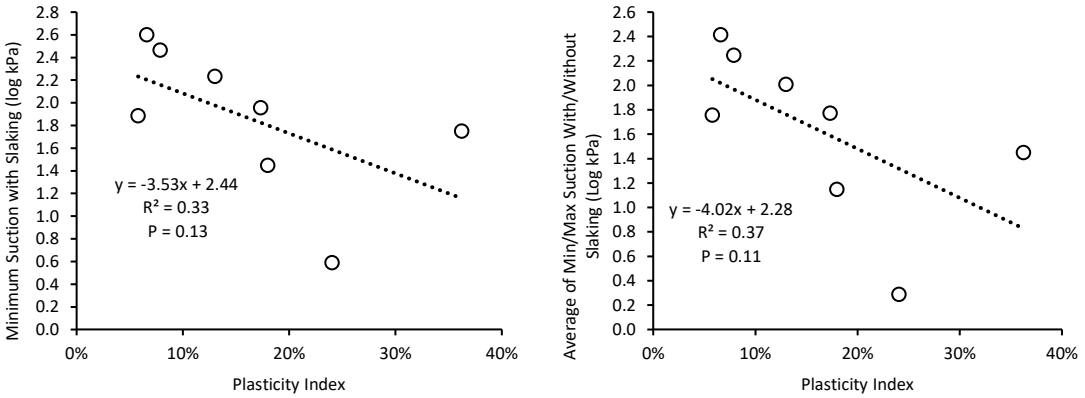

Figure 42: Effect of plasticity index on slaking threshold

4.6.4 Effect of Cation Exchange Capacity (CEC)

Cation Exchange Capacity (CEC) was not found to have a statistically significant effect on the slaking threshold based on the regression analysis conducted. CEC is considered a gauge of clay mineral cohesion, and typically cohesion increases as the cation exchange capacity increases (McAnnally, 1968). However, while not statistically significant, the relationships in Figure 1 suggest that the particle attractive forces which resist slaking increase with decreasing cation exchange capacity.

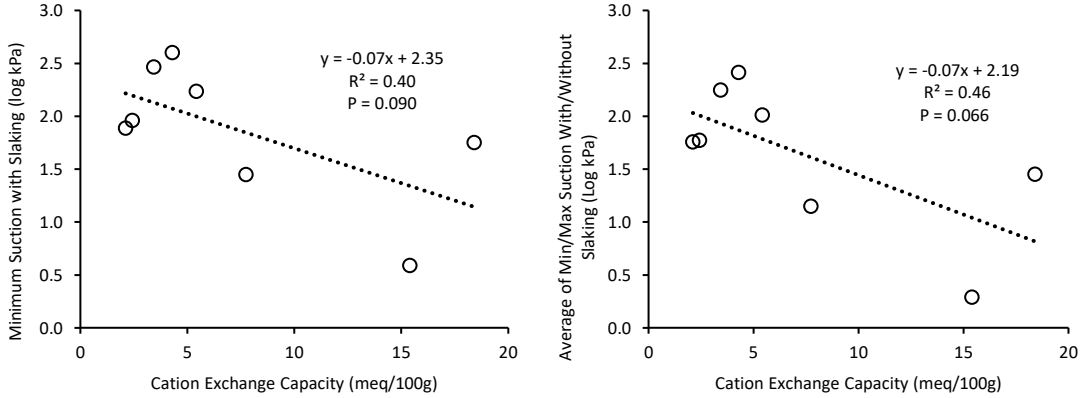

Figure 43: Effect of cation exchange capacity on slaking threshold

4.6.5 Stepwise Multiple Linear Regression

Stepwise multiple linear regression was conducted by performing multiple linear regression using all of the relevant variables and iteratively removing the variables with the largest p-value until the p-value of the remaining variables was less than 0.05. This process resulted in a linear model which considers the clay fraction and density. These results appear reasonable, since density may be indicative of a key attractive force between particles (Van der Waals force) and the clay fraction may be indicative of a key repulsive force between particles (swelling). The resulting multiple linear regression equations are as follows:

$$ST_{min} = 0.0048 \times \rho - 2.7 \times P_{clay} - 7.6 \quad (4\text{-}1)$$

$$ST_{mid} = 0.0049 \times \rho - 3.1 \times P_{clay} - 7.9 \quad (4\text{-}2)$$

Where ST_{min} is the predicted minimum suction with slaking, ST_{mid} is the predicted average of the maximum/minimum suction with/without slaking, ρ is density (kg/m^3), and P_{clay} is the clay fraction.

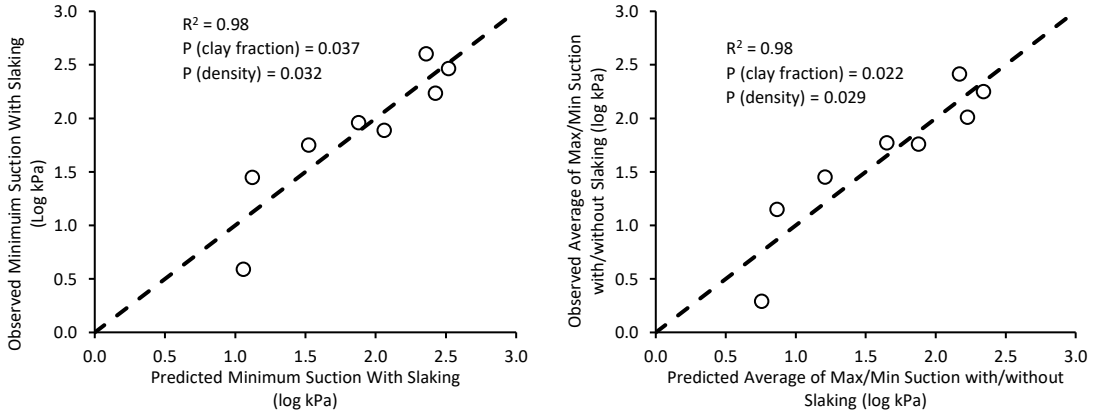

Figure 44: Observed and predicted slaking threshold based on two variable (clay content and density) linear regression model shown with 1:1 line

4.7 Effects of Lime Stabilization

Slaking and erosion tests were also conducted on Shelby tube puck samples which were stabilized with hydrated lime, as described in Chapter 3.7. The results of these tests are summarized in the following subsections.

4.7.1 Effects of Lime Stabilization on Slaking

To assess the effects of lime stabilization on slaking, the following six samples were subjected to air drying (dried until their moisture content was no longer decreasing):

- St. Laurent grab sample reconstituted without lime (SLGS)
- St. Laurent grab sample reconstituted with 2% lime (SLGS-L2)
- St. Laurent grab sample reconstituted with 4% lime (SLGS-L4)
- LSMOC grab sample reconstituted without lime (TP19-KGS-08-S4)
- LSMOC grab sample reconstituted with 2% lime (TP19-KGS-08-S4-L2)
- LSMOC grab sample reconstituted with 4% lime (TP19-KGS-08-S4-L4)

After air drying, these samples were submerged, and their slaking was observed. Both samples which were not stabilized with hydrated lime slaked and swelled significantly (approximately 1 cm), consistent with previously tested air-dried intact and reconstituted samples. Their surfaces could be easily prodded with a pocket penetrometer without any measurable resistance.

Conversely, all lime treated samples did not exhibit any measurable swelling. The LSMOC grab sample reconstituted with 2% lime exhibited some minor surface flaking, while the exposed surfaces of the remaining lime treated samples appeared completely intact. When prodded with a pocket penetrometer at its maximum applied compressive stress (4.5 kg/cm^2), no indent was observed on the surface of any of the treated samples. Figure 45 illustrates the difference in swelling between the treated and untreated LSMOC till samples.

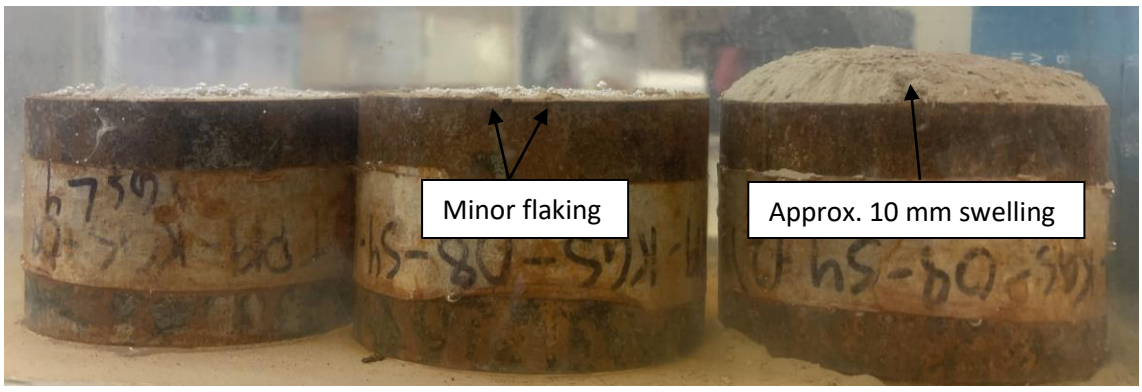

Figure 45: Swelling of LSMOC till reconstituted with 4% (left), 2% (centre), and 0% (right) hydrated lime content - subjected to air-drying prior to submergence

4.7.2 Effects of Lime Stabilization on Freeze/Thaw Deterioration

After assessing the effects of lime stabilization on slaking, the lime treated samples were then subjected to at least one 24 hour freezing period followed by a 24-hour (submerged) thawing period. At this point, the LSMOC till reconstituted with 2%

appeared to exhibit additional surficial flaking of the top 2 mm of material (only approximately 20% of its surface remained intact), while the LSMOC till reconstituted with 4% lime exhibited some minor surficial flaking (< 1 mm). Unlike previous untreated samples observed to slake, neither the detached flakes or remaining intact surface exhibited any apparent softening when submerged. The lime stabilized St. Laurent till did not exhibit any flaking after the freeze/thaw cycle and the surface of both samples remained completely intact.

4.7.3 Effects of Lime Stabilization on Erosion (Post Freeze/Thaw and Wetting/Drying Cycle)

After subjecting the lime treated samples to a wetting/drying cycle and a freezing/thawing cycle, incrementally increasing shear stresses were applied to the samples consistent with previous erosion tests (note sample SLGS-L4 was only subjected to 14 to 17 Pa). Figure 46 shows the pitted area measured prior to testing and after each applied shear stress. The initial pitted area of the LSMOC samples are a result of the previously noted surficial flaking. The surface of sample SLGS-L2 was pitted prior to any applied shear stress due to some damage during its installation into the sample panel, while the minimal initial pitted area shown for sample SLGS-L4 is a result of the moulding process.

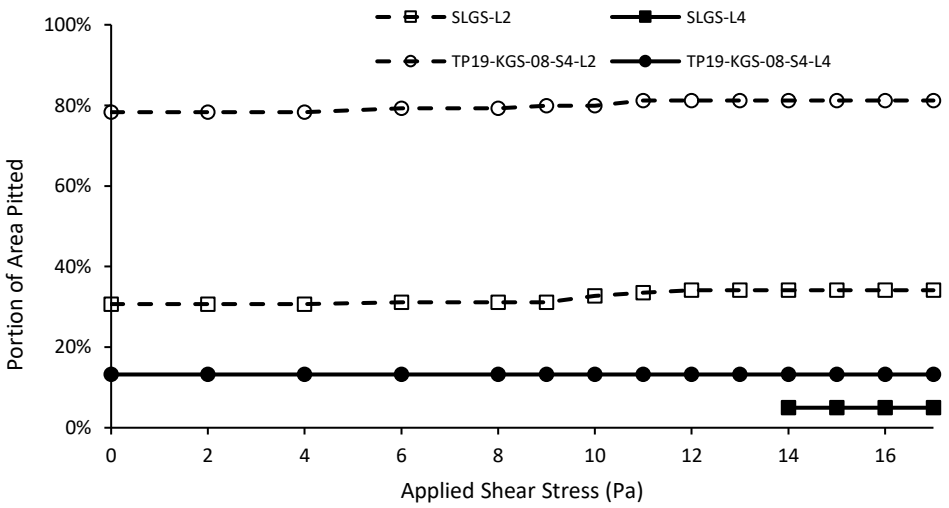

Figure 46: Portion of sample area pitted at increasing increments of applied shear stress – lime stabilized

As shown, lime stabilization effectively prevented erosion of samples which were previously subjected to freezing/thawing and wetting/drying cycles. Based on previous

erosion tests, untreated intact or reconstituted samples subjected to the same weathering conditions would have completely eroded after only a 2 Pa shear stress was applied.

Chapter 5: Discussion

Hydraulic flume tests conducted on the till samples included in this study showed that till which has not been subjected to weathering has a relatively high critical shear stress. Intact material from all sample locations was subjected to at least one erosion test with an initial moisture content/suction which did not exceed its slaking threshold. In each case, the critical shear stress of the unslaked material was shown to be in excess of 17 Pa, with the exception of one sample location which still maintained a relatively high critical shear stress of 13 Pa. These values lie within the wide range of critical shear stresses determined by previous researchers for glacial till. Pike (2014) estimated the critical shear stress of till obtained from Medway Creek (tested at its in-situ moisture content) as 7.9-8.3 Pa. Khan & Kostaschuk (2011) found the critical shear stresses of submerged Highland Creek till ranged from 17.5 Pa to 63.3 Pa. Other researchers have found the critical shear stress to be considerably lower, however it is unclear whether this till had been subjected to weathering. Assuming that a 17 Pa shear stress was applied to a non-cohesive sediment with a wide range of particle sizes, based on equation *(2-9*), particles with a diameter smaller than 8.9 cm would erode.

Unlike the intact till, material which been subjected to slaking has a relatively low critical shear stress estimated as less than 2 Pa. This is consistent with the critical shear stresses of air-dried Medway Creek till estimated by Pike (2014) as 0.9 Pa and 1.2 Pa. Similarly, the critical shear stress of exposed Highland Creek till was estimated by Khan and Kostaschuk (2011) as ranging from 0.0 to 0.2 Pa. As shown in Table 8: Critical Shear Stresses for Glacial Till Material material was found to exist naturally along the banks of the LSMEOC with a moisture content/suction both above and below its slaking threshold. As such, if the LSMEOC was suddenly operated (while at this same initial moisture content/suction condition) and all sample locations were inundated and subjected to an applied shear stress of 10 Pa (for example), it is anticipated that locations which slaked at their in-situ moisture content would erode (R1-L2, R1-L3, and R1-L4) while the remaining locations would exhibit only minor surficial erosion before becoming stable. This assumes that freeze/thaw and abrasion effects are negligible and that the loose overburden material (discussed in Chapter 3.2.2.1, unclear whether this material is weathered or was disturbed during construction) either does not exist

or erodes quickly. Based on these simplifications, erosion of intact material at a particular location is governed by both its moisture content/suction conditions prior to inundation and its slaking threshold, which is a function of its material properties.

Experiments were conducted which iteratively subjected till samples from eight locations to decreasing moisture contents/increasing matric suction prior to submergence to approximate their threshold value for slaking. These thresholds were then compared to various material properties and relationships were observed through linear regression analysis. For reasons previously discussed, this analysis focused on matric suction instead of moisture content or degree of saturation. Several material properties were shown to have a statistically significant relationship with the slaking threshold. The slaking threshold was shown to increase with increasing density and decrease with increasing clay content (note clay content was correlated with several other variables, including cation exchange capacity). A stepwise multiple linear regression model was prepared which ultimately considered density and clay fraction, however more data is needed to verify/improve this relationship. A model which considers density and clay content is reasonable since these may represent key particle attraction (Van der Waals force) and repulsion (dispersion) forces, respectively. Figure 47 shows the net effect of the double layer repulsive forces (dispersion) and van der Waals attractive forces. As shown, the van der Waals attractive forces dominate the double layer repulsive forces at very short particle distances (i.e. very high material density). However, as particle distance increases, van der Waals attractive forces decrease faster than the double layer repulsive forces decrease, and the resulting net force between particles transitions from a net attractive force to a net repulsive force. Since it is the clay particles within the soil matrix that are negatively charged and cause these double layer repulsive forces, increased clay content results in increased repulsive forces. However, these repulsive forces also depend on the concentration and valency of cations in the bulk solution, as well as on the cation exchange capacity of the clay minerals themselves (Tan, 2011). While cation exchange capacities of the tested till samples were measured, they were found to be highly correlated with the clay fraction and not directly representative of the specific clay minerals present. As such, the multiple linear regression model proposed is not expected to be valid for tills containing different clay minerals. However, the clay fraction of soils found in

Manitoba, Saskatchewan, and Alberta are known to be predominantly montmorillonite (Gardiner, 1965), so it may be appropriate to apply the relationship to this region. Methods exist to identify the clay minerals present (e.g. X-ray diffraction, infrared spectroscopy), however they were not determined as part of this study.

Till material which was allowed to saturate slowly via capillary rise did not disperse (i.e. the interparticle distances/net forces did not change). However, the compression of entrapped air caused by the submergence of unsaturated till material results in an additional repulsive force. This repulsive force (tensile stress) combined with the existing repulsive forces increases the interparticle distance, creating a positive feedback by allowing the double layer repulsive forces to dominate over the van der Waals attractive forces, further separating the particles until a new equilibrium particle distance is reached.

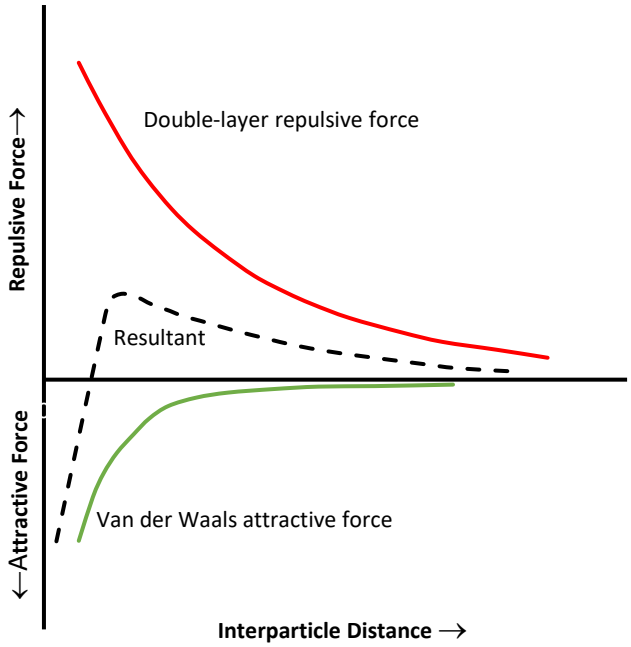

Figure 47: Double-layer repulsive and interparticle attraction (van der Waals) forces as a function of interparticle distance (adapted from Tan, 2011)

The effects of cementation, which is believed to be a significant particle attraction force, is not considered in the proposed multiple linear regression model or shown on Figure 47. As shown on Figure 5, cementitious bonds are brittle, as their strength reduces significantly at increasing strains. Therefore, under the initial tensile stress induced strain caused by the compression of entrapped air during submergence, cementitious bonds cause an additional particle attractive force. If the strain is large

enough, the cementitious bonds become broken and no longer have a significant effect on the net force balance between particles. The presence of cementitious compounds could also be determined using x-ray diffraction, among other methods.

Both the in-situ matric suction and degree of saturation of samples collected near the surface of the LSMEOC were found to vary reasonably with height above the water table and overburden material depth. It is anticipated that with improved measurement techniques and more extensive modelling efforts, the vertical variation in degree of saturation and matric suction could be predicted under a given set of boundary conditions.

The significant difference in erodibility between intact and slaked till suggests that till which is subjected to repeated wetting and drying cycles (e.g. the banks of the LSMOC) would be significantly more susceptible to erosion than till which is permanently submerged (e.g. the bed of the LSMOC). Material which has undergone major slaking, such as that shown in Figure 35, did not appear to exhibit any cohesive forces between particles, as the slaked material took on a fluid-like state and particles could be brought into suspension by only a slight movement of water within the submersion tank. Without any cohesion, erosion and transport of this slaked material would be governed by non-cohesive sediment transport principals such as those discussed in Chapter 2.6, and based on these principals, it is anticipated that almost all of the slaked material would be eroded. Assuming a shear stress of 7 Pa is applied to slaked channel bank material, equation (2-9) suggests that all particles smaller than 14 mm (the critical particle diameter) would be eroded (assumes a Shields parameter of 0.03 and a particle density of 2650 kg/m3). Based on the grain size distributions for samples collected along the LSMEOC, approximately 1-17% of material would be large enough to resist erosion. Taking the mean fraction greater than 14 mm for all materials tested (8%), equation (2-8) suggests that approximately 0.50 m of material would be eroded before a sufficient armour layer develops (assumes armour layer thickness of three times the critical particle diameter). This suggests that the rate of erosion for till subjected to wetting and drying cycles may be governed by the rate of weathering, or specifically, the thickness of weathered or slaked material which develops between and during high water levels, at least until a sufficient armour layer develops. The thickness of this slaked material layer is expected to be dependent on the slaking

threshold of the material and its moisture content prior to submergence. Since the shear stress required to erode slaked till is minimal, it is suggested that this process would impact shorelines with only minimal applied shear stresses or wave action.

Even with an understanding of the slaking threshold, the thickness of the slaked material layer which would develop between and during high water levels is difficult to understand or predict. Various softened layer thicknesses were observed along the banks of the LSMEOC (summarized in Table 2), however as noted, it was not clear whether this softened layer developed from weathering, deposited from upslope erosion, or was mechanically disturbed during construction of the channel.

It is anticipated that cyclic wetting and drying would be caused by both water level changes and rainfall. Cycles caused by rainfall are likely to be more frequent and also more rapid, at least for upper bank locations which would have a lower initial moisture content / greater matric suction (i.e. exceed their slaking threshold assuming submergence). Slaking which occurs due to rainfall causes rill erosion and interrill erosion (erosion between rills) (Moore & Simger, 1990; Shi et al., 2017). Rill erosion was observed to have caused scour depths along the rills in excess of 2 m relative to the adjacent bank elevation, as shown in Figure 12. Interrill erosion could not be measured in this way, however its effects are anticipated to be much less significant for the local glacial till material present since these areas would not be subjected to submergence or the same applied shear stresses. Without submergence, the particle separating forces caused by the compression of entrapped air would be less significant and without an applied shear stress to cyclically remove material, overburden pressure would supplement interparticle attractive forces. Additionally, fine surficial aggregate has been observed to form surface seals when wetted which impede infiltration and promote overland flow (Moore & Singer, 1990 as cited in Shi et al., 2017), further increasing erosion in rills relative to interrill areas. In the context of agricultural soils, the presence of organic matter (i.e. vegetation) has shown to greatly reduce slaking due to rainfall (Zaher & Caron, 2008). Organic matter reduces the wetting rate, which allows air to escape before significant pressure build-up, thus reducing the effects of slaking due to the compression of entrapped air.

While cyclic wetting and drying caused by rainfall events can result in considerable scour, particularly through rill erosion, this study focused on slaking and erosion caused by water level changes and channel hydraulics. This process of channel water level increase and the resulting vertical matric suction profile change leading to the potential for slaking is described in Figure 48. As shown, a change in water level of a channel is expected to be accompanied by a change in groundwater level in the adjacent channel banks, likely with some delay. If the rate of channel water level increase is slow enough, the near surface matric suction will be allowed to gradually decrease through capillary rise (due to the increasing groundwater level) such that it does not exceed the slaking threshold at the instant of surface immersion. However, if the rate of channel water increases fast enough, the near surface matric suction will exceed the slaking threshold at the instant of immersion and slaking will occur.

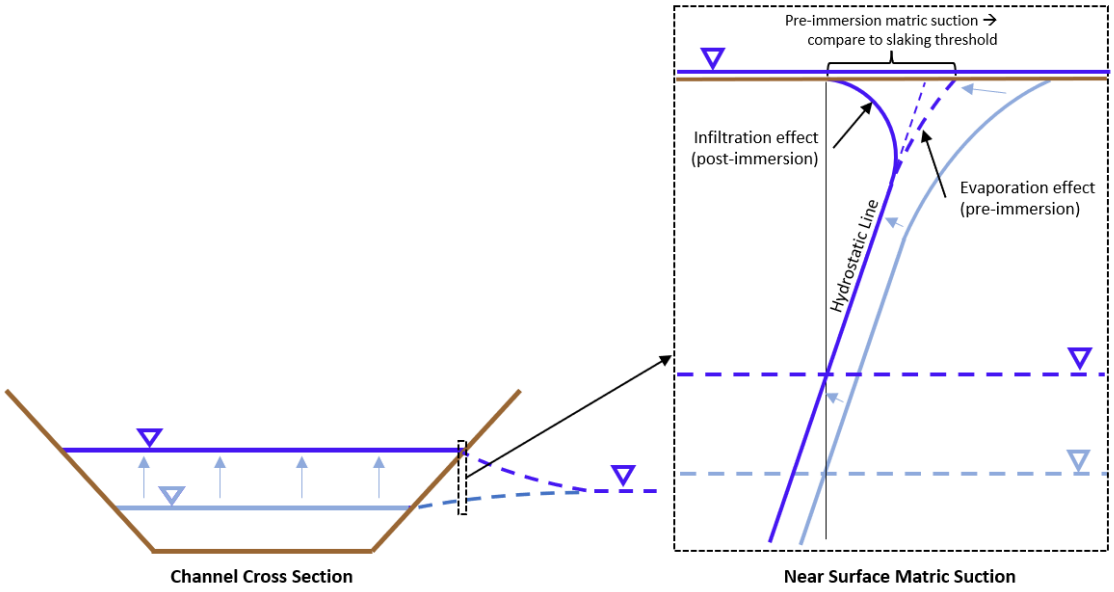

Figure 48: Matric suction at a point along a channel bank relative to channel and groundwater levels at an initial condition (light blue) and during immersion (dark blue)

As shown for all materials tested, slaking did not occur on the upper surface of Shelby tube puck samples which were allowed to saturate through capillary rise prior to submergence, since this method of saturation occurs at a much slower rate, allowing air to escape before being compressed in soil pores. Therefore, just as a slaking threshold exists for instantaneous submersion, a threshold wetting rate would also exist for each material tested and could be expressed as a rising water level. This wetting rate could be an important parameter for predicting erosion and moreover,

could serve as an important guideline for channel operation since ensuring that the channel water level does not rise faster than this threshold wetting rate could reduce the likelihood of erosion due to slaking.

Based on the erosion and slaking processes described above and specifically the relationship between matric suction and slaking, it is suggested that modelling of groundwater flow in the unsaturated zone could be used to estimate the rate of erosion for a till lined channel under a given set of environmental conditions (i.e. water levels, flow rates, rainfall conditions, etc.). At a given point along the channel slope, the erosion depth of intact till due to a high-water event is expected to be governed by the vertical matric suction profile immediately prior to submergence along with the matric suction slaking threshold of the material. For example, if the threshold matric suction is modelled to be 10 cm below the surface, the expected maximum erosion depth would be 10 cm. This would conservatively neglect the effects of overburden pressure which would supplement the attractive forces between particles to resist slaking. The relationship between modelled matric suction conditions immediately prior to submergence resulting from unsaturated groundwater flow and the associated slaking should be verified by observing slaking at various wetting rates (expressed as an increasing water level) as described above. Similar to how vegetation and organic matter reduces the wetting rate during rainfall, it is anticipated that the same effect would occur during a rising water level. However, as previously noted, vegetation did not establish itself along the banks of the LSMEOC in the native till material present.

Finally, the effect of lime stabilization on glacial till material obtained from the St. Laurent quarry site and the LSMOC alignment was assessed, and its feasibility as an alternative to conventional erosion protection was considered. Lime stabilization at a rate of 4% was found to effectively prevent weathering due to slaking and freeze/thaw cycles, while only minimal surficial slaking was observed for samples stabilized at a rate of 2%. Hydrated lime, when incorporated and compacted with soil, reacts with water and pozzolans to form cementitious bonds between aggregates which increase the attractive force between particles during wetting and can effectively prevent slaking. Stabilized samples were subjected to shear stresses up to 17 Pa and almost no erosion was observed. Untreated, intact till samples subjected to the same weathering conditions would have eroded completely from the application of a 2 Pa shear stress.

Past research has suggested that lime stabilization can be a more economical alternative to riprap, depending on the riprap haul distance, project scale, and the clay fraction and pozzolan concentration in the native soil.

Chapter 6: Conclusion

6.1 Conclusions

The primary objectives of this study were to determine the critical shear stress for erosion of the glacial till material local to the proposed LSMOC, assess the impacts of slaking on erodibility, and evaluate the effect of various material properties on slaking and erosion. The main findings of this study are summarized as follows:

- The extraction of intact samples using a manual Shelby tube hammer and the concurrent erosion testing of 12 intact Shelby tube "puck" samples using a recirculating unidirectional hydraulic flume proved to be an effective and practical method for assessing the erodibility of glacial till.
- The critical shear stress of unslaked till was determined to be greater than 17 Pa for eight of the nine sample locations considered and 13 Pa for the remaining sample location.
- The critical shear stress of slaked till was determined to be less than 2 Pa.
- The critical shear stress of till subjected to a freeze/thaw cycle ranged from 8 Pa to greater than 17 Pa for the four samples tested. In general, the effect of freeze/thaw cycles were observed to be less significant than the effect of slaking.
- Slaking was shown to be dependent on the moisture content / matric suction condition prior to submergence.
- Reducing the wetting rate of till samples by allowing them to saturate through capillary rise effectively prevented slaking for all samples at any initial moisture content / matric suction tested.
- Samples were shown to slake at varied initial matric suction conditions. Therefore, a slaking threshold exists for each sample based on its material properties. The slaking threshold was experimentally approximated for samples collected near the proposed LSMOC. They ranged from approximately 34 Pa to 400 Pa.
- Samples were found to exist naturally along the banks of the LSMEOC both above and below their slaking threshold. Most samples did not slake or erode at their in-situ moisture content. Three samples exhibited slaking and erosion

at their in-situ moisture content. The initial moisture content of identical samples (i.e. from then same Shelby tube) could be increased through capillary rise, past the slaking threshold, such that slaking and erosion did not occur when these samples were submerged and a shear stress was applied.

- The slaking threshold was found to increase with increasing density and with decreasing clay content. A multiple linear regression model is proposed and was found to be in good agreement with the observed data ($R^2 = 0.98$).
- Lime stabilization was shown to effectively prevent slaking as well as freeze / thaw deterioration. It is suggested that lime stabilization should be considered as an alternative to conventional erosion protection depending on the project scale, location, and the local material present.

6.2 Recommendations for Future Work

Further research on this topic would be useful to better understand the erosion and slaking process, as well as how it can be managed. Some suggestions based on this research are as follows:

- Additional drying/submersion iterations could be conducted to more accurately define the slaking threshold. This would help improve upon the regression analysis conducted between the slaking threshold and material properties.
- Additional experiments could be conducted to iteratively determine the threshold wetting rate for each material. This would help better understand what rate of water level increase is expected to initiate slaking.
- Further research and experimentation could be conducted to better understand slaking in the context of rainfall infiltration as well as rill and interrill erosion processes.
- Unsaturated groundwater modelling could be used; along with the estimated slaking thresholds, to estimate erosion under a given set of environmental/hydraulic conditions. Determining a threshold wetting rate (expressed as a rising water level) could be used to help verify this procedure.
- Additional experiments could be conducted to further understand the effects of overburden pressure on slaking. This would help improve the estimation / modelling of slaking depth after a given set of environmental conditions.

- X-ray diffraction could be used to better understand the mineral composition of the till. Specifically, the dominant clay mineral and gypsum content are expected to impact the slaking threshold.
- Additional experiments could be conducted to evaluate the effect of abrasion on the critical shear stress of unslaked till. Past conclusions regarding the importance of this mechanism appear mixed.
- Direct shear tests could be conducted to determine cohesion, which has been shown by past researchers to be a strong indicator of critical shear stress. These tests should be conducted using samples reconstituted using just the fine material, since coarse aggregate oriented along the shear plane would increase the determined shear stress but would not be representative of the cohesive bonds between particles.
- Further research and experimentation could be conducted to better evaluate the effectiveness and costs/benefits of lime stabilization as an alternative to conventional erosion protection (riprap).

Chapter 7: References

Alshameri, B., Madun, A., & Bakar, I. (2017). Comparison of Effect of Fine Content and Density towards the Shear Strength Parameters. *Geotechnical Engineering Journal of the SEAGS & AGSSEA*, *48*(2), 104–110.

ASTM. (1998). *Standard Test Method for Liquid Limit, Plastic Limit, and Plasticity Index of Soils.* West Conshohocken: ASTM International.

ASTM. (2007). Standard Test Method for Erodibility Determination of Soil in the Field or in the Laboratory by the Jet Index Method 1. *Astm D5852-00*, *00*(Reapproved 2007), 1–5. https://doi.org/10.1520/D5852-00R07E01.2

ASTM. (2013). *Standard Test Method for Identification and Classification of Dispersive Clay Soils by the Pinhole Test*.

ASTM. (2016). Standard Test Method for Measurement of Soil Potential (Suction) Using Filter Paper. *Astm International*, *04.08*(November 1994), 1–6. https://doi.org/10.1520/D5298-16.2

ASTM. (2017). *Standard Test Method for Particle-Size Distribution (Gradation) of Fine-Grained Soils.* West Conshohocken: ASTM International.

ASTM. (2017). *Standard Test Method for Particle-Size Distribution (Gradation) of Soils Using Sieve.* West Conshohocken: ASTM International.

ASTM. (2019). *Standard Test Method for Using pH to Estimate the Soil-Lime Proportion Requirement.* West Conhohocken: ASTM International.

ASTM. (2021). *Standart Test Methods for Laboratory Compaction Characteristics of Soil Using Standard Effort.* West Conshohocken: ASTM International.

ASTM. (2021). *Standard Test Methods for Determining Dispersive Characteristics of Clayey Soils by the Crumb Test*.

Bell, F. (1996). Lime Stabilization of Clay Minerals and Soils. *Engineering Geology*, 223-237.

Benn, D., & Evans, D. (2010). Glaciers and Glaciation. Routledge, London, UK.

Boudaghpour, S., & Majdzadeh, F. (2014). *Environmental Effects of Lime on Mechanical*

Characteristics of Stabilized Closed-texture Soils. *8*(1992), 60–64.

Carlson, E., & Enger, P. (1962). *Studies of tractive forces of cohesive soils in earth.* Denver, USA: US Department of the Interior Bureau of Reclamation.

Carter, W., & Gregorich, E. (2007). *Soil Sampling and Methods of Analysis.* Boca Raton: Canadian Society of Soil Sciences.

Chan, K. Y., & Mullins, C. E. (1994). Slaking characteristics of some Austrailian and British soils. *European Journal of Soil Science*, *45*, 273–283.

Chow, V. T. (1969). *Open Channel Hydraulics.* Tokyo: McGraw-Hill Book Company Inc.

Clarke, B. G. (2018). The engineering properties of glacial tills. *Geotechnical Research*, *5*(4), 262–277. https://doi.org/10.1680/jgere.18.00020

Couper, P. (2003). Effects of silt-clay content on the susceptibility of river banks to subaerial erosion. *Geomorphology*, *56*(1–2), 95–108. https://doi.org/10.1016/S0169-555X(03)00048-5

Debnath, K., & Chaudhuri, S. (2010). Cohesive sediment erosion threshold: A review. *ISH Journal of Hydraulic Engineering*, *16*(1), 36–56. https://doi.org/10.1080/09715010.2010.10514987

Dreismanis, A. (1989). Tills: their genetic terminology and classification. In R. Goldthwait, & C. Matsch, *Genetic Classification of Glacigenic Deposits* (pp. 17-83). Balkema, Rotterdam, the Netherland.

Dunn, I. (1959). Tractive resistance of cohesive channels. *Journal of Soil Mechanics and Foundations*, 1-24.

Durand, Z. (2014). *Experimental Study of Tailwater Levels and Asymmetry Ratio Effects on Three-Dimensional Offset Jets.* Winnipeg: University of Manitoba.

European Union. (2016). *Regulation (EU) No 528/2012 concerning .* European Union.

Fredlund, D., Rahardjo, H., & Fredlund, M. (2012). *Unsaturated Soil Mechanics in Engineering Practice.* Saskatoon: John Wiley & Sons.

Garcia, M. (Ed.). (2008). *Sedimentation Engineering; Processes, Measurements, Modeling, and Practice*. ASCE.

Gardiner, R. (1965). *Mineralogic and Chemical Composition of Some Prairie Clays.* Ottawa: National Research Council

Government of Canada. (2022, 08 10). *2011 Manitoba flood: status of community rebuilding and numbers of displaced persons*. Retrieved from https://www.sac-isc.gc.ca/eng/1392046654954/1535122238673

Graymont. (2022, July 7). *Lime and Limestone in Agriculture*. Retrieved from https://www.graymont.com/en/markets/agriculture#:~:text=Ag%2Dlime%20is%20often%20used,water%20percolation%20through%20the%20soil

Herrier, G., Campos, G., Nerincx, N., Bonelli, S., Puiatti, D., Tachker, P., & Cornacchioli, F. (2018). Lime Treatment of Soils: A solution for Erosion-Resistant Hydraulic Earthen Structures. *Dam World 2018*, *September*.

Herrier, G., Puiatti, D., Chevalier, C., Froumentin, M., Bonelli, S., & Fry, J. J. (2013). Lime treatment: New perspectives for the use of silty and clayey soils in earthen hydraulic structures. *WasserWirtschaft*, *103*(5), 112–115. https://doi.org/10.1365/s35147-013-0546-4

Investigating the Effect of Applied Shear Stress on Cohesive Riverbank Erosion by Navid Kimiaghalam A thesis submitted to the Faculty of Graduate Studies of the University of Manitoba in partial fulfillment of the requirements for the degree of Doctor of . (2016).

IOWADOT. (2015). *Engineering Properties of Soil and Rock*.

Jelisic, N. (2006). Geotechnical Properties of Stabilized Peat. *International Conference on Soil Mechanics and Foundation Engineering.* Osaka, Japan.

Jianfar, A. (2014). *EVALUATION OF EROSION RATES AND THEIR IMPACT ON RIVERBANK STABILITY.* Winnipeg: University of Manitoba.

Kamphuis, J. W., Gaskin, P. N., & Hoogendoorn, E. (1990). Erosion tests on four intact Ontario clays. *Canadian Geotechnical Journal*, *27*(5), 692–696. https://doi.org/10.1139/t90-082

KGS Group. (2016). *Assiniboine River & Lake Manitoba Basins Flood Mitigation Study LMB & LSM Outlet Channels Conceptual Design - Stage 2.* Winnipeg.

Khan, I., & Kostaschuk, R. (2011). Erodibility of cohesive glacial till bed sediments in urban stream channel systems. *Canadian Journal of Civil Engineering*, *38*(12), 1363–1372. https://doi.org/10.1139/L11-099

Kimiaghalam, N. (2016). *Investigating the Effect of Applied Shear Stress on Cohesive .* Winnipeg: University of Manitoba.

Lagasse, P. F., Zevenbergen, W. J., Spitz, W. J., & Arneson, L. A. (2012). *Stream Stability at Highway Structures*.

Laker, M. C., & Nortjé, G. P. (2019). Review of existing knowledge on soil crusting in South Africa. *Advances in Agronomy*, 189-242.

Lambert, S. (2018, January 12). *Judge approves $90M settlement for flooded Manitoba First Nations*. Retrieved from CBC News: https://www.cbc.ca/news/canada/manitoba/manitoba-first-nations-flooding-settlement-1.4482353

Lefebvre, G., Rohan, K., & Douville, S. (1985). Erosivity of natural intact structured clay: Evaluation. *Canadian Geotechnical Journal*, *22*, 508–517.

Lim, S. S. (2006). *Experimental Investigation of Erosion in Variably saturated Clay Soils*. University of New South Wales.

Manitoba. (2013). *2011 Flood: Technical Review of Lake Manitoba, Lake St. Martin and Assiniboine River Water Levels.* Winnipeg.

Manitoba. (2022). *Lake Manitoba and Lake St. Martin Outlet Channels Project Overview*. Retrieved from https://www.gov.mb.ca/mit/wms/lmblsmoutlets/overview/index.html

Mantz, P. (1977). Incipient transport of fine grains and flakes by fluids — extended. *Journal of Hydraulics Division*, 601–615.

Mazurek, K. A. (2010). Erodibility of a cohesive soil using a submerged circular turbulent impinging jet test. *2nd Joint Federal Interagency Conference*, 10. http://scholar.google.com/scholar?hl=en&btnG=Search&q=intitle:ERODIBILITY+OF+A+COHESIVE+SOIL+USING+A+SUBMERGED+CIRCULAR+TURBULENT+IMPINGING+JET+TEST#1%5Cnhttp://scholar.google.com/scholar?hl=en&btnG=Search&q=in

title:ERODIBILITY+OF+A+COHESIVE+SOIL+USING+A+

Mcanally, W. H. (1968). *Fine-Grained Sediment Transport*. 253–306.

McMullen, B. (2000). *SOILpak for vegetable growers*.

Medina-Cetina, J.-L. B. I. S. H.-C. C. and Z. (2019). Relationship Between Erodibility and Properties of Soils. In *Relationship Between Erodibility and Properties of Soils*. National Academies Press. https://doi.org/10.17226/25470

Mier, J. M., & Garcia, M. H. (2011). Erosion of glacial till from the St. Clair River (Great Lakes basin). *Journal of Great Lakes Research*, *37*(3), 399–410. https://doi.org/10.1016/j.jglr.2011.06.004

Mirauda, D., & Russo, M. G. (2020). *Modeling Bed Shear Stress Distribution in Rectangular Channels Using the Entropic Parameter.* Potenza, Italy: MDPI.

Mitchell, J. K., & Soga, K. (2005). *Fundementals of Soil Behavior* (3rd ed.). John Wiley & Sons.

Moore, D., & Simger, M. (1990). Crust Formation Effects on Soil Erosion Processes. *Soil Science Society Journal of America*, 1117-1123.

Moriwaki, Y., & Mitchell, J. (2009). The Role of Dispersion in the Slaking of Intact Clay. *Dispersive Clays, Related Piping, and Erosion in Geotechnical Projects*, 287-287–16. https://doi.org/10.1520/stp26994s

Munson, B. R., Young, D. F., & Okiishi, T. H. (2002). *Fundementals of Fluid Mechanics* (4th ed.). John Wiley & Sons.

National Lime Association. (2004). Lime-Treated Soil Construction Manual: Lime Stabilization & Lime Modification. *Bulletin*, *January*, 41.

National Lime Association. (2006). *Technical Brief: Mixture Design and Testing Procedures for Lime Stabilized Soil.* Arlington, VA: National Lime Association. Retrieved from Lime.

No, D. S., & Final, S. S. P. (2013). *Embankment Dams*. *13*.

Owen, M. W. (1975). *Erosion of Avonmouthmud*.

Painall, A. (1971). Concept of critical shear stress in loose boundary open channels. *Journal of Hydraulic Research*, 91-113.

Peters, M. (2015). *An experimental study of the hydraulic characteristics beneath a partial ice cover*.

Pike, L. (2014). *The dynamics of glacial till erosion : hydraulic flume tests on samples from Medway Creek , London , ON*.

Report, A. (2015). *the Making Available on the Market and Use of Biocidal Products*. *1*(528), 1–61.

Roy, S., & Dass, G. (2019). Statistical models for the prediction of shear strength parameters at Sirsa, India. *International Journal of Civil and Structural Engineering*, *4*(4), 483–498.

Seedsman, R. (1986). The behavior of Clay Shales in Water. *Canadian Geotechnical Journal*, 18-22.

Shi, P., Thorlacius, T., Keller, M., & Sculin, R. (2017). Soil aggregate breakdown in a field experiment with different rainfall intensities and initial soil water contents. *European Journal of Soil Sciences*

Shugar, D., Kostaschuk, R., Ashmore, P., Desloges, J., & Burge, L. (2007). In situ jet-testing of the erosional resistance of cohesive streambeds. *Canadian Journal of Civil Engineering*, *34*(9), 1192–1195. https://doi.org/10.1139/L07-024

Smerdon, E., & Beasley, R. (1961). Critical tractive forces in cohesive soils. *Agricultural Engineering*, 26-29.

Sturm, T. W. (2010). *Open Channel Hydraulics* (2nd ed.). McGraw-Hill Book Company, Inc.

Tan, K. H. (2011). *Principles of Soil Chemistry.* Boca Raton: Taylor & Francis Group.

Thorn, M. F. C., & Parsons, J. G. (1980). Erosion of cohesive sediments in estuaries: an engineering guide. *International Symposium on Dredging Technology*, 349–358.

Threshold Channel Design. (2007). In *Stream Restoration Design National Engineering Handbook*. United States Department of Agriculture.

Tolhurst, T. J., Black, K. S., Shayler, S. A., Mather, S., Black, I., Baker, K., & Paterson, D. M. (1999). Measuring the in situ erosion shear stress of intertidal sediments with the cohesive strength meter (CSM). *Estuarine, Coastal and Shelf Science*, *49*(2), 281–294. https://doi.org/10.1006/ecss.1999.0512

U.S. Department of the Interior. (1998). *Earth Manual.* Denver, Colorado.

USBR. (2013). Soil-Cement Slope Protection. In U. S. Reclaimation, *Design Standard No. 13: Embankment Dams.*

USDA. (2007). *Threshold Channel Design.* United States Department of Agriculture.

Zaher, H., & Caron, J. (2008). Aggregate slaking during rapid wetting: Hydrophobicity and pore occlusion. *Canadian Journal of Soil Science*, 85-97.

Appendix A – Soil-Water Characteristic Curves for LSMEOC Shelby Tube Puck Samples

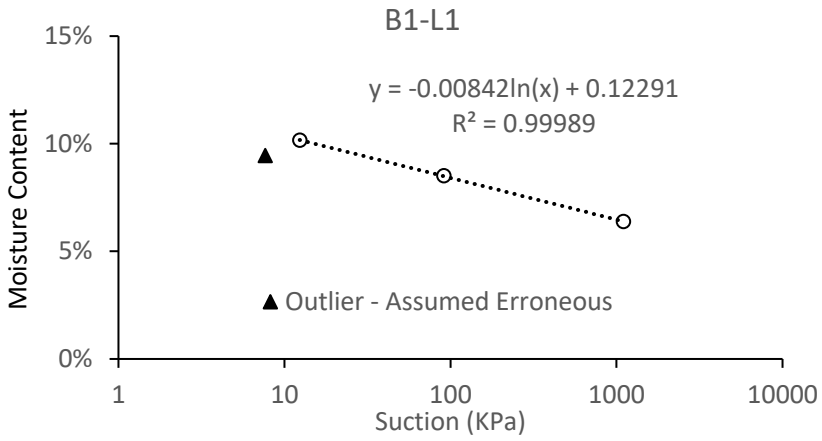
B1-L1
y = -0.00842ln(x) + 0.12291
R² = 0.99989
Outlier - Assumed Erroneous
Moisture Content
15%
10%
5%
0%
1
10
100
1000
10000
Suction (KPa)

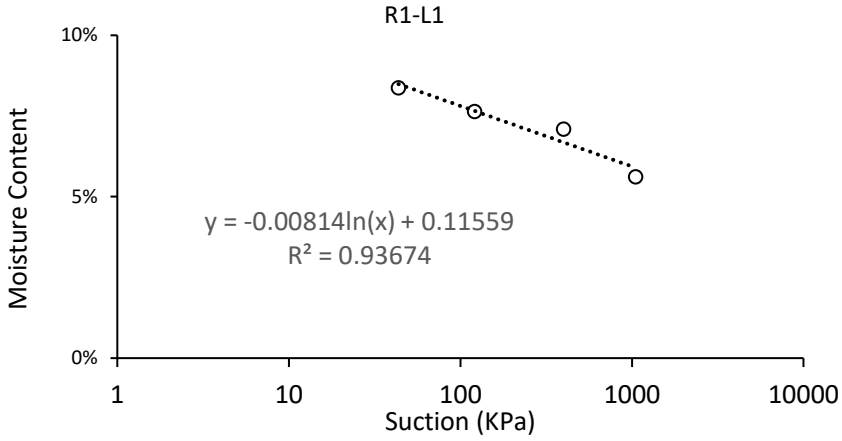
R1-L1
y = -0.00814ln(x) + 0.11559
R² = 0.93674
Moisture Content
10%
5%
0%
1
10
100
1000
10000
Suction (KPa)

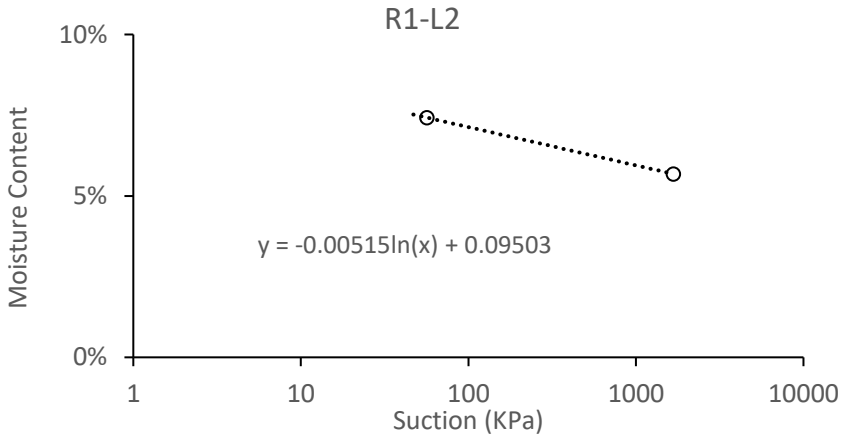
R1-L2
y = -0.00515ln(x) + 0.09503
Moisture Content
10%
5%
0%
1
10
100
1000
10000
Suction (KPa)

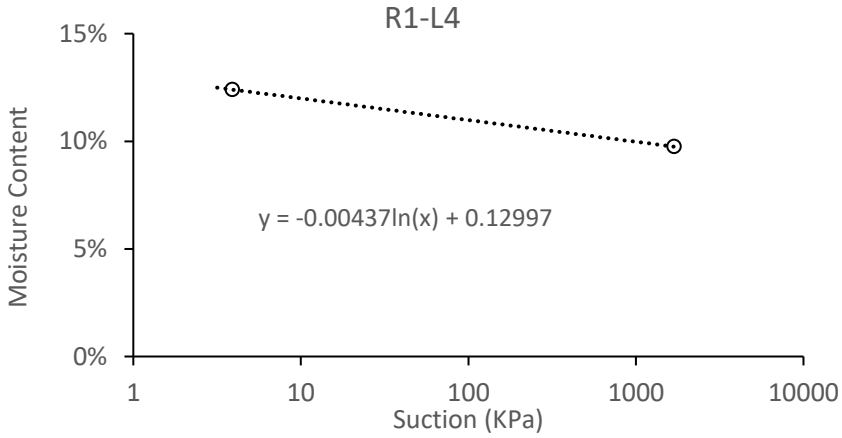
R1-L4
y = -0.00437ln(x) + 0.12997
Moisture Content
15%
10%
5%
0%
1
10
100
1000
10000
Suction (KPa)

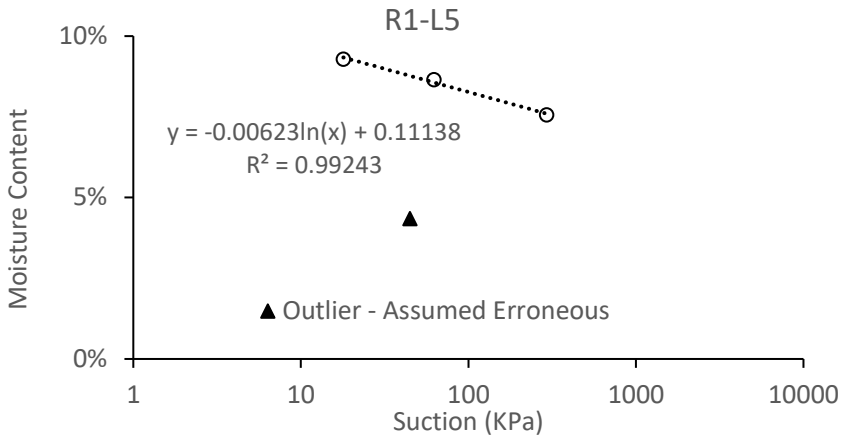
R1-L5
10%
5%
0%
Moisture Content
y = -0.00623ln(x) + 0.11138
R² = 0.99243
▲ Outlier - Assumed Erroneous
1
10
100
1000
10000
Suction (KPa)

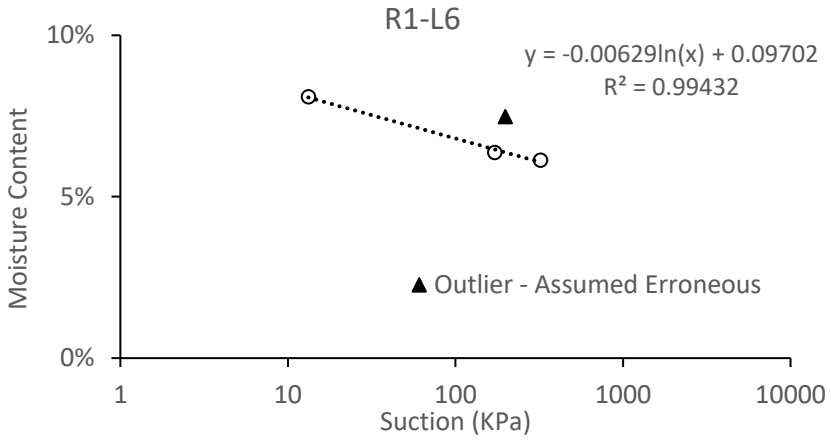
R1-L6
10%
5%
0%
Moisture Content
y = -0.00629ln(x) + 0.09702
R² = 0.99432
▲ Outlier - Assumed Erroneous
1
10
100
1000
10000
Suction (KPa)

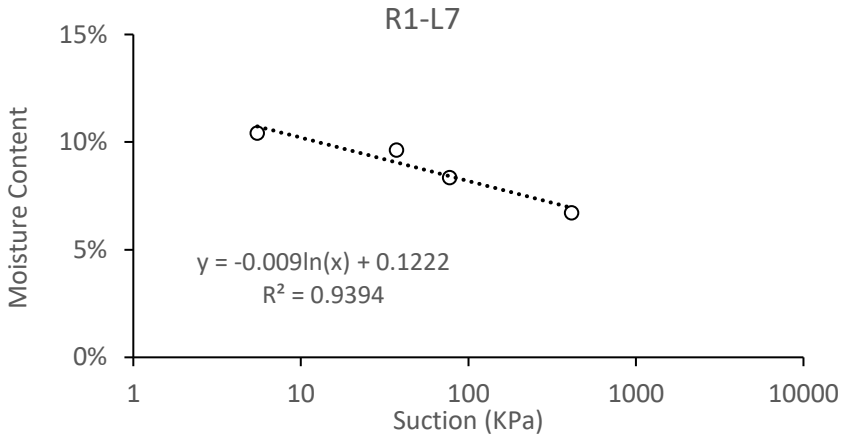
R1-L7
15%
10%
5%
0%
Moisture Content
y = -0.009ln(x) + 0.1222
R² = 0.9394
1
10
100
1000
10000
Suction (KPa)